University of Nevada, Reno

Disinfection By-Products in Potable Reuse Water and Interpretation of Their Relative Toxicities

A thesis submitted in partial fulfillment of the requirements for the degree of Master of Science in Civil and Environmental Engineering

by

Elizabeth McKenna

Dr. David Hanigan – Thesis Advisor

August 2020

THE GRADUATE SCHOOL

We recommend that the thesis
prepared under our supervision by

ELIZABETH MCKENNA

entitled

Disinfection By-Products in Potable Reuse Water and Interpretation of Their Relative Toxicities

be accepted in partial fulfillment of the
requirements for the degree of

MASTER OF SCIENCE

David Hanigan, Ph.D.

Advisor

Yu Yang, Ph.D.

Committee Member

Joanna Blaszczak, Ph.D.

Graduate School Representative

David W. Zeh, Ph.D., Dean
Graduate School

August, 2020

Abstract

To preserve water resources, many arid regions have started recycling water via direct or indirect potable reuse treatment systems. One of the pitfalls of reused water is the potential for disinfection by-products (DBPs) to form and persist in the systems– many of which are carcinogens. DBPs form from reactions between disinfectants and organic or inorganic matter.

Many methods have emerged to analyze and interpret DBP data. One such method, called “predicted toxicity,” has been used to compare the efficacy of different water treatments. Dividing each measured DBP concentration by an experimentally determined toxicological index, results in the relative contribution to the overall DBP associated toxicity of a sample, and summing the products results in a total “predicted toxicity” of a water sample, which is compared to other samples or water treatment methods. This thesis shows that this method of data use may result in biased conclusions due to the inability of any study to measure all DBPs. I removed or added actual or simulated DBP measurements to those of published studies which evaluated granular activated carbon as a treatment to reduce the relative toxicity of the effluent. In one example, removing measured haloacetaldehydes from the data caused the predicted cytotoxicity of a treated sample to decrease by up to 47%, reversing the initial conclusion that activated carbon increased the toxicity of the water. Though this additive approach should be carefully used when evaluating water treatments, it is an appropriate tool to demonstrate which species dominate toxicity. Understanding which compounds are more toxic than others can help inform future water regulations.

Nitrosamines, especially *N*-nitrosodimethylamine (NDMA), are potential human carcinogens that form from reactions of chloramines (a common disinfectant) with nitrogenous organic matter. These are persistent potential carcinogens and are best

prevented from forming by removing their precursors. I attempted to identify precursors at a potable reuse facility in California. The reuse facility's chemical additions, cleaning agents, UV/AOP process, and oxidant conditions were evaluated for NDMA precursor contribution by performing NDMA formation potential tests. Chemical additions and cleaning agents formed some nitrosamines but incorporating a conservative dilution factor to simulate the facility's conditions resulted in negligible contribution to the total NDMA formation observed at the plant. Precursor loading was higher in HOCl treatment train than in the H_2O_2 treatment train, but precursors were well removed across the treatment process for both oxidant trains. Finally, many nitrogen-containing anthropogenic compounds were subjected to simulated UV/AOP conditions to determine if they transformed into reactive nitrosamine precursors. Yields were generally less than 0.2%, except for diphenhydramine whose yield was 1.4%. Diphenhydramine (and similar compounds containing a tertiary amine outside of a ring structure) requires further study to determine the precursor load it contributes to the water reuse facility.

Acknowledgements

I had a lot of support as I pursued my master's degree and I want to thank everyone for propping me up. Thanks to my thesis committee, Dr. Yu Yang, Dr. Joanna Blaszczak, and Dr. David Hanigan for taking the time to serve on this committee and engaging with this thesis. I especially want to thank David for two years of career mentorship, reading many thesis drafts, and providing several opportunities for me, such as conferences, paper authorship, and scholarships. The research herein has been funded by the National Science Foundation under Grant No. 1804255, the Water Research Foundation (Project #5005, managed by Djanette Khiari), and AFRI grant no. 2017-69007-26309 from the USDA National Institute of Food and Agriculture.

The UNR Environmental Engineering Department has been extremely supportive with engaging classes, interesting seminar speakers, and top-notch professors. A huge appreciation goes to my first friend, Niloufar Gharoon Dastjerdi, for many cups of tea, being my go-to study buddy, and letting me drag you to events. I could not have succeeded academically or socially without you. Andy Poustie – thanks for acclimating me to the lab, especially the GC-MS. To the rest of my lab group – Mingrui Song, Junli Wang, Ibrahim Abusallout, Utsav Thapa, Priyam Sharma – your laboratory and writing advice saved me many times. Thanks for the incredible cultural exchange and tolerating my game nights.

Finally, to the rest of my support network– Whitney Bunts, Tacia Colon-Martins, Thulani Tsabedze, Taylor Scult, Emily Dement, and Hannah Kohn– thanks for being my accountability buddies and stress relievers. I am grateful for my family, especially my parents, Karen and Sean McKenna, for being built-in mentors and my biggest cheerleaders. I loved every unexpected visit to Reno, and I could not have gotten here without you.

Table of Contents

List of Tables

List of Figures

Chapter 1 Introduction and Structure of this Thesis

As climate change is exacerbated, we must find new ways to conserve energy, water, and other resources. An example of climate change can be seen in California, where the 2012-2015 drought highlighted the vulnerabilities of the environment and rural, poor communities during extreme climate events (Swain 2015). Technologies like water reuse help mitigate some of the results of climate change by recycling water for agricultural and potable use. California has been particularly forward thinking by using indirect potable reuse water in Orange County. At the Orange County Water District, secondary effluent from the Orange County Sanitation District is sent to an Advanced Water Purification Facility. Water is treated using microfiltration, reverse osmosis, an ultraviolet/advanced oxidation process, and finally decarbonated and treated with lime. Because this water is recycled, it is important to study the occurrence and persistence of disinfection byproducts (DBPs) to protect the public from adverse health effects.

The objectives of this thesis are to identify and quantify DBP precursors at the above indirect potable reuse facility, as well as critique a common DBP analysis method. DBPs in water reuse systems are generally well removed. However, since water is being reused, it is important that DBP precursors are also removed from the system to prevent future formation. *N*-nitrosodimethylamine (NDMA) is a DBP formed from a reaction with organic compounds and chloramines found in some drinking water treatment processes. Thus, the bulk of the laboratory research portion in this thesis focused on finding NDMA precursors that could be formed or introduced at potable reuse facilities. Though many NDMA precursors have been identified, it is estimated that only 10 – 50% of precursors have been discovered based on mass balance (Hanigan et al. 2015, Mitch and Sedlak 2004, Selbes et al. 2013). NDMA precursors persist through these facilities and later

react with residual chloramines. Precursors of interest include possible cleaning agents, chemical additions at the plant, and products of UV photolysis of pharmaceuticals and personal care products, which are discussed in Chapters 2 and 3.

Since nitrosamines are formed at extremely low concentrations, measuring such low concentrations can be difficult and requires sensitive instruments to quantify these compounds. Quadrupole instruments, liquid chromatography mass spectrometry (LC-MS) and gas chromatography mass spectrometry (GC-MS), are best used to measure known compounds' concentrations, while high resolution instruments can identify unknown precursors (e.g., nontarget analysis), such as FT-ICR, Orbitrap, and Time-of-Flight. These instruments can measure compounds invisible to most microscopes, but their use is highly complex. Chapter 4 focuses on common types of mass spectrometry instruments. It explains this type of instrumentation at a basic level for those who commonly use it i.e. operators, researchers, grad students, etc. My goal was to explain the instruments' analytical processes to help users optimize their data and appreciate how their data is generated. When the instrument fails, a better of understanding the instrument helps troubleshoot the issue.

Once DBPs have been quantified, meaning must be derived from the concentration data. One common method of interpretation is to use relative toxicity indices. First, the toxic potency of a DBP is found by measuring the geno- and cytotoxic responses of mammalian cells exposed to individual DBPs. Then, the measured DBP concentrations are divided by this potency factor, resulting in a weighted, unitless, toxicity index. The toxicological profile of the water is then determined by summing the toxicity indices of each measured DBP. However, I found that summing these indices may lead to biased data as it is impossible to capture the entire DBP picture in every water sample, as discussed in Chapter 5.

Literature Review

Introduction

This thesis discusses NDMA formation, analytical instrumentation, and DBP toxic potencies. For context, I first provide a brief review of instrumentation and toxic potencies. The bulk of this literature review contains information on NDMA as that is what the laboratory research focused on. A more extensive literature review of DBP toxic potencies can be found in the introduction of Chapter 5.

Advancements in analytical instrumentation have opened the door to identifying DBPs. Though the first GC-MS was developed in the 1950's (James and Martin 1952), it was not until 1974 that this technology reached the water research sector. The first group of DBPs that were discovered, trihalomethanes (THMs), were quantified using a new volatile organic compounds method for a GC-MS, allowing for measurements in nanogram quantities (Bellar et al. 1974, Rook 1974). Prior to this analysis technique, quantification and identification of these DBPs had been speculated about, but conclusions could not be drawn (Bellar et al. 1974). Since the 1970's, instrumentation has evolved to detect lower contaminant concentrations and better identify compounds using extensive libraries, multiple quadrupoles, electromagnetic pulses, and higher resolution instruments. In the 1980's, the development of electrospray ionization allowed liquid chromatography to be paired with a mass spectrometer (LC-MS) (Fenn et al. 1989, Pitt 2009). High resolution mass spectrometry instruments such as time-of-flight and Fourier transform ion cyclotron resonance were developed in the 1940's but were refined in the 1970's (Nier et al. 2015).

Studies had shown that THMs, such as chloroform and bromoform, were carcinogenic in mammals prior to detecting them in drinking water (Eschenbrenner 1945, National Cancer Institute 1976). So, with the development of analytical tools to measure

low concentrations of DBPs came the question, what concentration of a DBP is toxic to humans in drinking water? In 1976, the National Cancer Institute found that chloroform could cause cancer in rodents (National Cancer Institute 1976), and the US EPA implemented the first THM drinking water regulations in 1979 (EPA 1979). Plewa *et al.* (2008) created a system to compare DBP classes using mammalian cell cytotoxicity and genotoxicity assays. They developed a toxic potency value for each DBP they studied to assess how much a DBP contributes to the toxicity of a water sample. This is particularly useful for studying low-concentration DBPs because their aqueous concentrations are often too small to elicit toxic responses. As of 2017, 103 DBP cyto- and genotoxic potencies had been quantified (Wagner and Plewa 2017). While some cases have been shown to be additive (Lau et al. 2020, Stalter et al. 2020), Chapter 5 discusses how this use of toxicological indices should be used carefully in data interpretation.

NDMA Overview

N-nitrosodimethylamine (NDMA) is a disinfection byproduct (DBP) associated with chloramine disinfection. A drinking water lifetime exposure to 0.69 ng/L NDMA in drinking water leads to a 10^{-6} lifetime excess cancer risk, meaning one in one million people will have an increased risk of cancer. The California Department of Public Health regulated NDMA and two other nitrosamines with a notification level of 10 ng/L in drinking water (CDPH 2009), and the California Office of Environmental Health set a 3 ng/L NDMA public health goal (OEHHA 2006). This is only one of two states that regulate NDMA in the U.S., with Massachusetts regulating NDMA at 10 ng/L (Massachusetts Department of Environmental Protection 2004). The EPA has included NDMA in its list of drinking water contaminant candidates (USEPA 2016).

When the EPA implemented the Stage 2 DBP Rule, many water treatment facilities switched their disinfectants from chlorination to chloramination (USEPA 2006). This switch effectively reduced the formation of EPA-regulated DBPs (THMs and haloacetic acids [HAAs]), but increased the formation of nitrosamines, especially NDMA. As the water treatment sector concentrated on THM and HAA removal to stay in compliance with the EPA, there was less focus on removal of other unregulated toxic compounds, such as NDMA or brominated DBPs.

NDMA Formation

In drinking water, NDMA is formed through a reaction between dichloramines and organic nitrogenous precursors (Mitch et al. 2003), usually secondary, tertiary, and quaternary amines (Fiddler 1972, Mitch 2002). The main mechanisms between precursors and dichloramine are generally followed in Figure 1-1 (Schreiber and Mitch 2006).

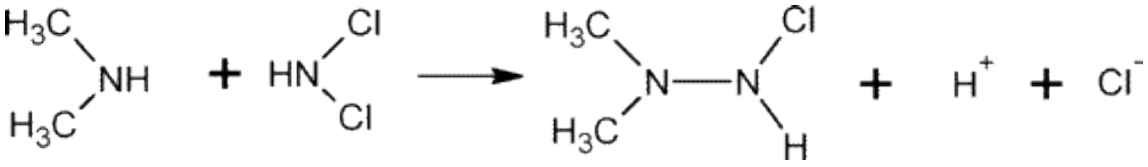

Figure 1-1 Formation pathway for NDMA precursor reaction with dichloramine. Figure from Schreiber and Mitch (2006).

The deprotonated amine precursor undergoes a nucleophilic substitution reaction with dichloramine. The N from the amine precursor attacks the dichloramine and a chloride ion is released. This results in a chlorinated unsymmetrical dialkylhydrazine intermediate which will then react with dissolved oxygen to form NDMA (Schreiber and Mitch 2006).

Though the bulk of NDMA forms from dichloramine and precursor reactions, NDMA also forms in the presence of high monochloramine concentrations. Monochloramine concentrations are highest at pH 6-8 (Figure 1-2A) (Abdessemed 2015), so the pH at treatment facilities is adjusted accordingly to maximize their disinfectant concentration. Though monochloramine is the dominant species at this pH, dichloramine is still present at equilibrium, and accounts for the majority of NDMA formation (Mitch and Sedlak 2002). As seen in Figure 1-2B, NDMA formation is also optimal at pH 6-8 due to higher rates of formation (Mitch and Sedlak 2002), resulting in the greatest yields at pH ~8.

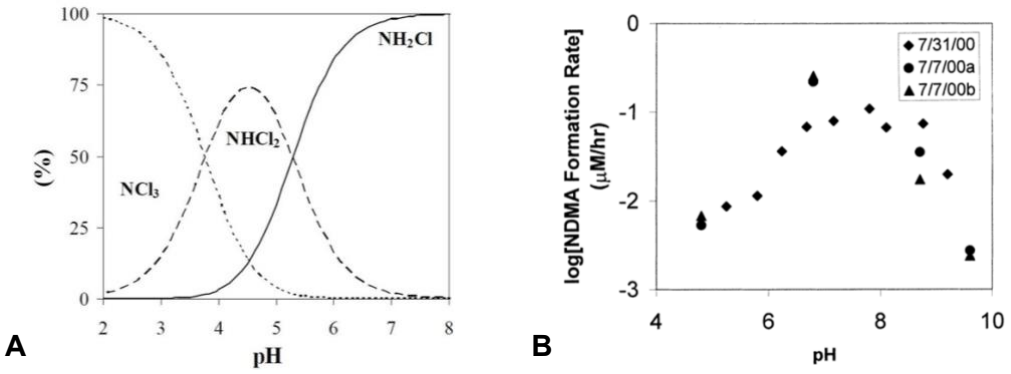

Figure 1-2 (A) Speciation of chloramines. Figure from Abdessemed *et al.* (2015). (B) The rate of NDMA formation from dimethlyamine depends on pH. Figure from Mitch *et al*. (2002).

Though NDMA is most commonly associated with chloramine disinfection, ozone can also contribute to its formation (Krasner et al. 2013). Schmidt and Brauch (2008) found that 30-50% of *N,N*-dimethylsulfamide (a decomposition product of a fungicide) was converted to NDMA when exposed to ozone. However, compared to chloramination, ozone tends to form less NDMA: Boyd *et al.* (2011) found that using ozone followed by chlorine disinfection resulted in a maximum of 12 ng/L NDMA in the

distribution system, while other studies using chloramination disinfection found that the maximum NDMA formed in the distribution systems ranged from 20 to 630 ng/L (Boyd et al. 2011, Krasner 2009, Russell et al. 2012). Krasner *et al.* (2013) concluded that while ozonation can produce high NDMA yields, this phenomenon seems contained to water with significant concentrations of industrial precursors.

NDMA's logK_{OW} (octanol-water partitioning coefficient) is -0.57, a small value indicating that it is hydrophilic (Sgroi et al. 2018). These characteristics of NDMA make it particularly difficult to remove via conventional treatment, air stripping, or activated carbon adsorption, so targeting its precursors is the more economical way of removing NDMA. Additionally, a long contact time (>45 hours) is required for chloramines to react with the NDMA precursors (Mitch and Sedlak 2002), which means NDMA is not formed at the facility, making it impossible to remove NDMA itself.

NDMA Precursors

As mentioned above, common NDMA precursors are organic secondary, tertiary, and quaternary amines. These functional groups may be found in wastewater from grey water sources (especially from laundry and shower), as well as pharmaceuticals and personal care products (PPCPs) found in blackwater (Zeng and Mitch 2015). Secondary amines, such as dimethylamine (DMA), are commonly found in human urine (Zeisel et al. 1985). In the case of tertiary amines, NDMA forms in yields of 2.5% when there is a DMA functional group (as seen with ranitidine and trimethyl amine) (Mitch and Sedlak 2004). This yield is much higher than those of tertiary amines that are part of an amide group (such as diuron or dimethylformamide), which have NDMA yields of 0.3% (Chen and Young 2008). Finally, quaternary amines may be found in some drinking water coagulants such as polyDADMAC and polyamine. They form NDMA because of their

ability to provide a DMA component during chloramination (Park et al. 2009b). Of relevance to the laboratory work done in this thesis is the ability of anion exchange resins (used in laboratory deionization devices) to shed precursors, especially quaternary amines. One study found that chloramination of water prior to resin treatment resulted in 20-400 ng/L of NDMA formation (Kemper et al. 2009).

Recently in the news, drug companies have recalled pharmaceuticals, such as the heartburn medication Zantac, for containing NDMA (Gumbrecht 2019, Ries 2020). In addition to NDMA, these pharmaceuticals are known to contain NDMA precursors, such as ranitidine, that enter the wastewater stream and form NDMA later in the treatment process. In fact, Shen and Andrews (2011) found ranitidine formed the most NDMA (90-94% yield) of 20 PPCPs tested. Selbes et al. (2013) found that compounds like ranitidine (only one carbon between the DMA and ring structure) were likely stabilized by resonance after the DMA group left, thus making NDMA formation favorable and producing yields of ~80%.

Precursors may also be formed during the treatment process through biofiltration. While some studies have found biofiltration to be an effective means to precursor removal, many others have shown that biofiltration actually increases the available NDMA precursors, subsequently increasing NDMA in the distribution system. In one study, drinking water storage facilities with nitrification were compared to facilities without nitrification – a phenomenon due to stagnation and poor mixing. As seen in Figure 1-3, a facility without nitrification formed significantly fewer nitrosamines than a facility with nitrification occurring. The soluble microbial products (SMP) produced from nitrifying bacteria led to an increase in NDMA formation when the bacteria was exposed to chloramines (Zeng and Mitch 2016).

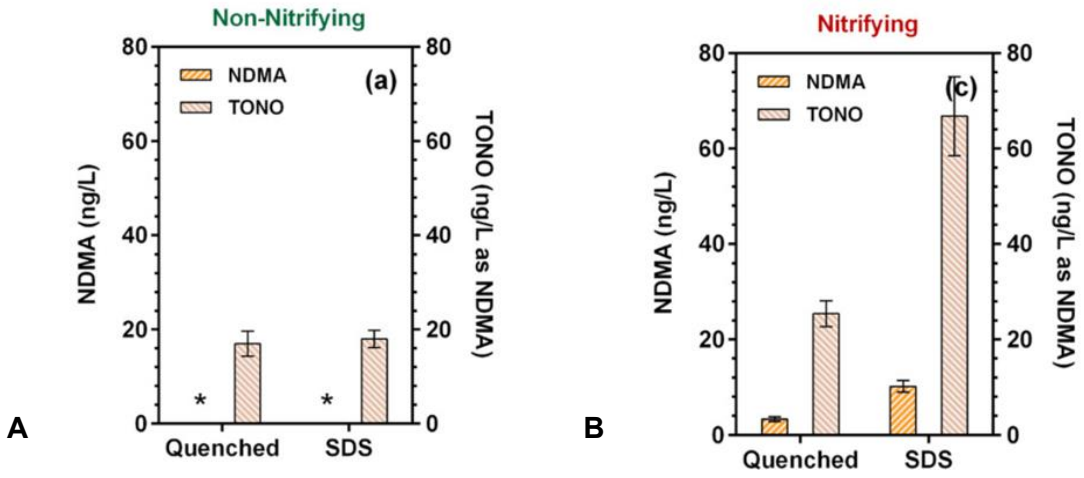

Figure 1-3 Concentrations of N-nitrosamines in non-nitrifying (A) and nitrifying (B) storage facilities. TONO = total nitrosamines (right y-axis). * = below the reporting limit (Zeng and Mitch 2016).

SMP as a source of precursors was found in another study of full-scale drinking water facilities. They found that biofiltration increased NDMA formation by 6 ng/L – indicating that biofiltration actually increases precursor loading (Krasner et al. 2018). They also found that biological material sloughed off a biological filter was a source of NDMA precursors. However, when this water was filtered, NDMA precursors decreased, indicating that most of the formed precursors were due to SMP.

Besides biofiltration, other treatment processes that might contribute to poor precursor removal or precursor formation include aging reverse osmosis membranes and advanced oxidation processes, respectively (Roback et al. 2018). Older membranes may pass more low-mass compounds that can lead to NDMA formation. Soltermann *et al.* (2013) found that NDMA formation increased in chloraminated pools that were exposed to sunlight, showing that exposure to UV can promote precursor formation, and subsequently NDMA.

Thesis Objectives

The objectives of this thesis span the various steps of DBP research. This thesis will not only focus on the EPA's priorities in regulating lower toxicity compounds, but also find NDMA precursors to reduce NDMA formation at a potable reuse facility. Objective 1 is to identify NDMA precursors that are either introduced to the treatment facility through chemical additions or transformed from nitrogenous organic matter into reactive precursors during UV/AOP treatment. Objective 2 is to explain how mass spectrometry generally works to a broad audience. This is the initial quantification step necessary to obtain data from the laboratory work. This step can be time consuming depending on understanding of the instrument and how well it is working. Finally, the data must be interpreted. Objective 3 is to show that a common analysis method, summation of relative toxicity indices, may result in biased conclusions.

Chapter 2 Contributions of Treatment Facility Chemical Additions and Cleaning Agents as Precursors to NDMA Formation

Introduction

I studied samples and chemicals from the Groundwater Replenishment System's (GWRS) Advanced Water Purification Facility (AWPF) in Orange County, California. This potable reuse facility treats tertiary effluent from the Orange County Sanitation Department (OCSD) to potable quality through 3 main steps: microfiltration (MF), reverse osmosis (RO), and an ultraviolet/advanced oxidation process (UV/AOP) (Figure 2-1). The treated water recharges the aquifer through either percolation or injection at spreading basins or wells, respectively. Aquifer recharge serves as an environmental buffer that reassures the public of their water quality and prevent seawater intrusion into the aquifer (Roback et al. 2018).

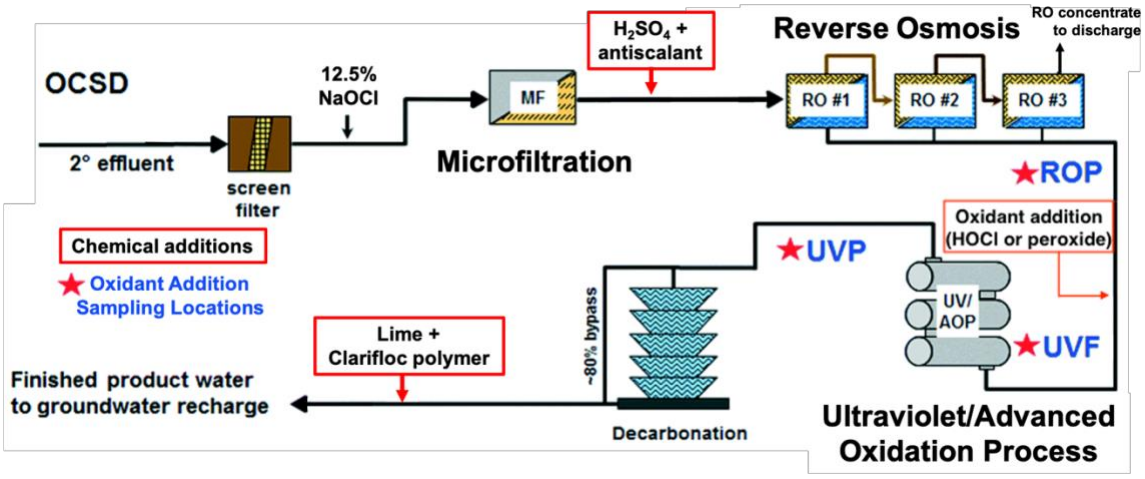

Figure 2-1 Schematic of the AWPF, a component of the GWRS. Five chemical additions and three sampling locations are highlighted. Modified from Roback *et al.* (2018).

This facility is the largest indirect potable reuse system in the world – treating 100 million gallons per day and soon expanding to 130 million gallons per day (MGD) (Roback et al. 2018). Its ability to purify sewage for indirect potable use is important in California for the area's vulnerability to droughts. Because the water is recycled, much related research focuses on the safety of the reused water, particularly the persistence of pollutants, anthropogenic disinfection by-products, and contaminant removal.

My research addressed the identification of processes and chemicals that could contribute to NDMA precursors. Finished product waters tested for NDMA were found to be non-detect (Roback 2017). However, after traveling 13 miles to the groundwater injection site, NDMA "rebounded" in concentrations of about 0.7 ng/L·h (Roback 2017). At another indirect potable reuse plant in California, NDMA concentrations increased from 10 ng/L in the finished product water to 14 ng/L after a one-day hold time, which indicated that NDMA precursors passed through the facility (Sgroi et al. 2015). These cases of NDMA rebound are worrisome because 1) NDMA is a persistent probable human carcinogen (U.S. EPA 1993) in water, so there are concerns it will form more readily (because of more available precursors reuse water) and 2) California has a 10 ng/L notification level and these levels of NDMA are close to that. We attribute this reformation phenomenon to NDMA precursors being added during treatment as in-plant chemicals, persisting through the facility from the influent wastewater, or being formed during some treatment process through transformation of otherwise benign organic matter. By identifying the NDMA precursor origins, we can alter the process or target specific precursors for removal to prevent the downstream NDMA formation. Additionally, NDMA is difficult and expensive to remove from water once formed, so precursors are often targeted to prevent NDMA formation (Leavey-Roback et al. 2016).

Cleaning Agents and Chemical Addition Experiments

Cleaning agents and chemical additions are used to maintain the equipment and infrastructure at the AWPF. In the microfiltration process, OCWD uses citric acid, caustic NaOH, and a MemClean detergent to clean membranes offline. Before reverse osmosis, sulfuric acid and an antiscalant are added to drop the pH and reduce build up on the membranes (Figure 2-1). Hydrogen peroxide is added before the UV/AOP process to aid in UV photolysis. The RO permeate water is corrosive due to the acid addition prior to RO treatment and low alkalinity levels resulting from the removal of dissolved minerals, so the pH is raised to preserve downstream infrastructure. To do this, the AWPF uses its own decarbonated product water system (DPW), as well as lime addition. After MF, RO, and UV/AOP treatment, 20% of the processed water is decarbonated using decarbonation towers (like artificial waterfalls) to remove CO_2 and raise the pH, then this DPW and the other 80% of the processed water is treated with lime to add minerals that prevent corrosion downstream. OCWD found the 20:80 ratio brought the water to the targeted pH and alkalinity levels. Thus, OCWD sent a liter of lime supernatant (a mixture of DPW and non-decarbonated water with lime added), rather than their stock $CaCO_3$. Finally, a polymer, Clarifloc A-210P (Polydyne), is added as a lime saturator and settler. I hypothesized that the NDMA reforming in the transmission lines to the injection/percolation sites could be from precursors contributed by the cleaning agents and chemical additions themselves or impurities in the stock solutions.

Oxidant Addition Sampling

In a separate sampling event, I analyzed water samples from the RO permeate (ROP), the UV feed water (UVF), and UV product water (UVP) (samples marked with red stars in Figure 2-1). The difference between the ROP and UVF is the separate

addition of two different oxidants, HOCl and H_2O_2 (Figure 2-1). My objectives for this chapter were to 1) determine if one oxidant was more effective than the other in removing precursors during UV/AOP and 2) extract nitrosamine precursors to measure the occurrence of nitrosamines at the plant, as well as extract organic matter to find potential nitrosamine precursors at the treatment plant.

Materials and Methods

Chemical Additions and Cleaning Agents

Five chemical additions (93% H_2SO_4, 50% H_2O_2, antiscalant, Clarifloc A-210P (Polydyne), lime supernatant) and three cleaning agents (NaOH, citric acid, MemClean detergent) were analyzed for their contribution to nitrosamines and nitrosamine precursors. Compounds were sent directly from OCWD's stock solutions. A 1 M borate buffer was made by dissolving 61.8g boric acid and 2.0 g NaOH in one liter of (MQ) water (18.2 MΩ·cm). The buffer was diluted 1000x to confirm it was buffering at pH 8. 5 mL of the 1 M borate buffer was added to raise the pH to 8.1. Prior to the formation potential process, the 93% H_2SO_4 was diluted 250 times in Milli-Q (MQ) water (to 69 mM) and adjusted the pH to 6.26 using ACS grade NaOH. The NaOH was diluted 250 times in MQ water and adjusted the pH to 5.9 with ACS grade H_2SO_4. 5 mL of a 1 M borate buffer was added to raise the pH to 8.1. H_2O_2 was diluted to 5 mg/L in 500 mL of MQ water. In the case of NDMA t_0, the peroxide solution was immediately quenched with 5 mL of 5mM ascorbic acid, buffered with 5mL of a 1 M borate buffer, and extracted the same as other samples. All other chemicals were diluted 1:500 and 1:1000 in MQ water. One clean, new, empty bottle from OCWD was filled with UNR's MQ water. 1 mL of this was diluted in 500 mL of MQ water for NDMA Formation Potential, NDMA t0, and Extraction & Concentration treatments.

Oxidant Addition

AWPF water was treated by two different oxidants prior to UV/AOP: HOCl and H_2O_2. Samples were taken from sites starred in Figure 2-1, including ROP, UVF, and UVP. Samples were sent overnight from OCWD to UNR in coolers with ice packs. Precursors were extracted using cation exchange (all samples) or hydrophilic-lipophilic cartridges (only UVF and UVP samples). Samples were also subjected to NDMA Formation Potential, NDMA t0, and Extraction & Concentration. For a visual representation of experiments, see Figure 2-2.

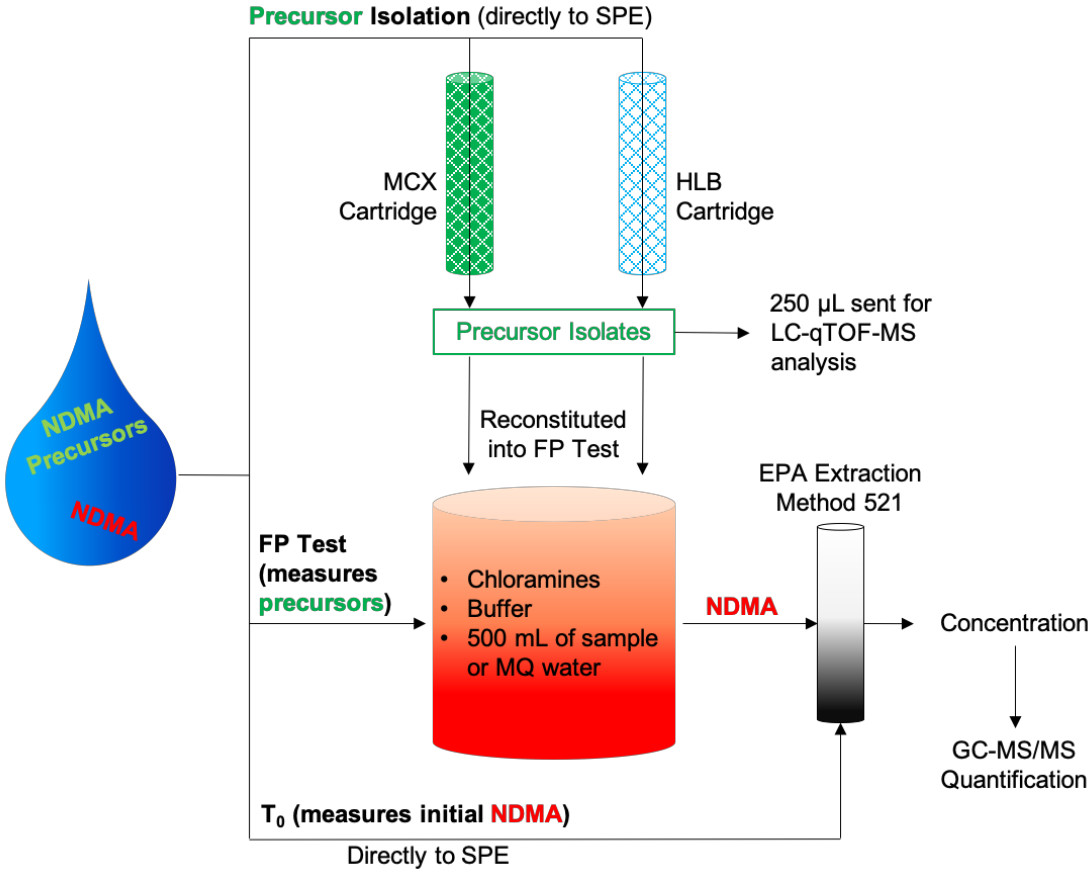

Figure 2-2 Schematic for how oxidant addition samples were tested for nitrosamines and nitrosamine precursors. Here, NDMA is used as an example but all nitrosamines were analyzed concurrently.

Precursor Extraction

MCX Precursor Extraction

The method for precursor extraction was from Hanigan *et al.* (2016). 2 L of each sample were acidified to pH ≤ 3 using 1 M H_2SO_4. Precursors were then extracted from the aqueous samples using an automated Dionex AutoTrace 280. This solid phase extraction (SPE) method used Oasis mixed-mode strong cation-exchange (MCX) 6 mL/500 mg cartridges (Waters Corporation, Massachussetts, USA). Cartridges were first conditioned with 20 mL of methanol, 30 mL of MQ water, then samples were loaded on the cartridges at a rate of 5 mL/min. Each sample was split into two, 1 L bottles and loaded onto separate cartridges to expedite the extraction process. Cartridges were dried for 45 min using ultra high purity (UHP) nitrogen gas, then eluted using 10 mL of a 5% ammonium hydroxide solution in methanol. Samples were evaporated to 1 mL in a TurboVap at 40°C using a gentle stream of UHP nitrogen gas. Using a 1 mL syringe, 1 mL total of like samples were combined into 2 mL amber vials and placed in the freezer. 250 µL of each isolated precursor sample were sent to Colorado for analysis by LC-qTOF-MS analysis.

HLB Extraction

This precursor extraction used the SPE method above, with the following exceptions. Only 1 L of an aqueous sample was loaded on to Oasis hydrophilic-lipophilic balance (HLB) 6 mL/200 mg cartridges. Samples were not acidified and were eluted with methanol. OCWD was interested in a non-target analysis of UV/AOP permeate for a profile of UV/AOP byproducts. So HLB cartridges were used to sorb and recover as much organic matter as possible and sent to Colorado for analysis by LC-qTOF-MS.

NDMA Formation Potential, NDMA t_0, and Extraction & Concentration

NDMA Formation Potential

Formation potential (FP) tests are a way to indirectly measure NDMA precursor concentrations by forcing any aqueous precursors to react with high concentrations of chloramines in ideal nitrosamine-forming conditions. This method was similar to Zhang *et al.* (2016). To begin FP tests, monochloramine was made by diluting 10 mL of a 5.65-6% sodium hypochlorite stock solution in 240mL of MQ water. The free chlorine was measured in a Hach DR 6000 UV-VIS spectrophotometer (Hach Company, Colorado, USA) using Program 80 (Chlorine F&T PP) and a DPD Free Chlorine Reagent pillow pack (Hach Company, Colorado, USA). The chlorine solution was diluted 2000 times into a square glass, 1-inch path length cuvette, gently mixed with the pillow pack contents for three minutes, then found the free chlorine concentration using Program 80. This free chlorine concentration (mg Cl_2/L), [X], was used in Equation 1 to determine the required ammonium chloride (NH_4Cl) based on a N:Cl molar ratio of 1.2.

(1) grams of NH_4Cl required = $\frac{[X]\text{mg } Cl_2}{\text{L}} * \frac{1 \text{ mmol } Cl_2}{71 \text{ mg } Cl_2} * \frac{1.2 \text{ mmol N}}{\text{mmol } Cl_2} * \frac{\text{mmol } NH_4Cl}{\text{mmol N}} *$

$\frac{53.5 \text{ mg } NH_4Cl}{\text{mmol } NH_4Cl} * \frac{1 \text{ g}}{1000 \text{ mg}} * \text{ Dilution factor } (2000) * 0.5 \text{ L}$

The required NH_4Cl was dissolved in 245 mL of MQ water and 5 mL of the 1 M borate buffer in a 500 mL amber bottle. As this solution was rapidly stirred, the sodium hypochlorite solution was added dropwise to the NH_4Cl solution using a burette or separatory funnel. Slow addition of the free chlorine to the NH_4Cl solution promotes monochloramine formation, rather than di- and trichloramine. Though monochloramine formation was measured, dichloramine was the targeted formation product because of its dominant role in NDMA formation and is always present in predominantly

monochloramine mixtures as a trace species (see Chapter 1, NDMA Formation). Since dichloramine is difficult to measure and varies across batches, it is important to 1) be consistent in preparation across batches and 2) use the same batch of chloramines across the same set of samples (i.e., for the oxidant addition samples from OCWD, the same chloramines were used for all FP samples). Once combined, the 500 mL monochloramine was allowed to equilibrate for one hour in the dark. The final concentration of monochloramine was measured using the same Hach instrument as above. The monochloramine solution was diluted 1000 times into a 1-cm path length plastic cuvette and the contents of a Monochlor F Reagent powder pillow pack (Hach Company, Colorado, USA) were added and gently stirred for 5 minutes. A chloramine measurement, [Y] (mg Cl_2/L] was taken using Program 66 (Monochloramine LR), which was then used to determine the required volume to add to 500 mL samples, assuming a monochloramine dose of 18 mg Cl_2/L (Equation 2):

(2) Required volume of chloramines: $$\frac{18\frac{\text{mg}}{\text{L}}\ \text{Cl}_2 * 500\ \text{mL}}{\frac{[\text{Y}]\ \text{mg}\ \text{Cl}_2}{\text{L}} * \text{dilution factor}\ (1000)}$$

The required volume of monochloramine was added to 1 L amber bottles for FP tests containing 5 mL of the 1 M borate buffer and either 1) 500 mL of water samples shipped from OCWD (oxidant addition samples) 2) 500 mL of MQ water as blank controls 3) 500 mL of MQ water into which 250 µL of precursor isolates were spiked or 4) 500 mL of MQ water into which 1 mL or 0.5 mL (depending on the targeted dilution factor) of chemical additions were spiked. The samples were then stored for 72 hours at room temperature in the dark. The samples were quenched with 5 mL of a 0.5 M (88 g/L) ascorbic acid solution to stop the FP reaction (final concentration was 5 mM in the samples). Samples

were then extracted and concentrated via SPE and analyzed with a GC-MS/MS (see Extraction, Concentration, and GC-MS/MS sections).

NDMA t_0

An NDMA t_0 test is a means to determine the initial amount of NDMA in a sample shipped from OCWD, before FP tests. Some chloramine residual is present upstream and downstream of the RO membranes to prevent biological growth on the membranes, and therefore some NDMA (NDMA t_0) is present in the samples sent to UNR. To test this initial NDMA (and 7 other nitrosamines), 500 mL of treated water samples sent from OCWD were extracted, concentrated, and analyzed in the following steps.

Extraction & Concentration

1 mL of a 100 µg/L NDMA-d_6 (Cambridge Isotope Laboratories, Massachusetts, USA) isotope solution was added to each sample for a final concentration of 0.2 µg/L. NDMA was then extracted from the aqueous samples using an automated Dionex AutoTrace 280. The SPE method conformed to EPA's Method 521 (Munch and Basset 2005), which used EPA 521 6 mL cartridges (Restek Corporation, Pennsylvania, USA). Cartridges were first conditioned with dichloromethane (DCM), methanol, and MQ water, then samples were loaded at a rate of 5 mL/min. Cartridges were dried for 30 min using ultra high purity (UHP) nitrogen gas, then eluted using 5 mL of DCM. The extracted samples were then passed through anhydrous sodium sulfate cartridges (Agilent Bond Elut JR-Sodium sulf. 1.4 gm) to remove any residual water and into glass conical centrifuge vials. Samples were evaporated to 1 mL in a TurboVap at 40°C using a gentle stream of UHP nitrogen gas. Using a 1 mL syringe, samples were transferred to 2 mL amber vials and placed in the freezer.

NDMA GC-MS/MS Electron Ionization Analysis

This method was adapted from a Shimadzu Application Note (Prakash et al. 2016). Concentrations of eight nitrosamines (NDMA, NMEA, NDEA, NDPA, NDBA, NPIP, NPYR, and NMOR) were determined using a Shimadzu GC-MS/MS TQ8040 in electron impact positive ionization mode and a Restek StabilWax column (30 m, 0.25 mm i.d., 0.25 µm). 2 µL splitless injections were injected into a 200°C injection port and used helium as the carrier gas. The inlet pressure was pulsed at 300 kPa for 1 minute, followed by 1.22 mL/min column flow. The initial oven temperature was held at 50°C for 2 min, ramped to 130°C at 15°C/min (no hold), ramped to 220°C at 20°C/min and held for 4 min. The MS acquisition mode was set to MRM using argon as the collision gas. The interface temperature was 220°C and the ion source temperature was set to 200°C. Ions monitored are included in the Table 2-1. The method detection limits were 1 ng/L based on a S:N ratio of 5.

Table 2-1 List of all precursor and product ions monitored during GC-MS/MS analysis based on a Shimadzu Application Note (Prakash et al. 2016). *m/z* = mass to charge ratio. “Precursor ion > product ion” indicates the precursor ion was fractured into the monitored product ion in the second quadrupole (see Chapter 4’s Quadrupole Mass Spectrometry). Qualifier ions were used to verify the compound identified by the quantification ion.

Compound	Abbrev.	Ions Monitored (*m/z*)			
		Precursor Ion	Quantification Product Ion	Qualifier Ions (Precursor Ion > Product Ion)	
N-nitrosodimethylamine-d_6	NDMA-d_6	80	50.1	46.1	30
N-nitrosodimethylamine	NDMA	74	44.1	42.2	30
N-nitrosomethylethylamine	NMEA	88	71.1	73.1	57.1
N-nitrosodiethylamine	NDEA	102	85.1	56.1	87.1
N-nitrosodi-n-propylamine	NDPA	130	113.2	113 > 71.1	130 > 88.1
N-nitrosodi-n-butylamine	NDBA	116	99.1	158 > 99.1	84.1 > 56.1
N-nitrosopiperidine	NPIP	114	84.1	55.1	97.1
N-nitrosopyrrolidine	NPYR	100	55.1	70.1	68.1
N-nitrosomorpholine	NMOR	116	86.1	116 > 56.1	86 > 56.1

Results and Discussion

Chemical Additions and Cleaning Agents

I dosed the cleaning agents and chemical additions into formation potential bottles to measure the nitrosamine precursor load contributed by them. To find the estimated concentrations at the AWPF, I conservatively assumed that chemicals would be diluted about 10,000-fold at the facility (Figure 2-2). For example, the antiscalant is dosed at 2.5 mg/L at the AWPF, a dilution factor of about 1E6. The Clarifloc A-210P polymer is dosed at 2-3 mg/L at the AWPF, a dilution factor of about 1E6, however it is only added to the saturators and is assumed to be completely removed from solution before the supernatant is added to the final product water. Finally, the peroxide is dosed at 3 mg/L for a dilution factor of 1E6. Just using this conservative dilution, I found that the NDMA and other nitrosamines formed from these chemical additions were unlikely to be the major contributors of the NDMA "rebound" downstream.

As seen in Figure 2-3, all but one of the chemical additions formed nitrosamines, though only two (lime supernatant and H_2O_2) formed NDMA above the MQ blank's NDMA formation when accounting for dilution. The lime supernatant formed about 0.28 ng/L of NDMA (accounting for MQ formation and dilution). This is consistent with previous work from OCWD that found 0.3 ng/L of NDMA (Plumlee 2020). The peroxide formed the most *N*-nitrosodibutylamine (NDBA) at 0.5 ng/L. However as mentioned above, this formation is negligible as the dilution factor is extremely conservative. Though six other nitrosamines were measured (NMEA, NDEA, NDPA, NPIP, NPYR, and NMOR), they were not detected (detection limit = 0.05 ng/L with incorporated dilution factor). The Clarifloc A-210P polymer forms some NDMA, but not as much as cationic polymers, such as aminomethylated polyacrylamide (Mannich polymer) or poly(epichlorohydrin-dimethylamine) (polyamine) (Park et al. 2009a). This is because

Clarifloc A-210P is an anionic polyacrylamide polymer, so it does not have a DMA functional group. The low contribution of NDMA precursors from Clarifloc A-210P is consistent with a previous NDMA FP study showing that anionic polyacrylamide polymers, specifically Clarifloc A-210P, did not increase NDMA yields at wastewater treatment plants (Sgroi et al. 2016).

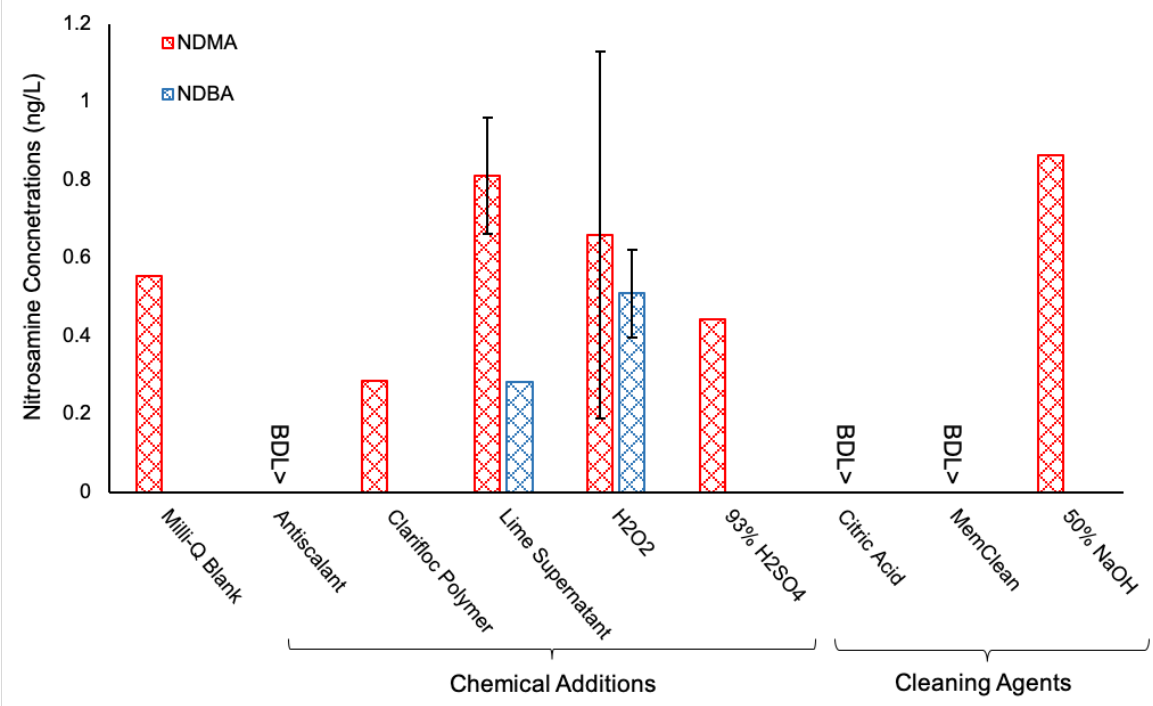

Figure 2-3 Concentrations of NDMA and *N*-nitrosodibutylamine (NDBA) (ng/L) formed from chemical additions and cleaning agents at OCWD's AWPF, assuming a 10,000x dilution. All samples were subjected to formation potential tests. Six other nitrosamines (NMEA, NDEA, NDPA, NPIP, NPYR, and NMOR) were also measured, but were not detected. Error bars represent deviation from the mean. Detection limit was 0.05 ng/L.

The only cleaning agent to form NDMA was the 50% NaOH at 0.86 ng/L. This formation may be due to impurities in the MQ water used for the FP test since the MQ blank itself is high. Additionally, the NaOH was titrated with the laboratory's stock H_2SO_4,

which could have been contaminated and passed on precursors to the NaOH sample. Finally, this NDMA formation is not alarming because NaOH is used to clean the MF cells, which undergo chemical cleaning only every 21 days. Thus, in addition to the assumed 10,000x dilution, these results are further diluted by 21 days of water flow.

I hypothesized that a chemical addition or cleaning agent in the AWPF process would contribute enough NDMA precursors to explain the 0.7 ng/L·h NDMA rebound downstream in the transmission pipeline. However, after formation potential testing, I found that none of the chemicals tested contributed enough NDMA precursors to account for the reformation downstream.

Oxidant Addition

To address the first objective of this chapter, OCWD samples treated with either H_2O_2 or HOCl prior to UV/AOP were tested for nitrosamine precursor removal. Of the eight nitrosamines measured, the most frequently detected compounds were NDBA and NDMA, while NMEA, NDPA, NPIP, NPYR were not detected at all. NMOR precursors were only measured in the ROP HOCl reconstituted MCX isolate (6 ng/L) and NDEA precursors were measured in the reconstituted HLB isolate (5 ng/L), two NDEA FP tests (each about 46 ng/L), and one NDEA t_0 test (42 ng/L) (See Table 2-1 for all data). Notably, the two travel blanks sent from OCWD formed 78% more NDMA in the FP test than the average of all other NDMA FP tests. However, due to low nitrosamine formation in the samples, expected removal across the plant, and no nitrosamines detected in the MQ water, it is likely the two travel blanks were contaminated by OCWD's deionization system prior to shipment.

Table 2-1 Raw data for oxidant addition samples. The Limit of Quantitation (LOQ) is based on the concentration at the lowest signal to noise ratio ≥ 5. MDL = method detection limit, N/A = not applicable. Compounds labeled >MDL were above the detection limit but below the LOQ.

Detection Limit: 1 ng/L LOQ: 11 ng/L	**Compound: [NDMA], ng/L**					
Sample	**NDMA t_0**	**FP**	**FP - t_0**	**Reconstituted MCX Isolate FP**	**Precursors Recovered in MCX Isolate**	**Reconstituted HLB Isolate FP**
ROP (tied to UV/HOCl)	21.14	41.22	20.08	13.84	69%	Not tested
UVF HOCl	17.05	32.27	15.22	<MDL	<10%	<MDL
UVP HOCl	<MDL	11.09	11.09	<MDL	<10%	<MDL
ROP (tied to UV/H_2O_2)	18.84	28.88	10.04	11.30	113%	Not tested
UVF H_2O_2	14.87	27.84	12.97	<MDL	<10%	<MDL
UVP H_2O_2	<MDL	<MDL	N/A	<MDL	N/A	<MDL
Travel Blank	<MDL	52.10	52.10	Not tested	Not tested	Not tested
MQ Blank	Not tested	Not tested	Not tested	<MDL	Not tested	Not tested

Detection Limit: 2 ng/L LOQ: 5 ng/L	**Compound: [NDEA], ng/L**					
Sample	**NDEA t_0**	**FP**	**FP - t_0**	**Reconstituted MCX Isolate FP**	**Precursors Recovered in MCX Isolate**	**Reconstituted HLB Isolate FP**
ROP (tied to UV/HOCl)	<MDL	<MDL	N/A	<MDL	N/A	Not tested
UVF HOCl	<MDL	46.76	46.76	<MDL	<5%	5.08
UVP HOCl	<MDL	<MDL	N/A	<MDL	N/A	<MDL
ROP (tied to UV/H_2O_2)	<MDL	>MDL	N/A	<MDL	N/A	Not tested
UVF H_2O_2	41.77	<MDL	-41.77	<MDL	N/A	<MDL
UVP H_2O_2	<MDL	46.01	46.01	<MDL	<5%	<MDL
Travel Blank	<MDL	<MDL	N/A	Not tested	Not tested	Not tested
MQ Blank	Not tested	Not tested	Not tested	<MDL	Not tested	Not tested

Detection Limit: 1 ng/L LOQ: 3 ng/L	**Compound: [NDBA], ng/L**					
Sample	**NDBA t_0**	**FP**	**FP - t_0**	**Reconstituted MCX Isolate FP**	**Precursors Recovered in MCX Isolate**	**Reconstituted HLB Isolate FP**
ROP (tied to UV/HOCl)	6.42	<MDL	-6.42	3.92	>100%	Not tested
UVF HOCl	<MDL	>MDL	N/A	<MDL	N/A	19.89
UVP HOCl	>MDL	6.00	6.00	4.95	82%	<MDL
ROP (tied to UV/H_2O_2)	<MDL	<MDL	N/A	<MDL	N/A	Not tested
UVF H_2O_2	<MDL	<MDL	N/A	3.36	>100%	11.58
UVP H_2O_2	<MDL	7.66	7.66	3.75	49%	4.96
Travel Blank	<MDL	<MDL	N/A	Not tested	Not tested	Not tested
MQ Blank	Not tested	Not tested	Not tested	5.37	Not tested	Not tested

Detection Limit: 2 ng/L LOQ: 5.9 ng/L	**Compound: [NMOR], ng/L**					
Sample	**NMOR t_0**	**FP**	**FP - t_0**	**Reconstituted MCX Isolate FP**	**Precursors Recovered in MCX Isolate**	**Reconstituted HLB Isolate FP**
ROP (tied to UV/HOCl)	<MDL	<MDL	N/A	5.90	>100%	Not tested
UVF HOCl	<MDL	<MDL	N/A	<MDL	N/A	<MDL
UVP HOCl	<MDL	<MDL	N/A	<MDL	N/A	<MDL
ROP (tied to UV/H_2O_2)	<MDL	<MDL	N/A	<MDL	N/A	Not tested
UVF H_2O_2	<MDL	<MDL	N/A	<MDL	N/A	<MDL
UVP H_2O_2	<MDL	<MDL	N/A	<MDL	N/A	<MDL
Travel Blank	<MDL	<MDL	N/A	Not tested	Not tested	Not tested
MQ Blank	Not tested	Not tested	Not tested	>MDL	Not tested	Not tested

NDMA t_0 and NDMA concentrations decreased after each unit process for both oxidant treatment trains, i.e. ROP > UVF > UVP (Figure 2-4). This indicated that the facility's processes were effective in removing most of the NDMA and NDMA precursors. Overall, the peroxide treatment train removed more NDMA precursors and contained no detectable NDMA precursors in the UV permeate compared to the HOCl treatment train.

Though the HOCl UVP FP contained NDMA precursors, only 11 ng/L of NDMA formed in one sample at the LOQ and was not detected the duplicate. Thus, the concentration in the duplicate was assumed to be 5.5 ng/L, or half the LOQ.

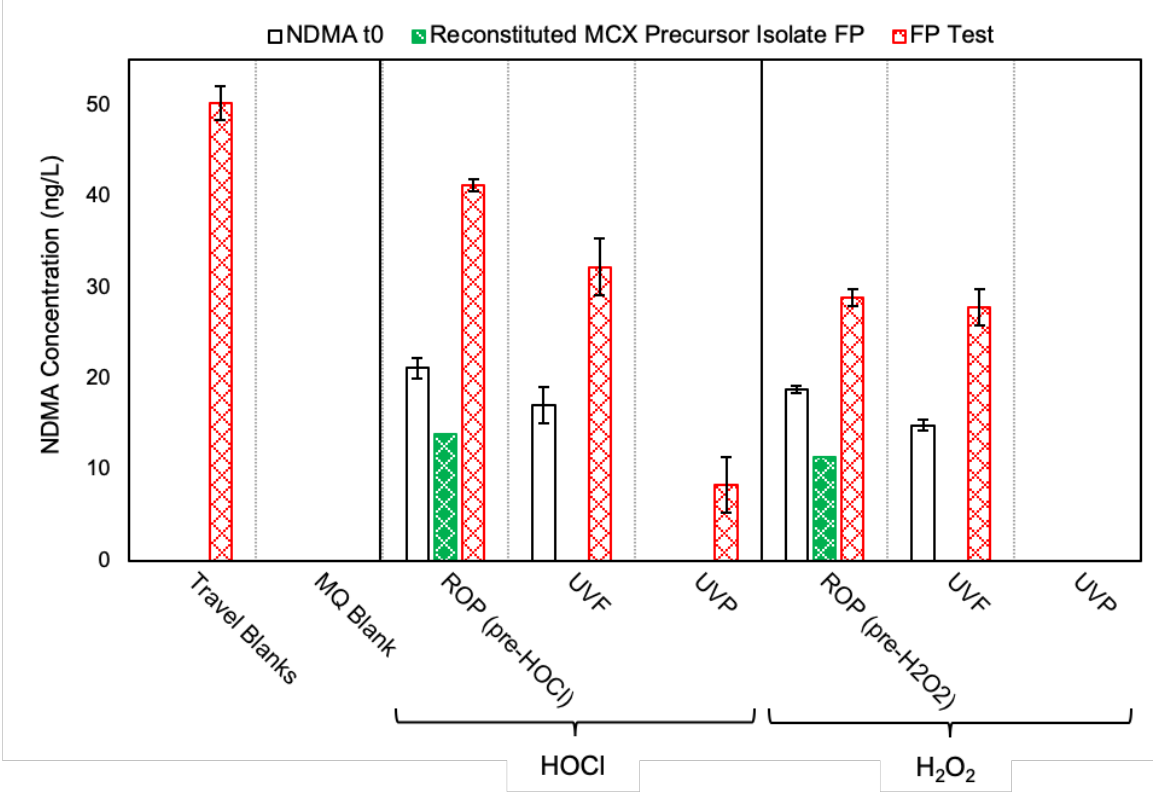

Figure 2-4 NDMA concentrations in samples from different oxidant conditions. Reconstituted HLB precursor isolates did not form NDMA under FP conditions. Detection limit was 1 ng/L. MQ blank sample was from UNR's MQ system, whereas the travel blank was provided by OCWD.

The second objective of this chapter was to extract organic matter using HLB cartridges and measure the total recovery of precursor material using MCX cartridges to extract cationic precursors. These extracts were sent to the University of Colorado, Boulder for non-target analysis by Imma Ferrer and Michael Thurman. The outcomes of

the work at the University of Colorado, Boulder are mostly outside the scope of this thesis, but it was generally found that MCX cartridges retained more NDMA precursors than the HLB cartridges, and more compounds were found in the HOCl treatment train than the H_2O_2 train.

These precursor extracts were also reconstituted into FP tests to quantify the formation of NDMA and other nitrosamines. Precursors detected from MCX extraction were not replicated due to the high sample volume required for analysis, and thus lack error bars. I measured precursory recovery by comparing NDMA measured from FP samples to NDMA measured from reconstituted precursor isolate FP tests as seen in Equation 1:

$$(1) \qquad \frac{\text{Reconstituted Precursor Isolate FP}}{\text{NDMA formed from FP} - \text{NDMA } t_0} * 100 = \text{Precursor recovery from extraction cartridge}$$

I found 69% and 113% of NDMA precursors were recovered using the MCX cartridges in the ROP HOCl and ROP H_2O_2 samples, respectively. Since ROP is the least treated water of the three unit processes analyzed, it is reasonable that the most precursors would be found in these samples. Because MCX samples were not duplicated, the recovery above 100% is likely due to variability in the sample itself. Hanigan et al. (2016) found MCX recoveries as high as 168%, which was attributed to experimental error in determining low concentrations of NDMA FP.

The NDMA MCX recovery was higher than that of the HLB cartridges (0%) for all samples (See Table 2-1 for raw data and all precursor recoveries). This shows that NDMA precursors were poorly extracted using HLB cartridges and that the majority of these precursors were best extracted when protonated, which was expected based on work by Hanigan *et al.* (2016). Though the MCX cartridges extracted NDMA precursors well, they recovered <5% of NDEA precursors, and 0% of all NMOR precursors, except

for one sample, ROP HOCl. In this case, only 5.9 ng/L of NMOR was measured in the ROP HOCl but was not found in any other sample or treatment. This data point is likely an outlier as it was detected at the LOQ and likely due to the variability in the MCX sample.

After NDMA, NDBA had the highest MCX cartridge recoveries. The precursor recoveries for UVP HOCl and UVP H_2O_2 were 82% and 49% respectively (Figure 2-5). Recoveries for the ROP HOCl and UVF H_2O_2 were both >100%, which was likely due to low NDBA FP formation. However, the MCX NDBA formation in the MQ blank was higher than all MCX NDBA samples. So, while MCX cartridges might have effectively isolated NDBA precursors, these precursors may have been contributed by the MQ water used, resulting in 0% recovery.

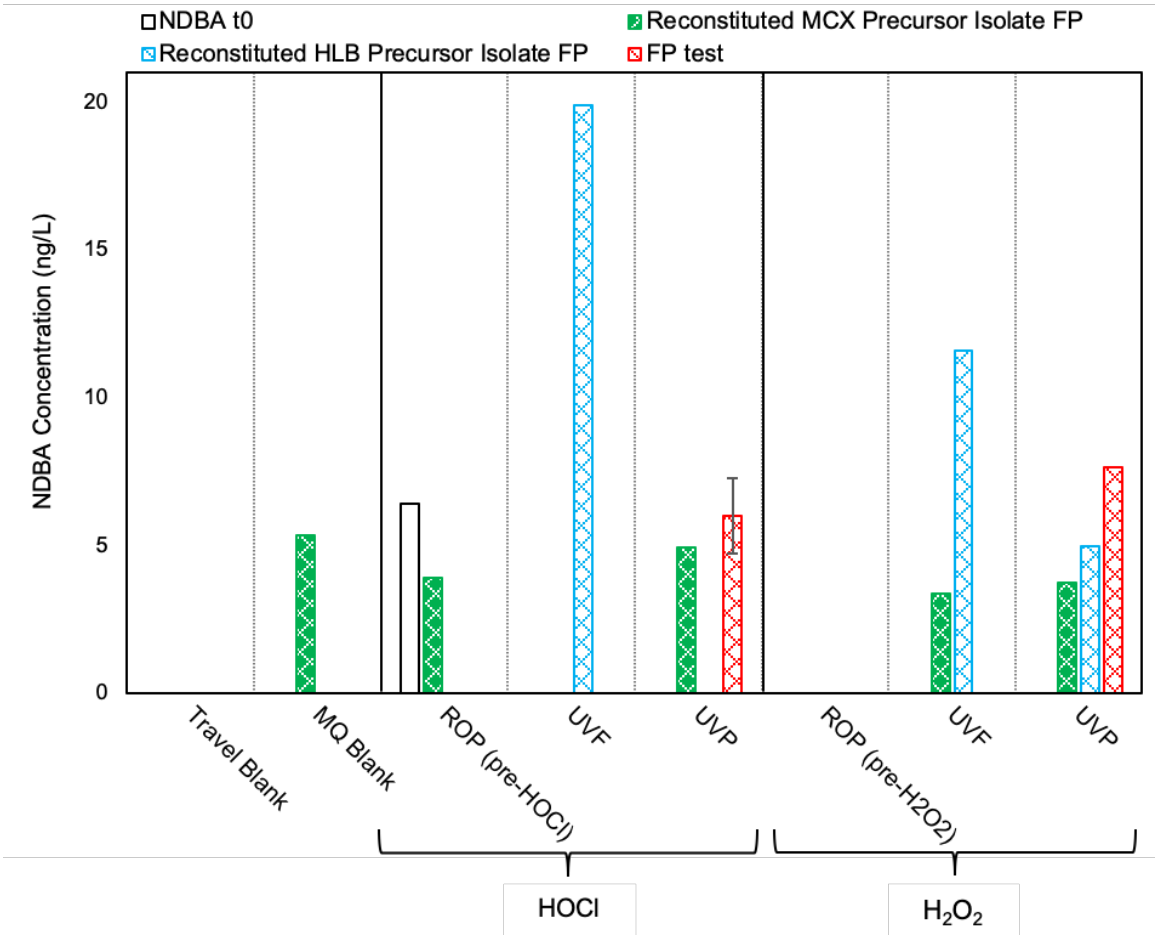

Figure 2-5 NDBA concentrations in samples from different oxidant conditions. Detection limit was 1 ng/L.

Though MCX likely did not isolate NDBA precursors, HLB cartridges recovered more NDBA than all other nitrosamines studied (Figure 2-5). The only other nitrosamine detected was 10% of recovered NDEA precursors in the NDEA UVF HOCl (Table 2-1). Of the three samples with HLB NDBA precursor measurements, only the UVP H_2O_2 sample set contained measurements for both HLB FP and NDBA FP, resulting in 65% recovery. Since NDBA FP was not detected for the other samples where HLB FP formed NDBA, recoveries appeared to be >100%. HLB cartridges may be more effective than MCX cartridges in extracting NDBA precursors, which could be attributed to the resin's

lipophilic properties. NDBA has the most alkyl constituents of the eight nitrosamines studied (two, 4-carbon components), so more precursors may have sorbed to the HLB cartridge than to the MCX cartridge. However, this does not explain the lack of NDPA (two, 3-carbon components) HLB precursor recovery, unless NDPA precursor concentrations were undetectable in the samples. Thus, future HLB extraction experiments should attempt NDPA and NDBA precursor isolation with higher concentrations of known precursors to compare t_0 and FP tests with reconstituted HLB precursor isolate FP tests.

Overall, chemical additions to the AWPF contributed few nitrosamine precursors and were unlikely to contribute to NDMA rebound in the transmission pipeline. Both oxidant treatment trains removed nitrosamines and nitrosamine precursors well. I found that MCX extraction cartridges recovered 69% to 113% of NDMA but recovered other nitrosamine precursors poorly. HLB cartridges were used to extract organic matter and were analyzed at another laboratory. In my research I found that the HLB cartridges were ineffective at sorbing and eluting nitrosamine precursors (as expected based on previous research) but did recover NDBA precursors well with recoveries of 65% to >100%. Future research should investigate HLB recovery of lipophilic nitrosamine precursors, such as those of NDBA and NDPA.

Chapter 3 Potential Transformation of Nitrogenous Organic Matter During UV/AOP into Reactive NDMA Precursors

Introduction

Benzotriazole is an example of an anthropogenic compound potentially transformed during water treatment into nitrosamine precursors. It is commonly used as a corrosion inhibitor in dishwasher detergent and aircraft deicing fluids (Cornell et al. 2000), resulting in high concentrations in surface water and wastewater (Giger et al. 2006, Voutsa et al. 2006).

According to Roback *et al.* (2018), benzotriazole was present in the RO permeate at OCWD's AWPF, but was not found in the UV product water (Figure 3-1), indicating that benzotriazole was transformed by the UV/AOP process. The benzotriazole may have been polymerized into various isomers during the UV/AOP process. Though one publication identified benzotriazole UV/AOP degradation products, they relied on stable products that could be quantified by HRMS (Chen et al. 2018), and used persulfite as the oxidant, rather than H_2O_2, the oxidant used at the AWPF. This study found that one ring was opened by UV/AOP treatment, but they did not pursue products or transformation of the nitrogenous ring. Finally, there is no literature studying the degradation or reactivity of the polymerized benzotriazole or its potential isomers. Benzotriazole contains three nitrogens, making it a candidate for transforming into NDMA precursors. I hypothesized that benzotriazole could be transformed by UV/AOP into more reactive nitrosamine precursors due to its high nitrogen content. To test this, I exposed benzotriazole at varying concentrations, UV doses, and oxidant concentrations

to see whether benzotriazole could transform into NDMA precursors, causing the NDMA reformation later in the distribution system.

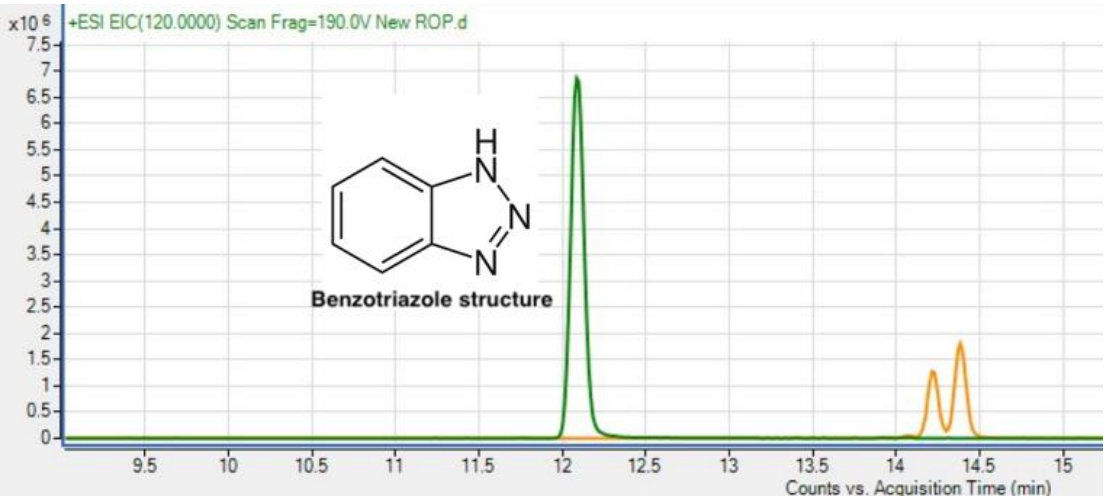

Figure 3-1 Benzotriazole (green) in the RO permeate and methylbenzotriazole isomers (yellow) found in the UV product water. Disappearance of benzotriazole peak at 12 minutes may indicate it is photolyzed into NDMA precursors. Figure modified from Roback *et al.* (2018).

In addition to benzotriazole, I tested five other anthropogenic compounds to see if they formed nitrosamine precursors in the presence of a simulated UV/AOP system: trimethoprim, sulfamethoxazole, diphenhydramine, caffeine, and natural organic matter (NOM). Trimethoprim and sulfamethoxazole are the most frequently detected antibiotics in wastewater (Karthikeyan and Meyer 2006). Diphenhydramine is used as an antihistamine and is also found in wastewater, most notably in soils watered with reclaimed water (Kinney et al. 2006). Caffeine is a commonly consumed stimulant which is consequently excreted into wastewater and found ubiquitously in surface waters (Buerge et al. 2003). These compounds were chosen for having nitrogen in their structures or containing a tertiary amine. So, similar to benzotriazole, I hypothesized that

these anthropogenic compounds would form reactive NDMA precursors after simulated UV/AOP tests.

Materials and Methods

Benzotriazole, NOM, trimethoprim, sulfamethoxazole, diphenhydramine, and caffeine were diluted in MQ water to 18.5 µM (resulting in 74 nM in the FP sample bottles). This concentration was chosen because it corresponded to 10x the NDMA LOQ on the GC-MS/MS to ensure quantifiable data (other preliminary tests resulted in low concentrations that were difficult to quantify) with an assumed precursor to NDMA yield of 1%. A solution of 5 mg C/L of NOM (International Humic Substance Society's Suwanee River 2R101N, 50% C w/w) was made in MQ water (resulting in 20 µg C/L in the FP samples).

A phosphate buffer was chosen based on a study that degraded DBPs using a UV/H_2O_2 AOP process (Chuang et al. 2016). A 0.1 M stock phosphate buffer was prepared by dissolving 4.36 g of monobasic sodium phosphate and 9.7 g of dibasic sodium phosphate in 1 L of Milli-Q (MQ) water. The pH was adjusted to pH 7.2. The phosphate buffer was added to each diluted compound for a final buffer concentration of 0.02 M. A 30% H_2O_2 stock solution was added just before exposure to the UV lamps to avoid any degradation. Peroxide concentration was dosed at 3 mg/L in the reactor, the same dose as used at the AWPF. The solution containing phosphate buffer, compound of interest, and peroxide was mixed, then loaded into quartz cuvettes, ranging from 15.7 cm_3 to 37.7 cm_3.

One 254 nm lamp (Phillips TUV 8W, G8T5) was allowed to warm up for 20 min before samples were exposed. The lamp was placed as close as possible to the cuvettes to reduce distance between the light source and the samples (see Appendix A

for UV/AOP Simulation SOP). Aluminum foil encased the samples and lamp to reflect as much light as possible into the cuvettes. Depending on the experiment, samples were removed from the light at 0 min (never exposed to the lamp), 2, 5, 10, 15, 20, 30, 40, 60, 80, 100, and 120 min and 2mL of the sample was pipetted into a 500 mL formation potential bottle. Samples were placed back into the light until the experiment finished. The AWPF uses a UV dose of about 1000 mJ/cm$_3$, which corresponds to about 20 min of exposure using the laboratory lamp. The formation potential experiments were prepared and analyzed exactly as described in Chapter 2's Materials and Methods: NDMA Formation Potential, NDMA t0, and Extraction & Concentration and NDMA GC-MS/MS Electron Ionization Analysis.

Results and Discussion

Benzotriazole, NOM, trimethoprim, sulfamethoxazole, diphenhydramine, and caffeine were exposed to UV and H_2O_2 doses that simulated the UV/AOP unit process at the AWPF to determine whether nitrosamine precursors were formed. For all compounds tested, the only nitrosamine detected was NDMA. Diphenhydramine formed the most NDMA after UV/AOP exposure and FP tests (268 ng/L) (Figure 3-2). This was expected because a study by Chen *et al.* (2009) found that when exposed to simulated sunlight and humic substances, diphenhydramine photodegraded such that the tertiary amine group was removed from the rest of the molecule to form three compounds: diphenylmethane, diphenylmethanol, and benzophenone. Lopez et al. (2017) also found that diphenhydramine degraded into these three products when exposed to UV/AOP conditions. All other compounds produced similar concentrations of NDMA to the MQ blanks. Though the trimethoprim formed more NDMA than the other low-yield compounds, the yield was only 0.6%. Excluding NOM and diphenhydramine, all

compounds' nitrogen atoms were bound by aromatic rings (extremely stable structures), making it more difficult to break the stable structure and form reactive nitrosamine precursors.

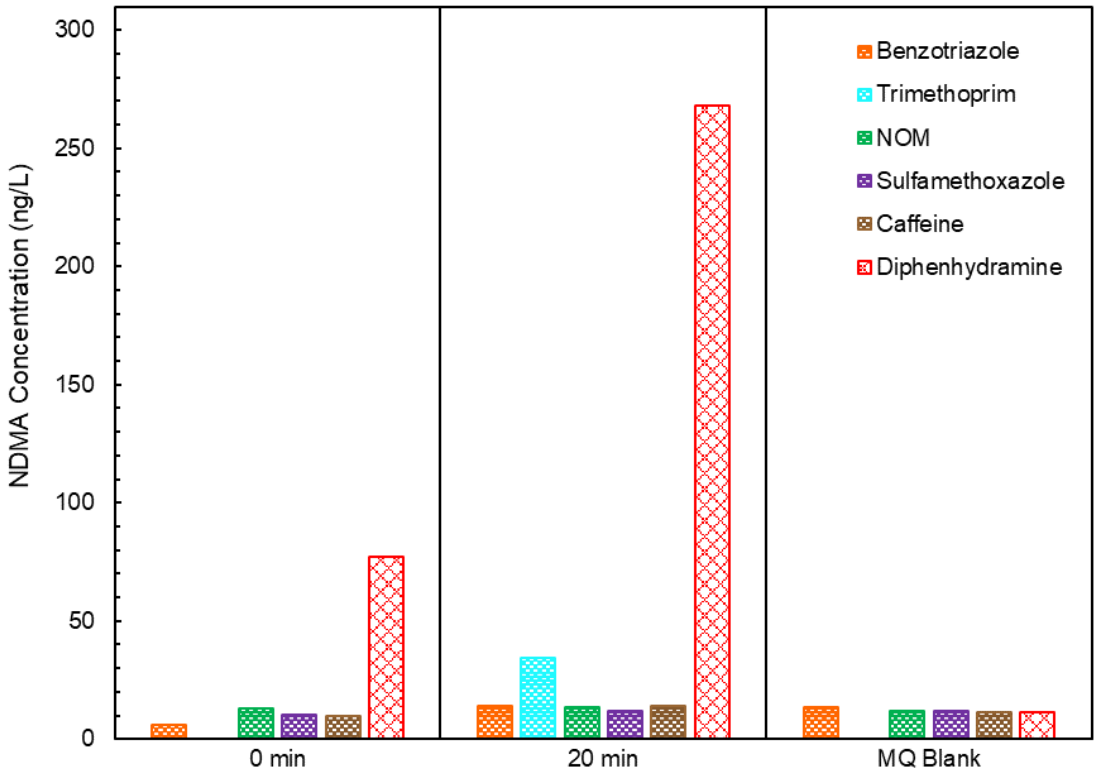

Figure 3-2 NDMA formation after simulated UV/AOP treatment for benzotriazole, trimethoprim, natural organic matter (NOM), sulfamethoxazole, caffeine, and diphenhydramine. To eliminate redundancy for data visualization purposes, only 0 min and 20 min samples are shown. Detection limit was 1 ng/L.

Excluding diphenhydramine, the average change in experimental NDMA yields was 0.16%, indicating that the PPCP UV products did not transform into NDMA precursors (Figure 3-3). However, diphenhydramine's yield increased by 1%, which is what was expected based on the experimental design. Further experiments are needed to understand the potential of diphenhydramine to produce NDMA precursors when

exposed to UV/AOP, specifically testing concentrations likely found at the facility, formation at UV doses between 0 and 20 min, and formation in the presence of NOM to simulate wastewater conditions. Additionally, compounds with similar structures to diphenhydramine should be tested.

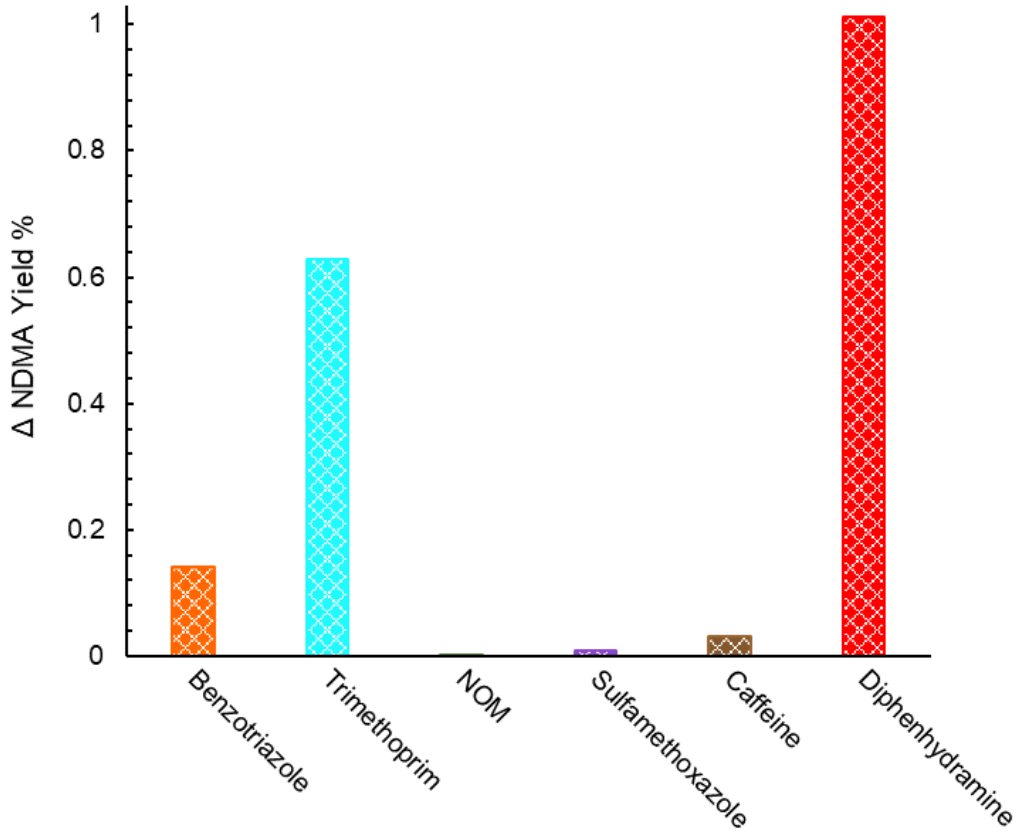

Figure 3-3 Change in NDMA yields (0 min to 20 min) after simulated UV/AOP processes for benzotriazole, trimethoprim, natural organic matter, sulfamethoxazole, caffeine, and diphenhydramine.

Most anthropogenic chemicals in this section did not form reactive NDMA precursors after simulated UV/AOP treatment as shown by an average NDMA FP delta yield of 0.16%. The exception, diphenhydramine, had a yield increase of 1%, which was expected based on the literature. Future research should use doses between 0 and

1000 mJ/cm$_3$ to understand how diphenhydramine's NDMA precursor yields change with UV exposure. Other compounds similar to diphenhydramine (i.e. contain tertiary amines that are not in a ring structure), such as erythromycin and dimethylaminoacetonitrile, should undergo similar UV/AOP tests to determine nitrosamine precursor formation.

Chapter 4 A Layman's Guide to High Resolution Mass Spectrometry

Relevance to Thesis

The following publication provides an overview of different types of high-resolution mass spectrometry (HRMS) for water industry professionals. This fits into my Thesis Objective 2: to explain the basics of mass spectrometry to a broad audience. All lab work presented in this thesis culminated in GC-MS/MS analysis to detect low concentrations of compounds, thus demonstrating the importance of mass spectrometry and my experience gained from repeated use and care of the instrument. Given the authors' collective experience with HRMS, we compiled a guide on instrumentation basics, as an expert understanding is not required for operation. We believed this publication would help operators, water professionals, and graduate students better troubleshoot their instrumentation problems, comprehend the conclusions and limitations of current research, realize the full capabilities of their laboratory instruments, and understand the complexities involved in measuring regulated and unregulated water contaminants. I led the production of the manuscript as first author. My contributions include the sections on Quadrupole Mass Spectrometry, Triple Quadrupole Mass Spectrometry, part of Chromatography, Figures 4-1, 4-2, and 4-3, and parts of Figures 4-5 and 4-6. Coauthors drafted the remaining sections on HRMS. Below is a citation to the publication, and the manuscript follows. (McKenna et al. 2020a)

Citation:

McKenna, E., Sharma, P., McCurry., D.L., and Hanigan, D. 2020a. A Layman's Guide to High-Resolution Mass Spectrometry. Journal American Water Works Association 112 (4), 40-49.

Key Takeaways

- Mass spectrometry is a tool that allows researchers to identify and quantify molecules using their known mass.
- The entertainment industry has made lab analysis seem easy but identifying chemicals in a solution is very complex.
- There are different types of mass spectrometry, each with variable analytical power and associated cost.
- Understanding the basics of mass spectrometry helps water professionals realize the full capabilities of lab instruments and comprehend the conclusions and limitations of water research.

The entertainment industry has led the public to believe that scientists are able to take a sample of anything and quickly identify specific toxicants that might be present. The popular television show *Crime Scene Investigation* includes a (darkly lit) forensics lab that quickly produces unequivocal identification of chemicals and poisons in blood or other random solutions. Until relatively recently, being able to identify an unknown compound in a complex mixture of other organic compounds was mostly a fallacy. However, the wider adoption of high-resolution mass spectrometry (HRMS) has permitted identification of unknown toxicants, bringing fiction closer to reality.

Although HRMS has been used in thousands of publications, one recent water-related example that follows the *Crime Scene Investigation* concept comes from the lab of Edward Kolodziej at the University of Washington, Seattle. Kolodziej's research group took samples of urban stormwater during rain events that resulted in coho salmon fish kills. Using HRMS, the researchers identified organic chemicals that co-occurred in storm events and runoff sources, showing that organic chemicals leaching from tire wear particles were a likely cause of the coho salmon mortality (Peter et al. 2018).

In this article, it is our goal to inform water industry practitioners—who may not be well versed in chromatography or mass spectrometry—how such forensic feats can be accomplished by the labs in their own backyards. This will help water professionals conceptualize what happens to their samples when they are sent for analysis, better understand the limitations of the data, and help troubleshoot problems in-house instrumentation. The variety of techniques covered here will inspire others to the possibilities of what they can measure and think more critically about current water research.

Chromatography

Complex environmental samples are mixtures of hundreds or thousands of different chemical compounds; the goal of chromatography is to separate compounds across time to enable their separate detection. Nearly all HRMS systems first use either gas or liquid chromatography (GC or LC) to make identification simpler. In either case, the real work of chromatography occurs inside a chromatography “column,” a flexible or rigid tube filled with a stationary phase. The stationary phase is composed of solid particles or film coatings with specific chemical properties that help separate chemical compounds. Figure 4-1, part A, shows the chromatographic separation of multiple compounds.

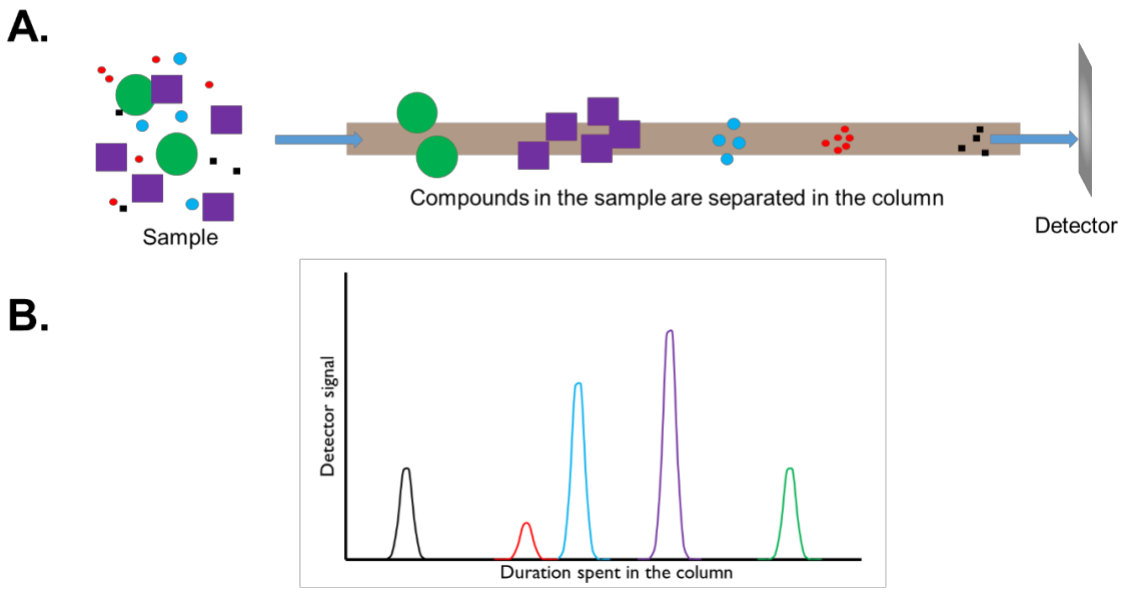

Figure 4-1 Sample passes through a column and is separated by its chemical properties (1A). The black chemicals elute more quickly and thus appears first in the plot of signal vs time (1B).

As the mobile phase (a liquid or gas) passes through the column, it flows through the stationary phase. The sample is injected into the mobile phase, and the chemical compounds stick to or interact with the stationary phase where they are retained for longer or shorter periods of time based on their chemical properties. As an analogy, let's say we're looking for two specific people in New York City. It might be hard to find them among 8.6 million people, but if everyone in the city is made to run a marathon and we stand at the finish line looking for our two individuals, we'll have a much better chance of finding them because they'll be separated by their running speed and the time they have to run. In this analogy, the interaction with the mobile phase is the fitness level, and the compounds that remain with the stationary phase longer are the slower runners who will inevitably finish the race (i.e., leave the column) last.

GC and LC are the most common chromatography techniques used for environmental applications. For GC, a sample is first heated to a vapor, and then an inert gas—usually hydrogen or helium—acts as the mobile phase, pushing the vaporized sample into a relatively low-temperature column (approximately 50 °C). Chemical compounds in the sample may stick to the stationary phase or even recondense in the column. An oven heats the column slowly, decreasing some chemicals' affinity for the stationary phase before others and causing them to separate over time by boiling point (i.e., low boiling point compounds will exit the column first).

LC uses a liquid (like water) for the mobile phase instead of a gas. For LC, a sample is injected into the mobile phase stream, which then flows through the column. Valves allow the mobile phase to be slowly changed over time, usually 5–30 minutes where the liquid is converted from 100% water to 100% of a less-polar solvent (e.g., methanol). The less-polar solvent changes the polarity of the mobile phase and thus slowly reduces the chemical compounds' affinity for the stationary phase. This causes them to leave the column at different times roughly according to polarity (i.e., more polar compounds will exit the column first).

Sensors at the end of the column detect chemical compounds as they exit. Figure 4-1, part B, shows a chromatogram of different compounds eluting across time. However, going back to our analogy, what if one of the two individuals we're looking for at the marathon finishes the race with a very large group of other runners? In practice, this would be like if we shifted the black peak on top of the red peak and would require us to be able to look for the black or red or both lines together. This situation occurs when two distinct chemicals have the same elution time, and for simple detectors it can make identifying one specific chemical problematic.

Quadrupole Mass Spectrometry

Running with the marathon analogy, let's say Waldo is one of the individuals we're trying to spot as he finishes the race. Waldo has a very distinctive appearance (skinny guy in red-and-white-striped shirt and hat, blue pants), and yet he's difficult to find when there are many other people surrounding him. How can we differentiate him from every other runner? With enough time, we can search the post-race photos for Waldo's smiling face which is akin to using quadrupole mass spectrometry; in chromatography, however, we have only a short time to pick Waldo out from all the racers finishing at the same time.

After chromatographic separation, the mobile phase containing the now-separated chemical compounds is directed to a mass spectrometer. The use of a quadrupole mass spectrometer (MS) in tandem with chromatography is important in the water industry and fairly common because there are many compounds present in a water sample. An MS addition helps identify low concentration compounds. The sample is ionized in the MS, imparting an electric charge. The charged molecules then enter a quadrupole, which selectively allows molecules through. A quadrupole is composed of four parallel rods (Figure 4-2) in a vacuum, which removes air and other interfering molecules that might be present. Electrical current is applied to the rods, producing four electromagnetic fields.

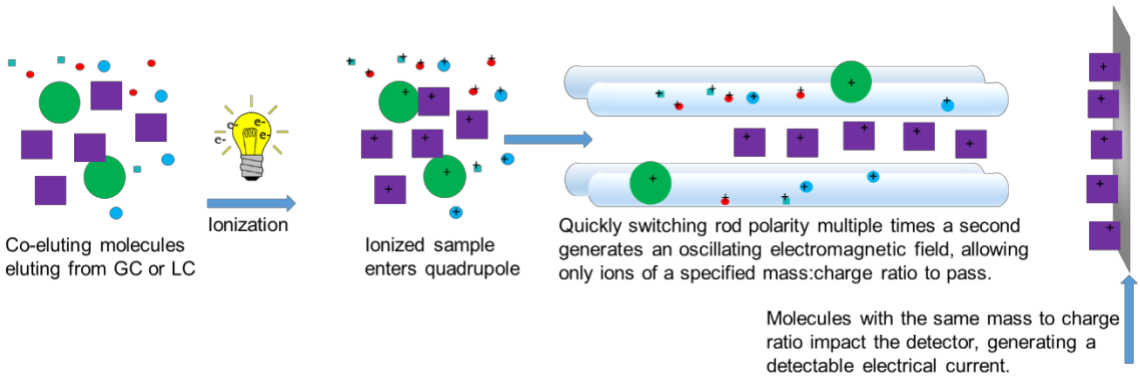

Figure 4-2 Quadrupole mass spectrometry. A sample is ionized before entering the quadrupole. The quadrupole filters by mass, so only the compound of a specified mass (purple squares) pass the quadrupole. Others are removed as neutral gas molecules after impacting the rods (poles).

When the ionized molecule enters the quadrupole, it is repelled by like-charges and attracted by opposite ones. The polarity of the rods is oscillated by reversing the current many times per second and thus an ion is pushed back and forth between the rods as it travels through them. Carefully tuning the oscillating electromagnetic fields ensures that only molecules of a specific mass-to-charge ratio (m/z) will make it the length of the four parallel rods without touching them. Molecules that are heavier or lighter than the target molecule are pushed harder or not hard enough to maintain a central path through the rods, so they impact the rods. Molecules that touch a rod gain or lose electrons from the rods themselves; first they lose their charge, then they are removed by the vacuum pump. Molecules that make it through without deviating from the central path impact the detector at the end of the quadrupole, which produces an electrical signal that is recorded by the computer. Importantly, the detector produces an electrical signal via the exchange of electrons with the ionized molecule for any ion that impacts it, so the mass filtering of the quadrupole is essential for discriminating the

target molecules (that follow the central path) from other molecules (that impact the rods and are removed).

Referring back to the marathon analogy, quadrupole mass spectrometry (GC-MS or LC-MS) is like having Waldo telling us his weight before the race. To find him, we'll weigh all the runners as they cross the finish line. Anyone who doesn't have the same weight as Waldo will be directed to a special waiting area, and any runners with the same weight as Waldo will be pushed across the finish line; this gives us a much better chance of finding Waldo.

Until this point, we've used the analogy of a marathon, which has probable finishing times on the order of hours—but what if we make the timeline much shorter? A typical chromatography analysis, for example, is completed in less than 30 minutes, so it's conceivable that with millions of runners (or molecules), many will have the same weight as Waldo does and will finish at close enough to the same time that it's nearly impossible to find Waldo. We need another filter.

Triple Quadrupole Mass Spectrometry

Unfortunately, the next analogy is not very nice to Waldo. A quadrupole filters chemical species by mass, but there are many molecules with the same mass: for example, water (H_2O = 16 + 1 + 1 = 18 atomic mass unit [amu]) and an ammonium ion (NH_4 = 14 + 1 + 1 + 1 + 1 = 18 amu). Triple quadrupole mass spectrometry takes advantage of three quadrupoles in a row to further separate compounds of interest from other organic compounds in a sample. The first quadrupole filters the species present by mass with an electromagnetic field, as described in the previous section. However, instead of then going into the sensor, the sample then passes into a second quadrupole (called a collision cell) that is filled with an inert gas such as argon or nitrogen. The

analyte molecules (or the parent ions) collide at high speed with the inert gas molecules, causing them to fragment in a predictable pattern specific to the analyte molecule. The fragments (or product ions) then enter a third quadrupole that filters out the fragments except those that are known to have come from the parent molecule of interest (Figure 4-3). If the correct fragment is detected at the right time, it can be known with relative certainty that the molecule is the target molecule, despite the thousands of other molecules in the sample.

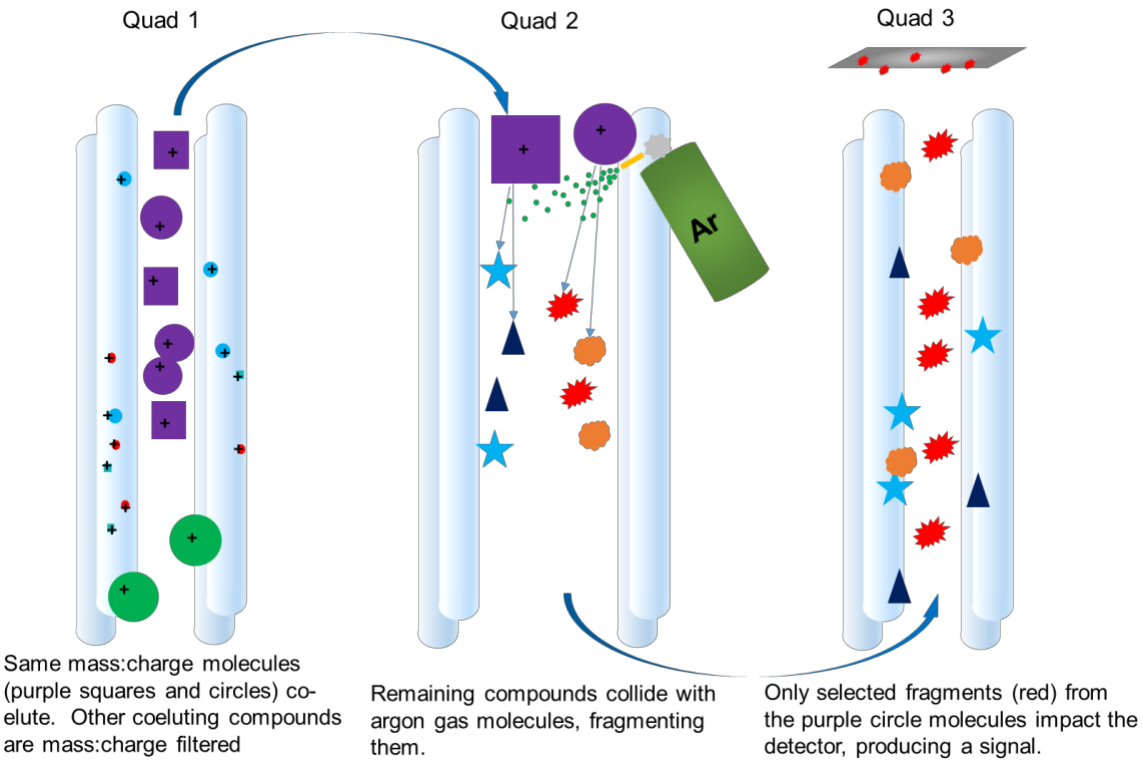

Figure 4-3 Triple quadrupole mass spectrometry. Many compounds may co-elute during chromatography and some may have the same mass (as seen with the purple squares and circles). Thus, the collision cell (quad 2) is filled with an inert gas (argon is shown), which fragments the molecules in a known or predictable way. These fragments enter the third quadrupole which, similarly to the first quadrupole, filters by mass. It only selects for the masses of the daughter or product ions (red) of the desired compound (purple circles), which strike the detector, causing an electric signal which can be used for quantification.

Let's imagine Waldo finishes the race (chromatography) at a similar time as may other runners. He stands on a scale (first quadrupole), which selects him and a few others that finished the race at the same time and have the same weight to begin a bike race. During the bike race, he rides into a pole, which causes his shoes and hat to fly off

(argon gas colliding with the parent ion in the collision cell). Other contestants also ride into poles, but they're wearing different hats and shoes. Race organizers clean up all the hats and shoes (third quadrupole), leaving only the hat and shoes that belong to Waldo. Through these multiple filtering mechanisms—time, mass, and fragment mass—specific molecules can be unequivocally identified and quantified in extremely complex mixtures.

In the analogy so far, if Waldo hadn't told us his weight or mentioned the color and appearance of his shoes, or if we had never met Waldo, or if we didn't even know Waldo was running the race, the mechanisms described thus far for finding him would be useless. This isn't entirely true for quadrupole mass spectrometry, however, as instruments may be operated in "scan mode" where the quadrupoles scan through one mass at a time looking for compounds of that mass. This is a full topic on its own, but in short, these methods result in poor sensitivity (high detection limits) and can't unequivocally identify molecules in the mass range a lab might be interested in.

HRMS

The goal of HRMS is to measure the mass of molecules as accurately as possible (i.e., as closely as possible to their known exact mass, equal to the sum of the exact masses of the elements that make up the molecule). If mass is measured accurately enough, it can be used to obtain the elemental composition of a molecule, and from that, a structure can be proposed and confirmed. Determining the elemental composition of a molecule is the first step in identifying the molecule and has been used recently to identify a slew of human produced chemicals such as pharmaceuticals in wastewater, drinking water, and the environment. This is sometimes called "nontarget" mass spectrometry, where the molecules of interest are not known from the beginning,

and instead the scientists or engineers attempt identify as many molecules in the sample as possible.

To better understand HRMS, we will use something less abstract. If we have US$6 in bills in our wallet, we would have either six $1 bills, or a $5 and a $1 bill. However, if we have $1000 in our wallet, the combination of potential bills is much greater. But there is still a finite number of possibilities of bills in our wallet that can be relatively easily determined (10 $100s, 20 $50s, etc.)

Going back to HRMS, assume the mass of an unknown molecule is measured to be 67.10 amu (it's notable that this is a nominal mass, not an "exact mass," but it is valuable as an example and likely the best measurement that could be achieved from a quadrupole instrument, which is not a high-resolution instrument). Think of this as the total value of all the bills in your wallet. If it is assumed that only carbon, hydrogen, nitrogen, oxygen, and sulfur are present, which is a reasonable assumption for organic molecules, a system of equations can be used to solve for the summed masses of the variables C, H, N, O, and S (simplified to Eq 1) by using their nominal masses of 12.01, 1.01, 14.01, 16.00, and 32.06 amu, respectively (similar to the sum of the $100s, $50s, $20s, $10s, and $1s). Solving for each of these elements is equivalent to figuring out the number of each type of bill that are in your wallet.

$$12.01\ C + 1.01\ H + 14.01\ N + 16.00\ O + 32.06\ S = 67.10\ \text{amu} \quad (1)$$

Since the number of atoms (variables C, H, N, O, and S in Eq 1) must be integers (i.e., no half atoms or half $50 bills), there is only one solution to this equation: four carbons, five hydrogens, one nitrogen, and no oxygen or sulfur (C_4H_5N). From the atomic composition, this compound could be assumed to be pyrrole, although it could also be another compound with the same formula (e.g., allyl cyanide), depending on the

structure. For small enough molecules, the atomic composition can be determined using a nominal mass measurement from an instrument such as a quadrupole mass spectrometer, and without highly accurate measurements of mass, although typically one cannot jump from atomic composition to structure.

For larger molecules, the number of possibilities increases exponentially because there are many ways to substitute elements with the same summed nominal mass, similar to if you have more and more cash in your wallet and only tell me the total, the possibilities of bills that are present becomes exponentially greater. To explain how HRMS instruments resolve this issue, we must first explain that isotopes are forms of the same element with the same number of protons but different numbers of neutrons—meaning, they have different atomic mass but the same chemical properties. On the periodic table of the elements, the atomic masses are averages of the atoms' isotopes, weighted by their environmental abundance. For example, chlorine occurs naturally as the principal isotopes of $_{35}Cl$ and $_{37}Cl$, where 75.8% of chlorine occurs as $_{35}Cl$ and 24.2% as $_{37}Cl$. With masses of 34.9689 and 36.9659 amu, respectively, the abundance-weighted average of the two is 35.45 amu, which is found on the periodic table. For molecules, the summed masses listed on the periodic table (i.e., nominal mass) of the individual elements that make up the molecule can be used with a low-resolution instrument (e.g., quadrupole), but this approach isn't very useful because the number of compounds that can be identified using nominal mass is very small and limited to low-molecular-weight compounds. Most molecules of interest in our field are considered low molecular weight by the general field of chemistry, but, unfortunately, not low enough for quadrupole instruments to be helpful in identifying them.

For a high-resolution instrument, it's important to consider that a compound will exist with a distribution of its natural isotopes. For example, consider C_4H_4NCl, which

has a mass of 101.0032 amu if only the isotopes of highest environmental abundance are present ($_{14}N$, $_{12}C$, $_{1}H$, and $_{35}Cl$). With a high-resolution instrument, we can expect to detect this compound at this mass, assuming no other atoms become attached during ionization in the instrument source (this is a poor assumption but allows for the most simplistic example). Similar to Eq 1, we may solve for the elemental composition given that the number of each element must be an integer, except with incorporation of the more accurate masses of the highest abundance isotopes rather than nominal masses (Eq 2).

$$12.0000\ C + 1.0078\ H + 14.0031\ N + 15.9949\ O + 34.9689\ Cl = 101.0032\ amu \quad (2)$$

As the measurement of mass accuracy increases, it becomes very difficult to substitute one element for multiple other elements and still arrive at the same exact mass, making HRMS a powerful tool for determining the elemental composition of a compound. Although these calculations can be conducted by hand, it becomes quite laborious as the number of potential elements increases, and therefore modern HRMS instrument software includes these calculations.

In nature, some molecules will inevitably contain $_{37}Cl$ rather than $_{35}Cl$, so a signal at 103.0003 amu of 0.31 times the intensity of the 101.0032 amu molecule (i.e., ratio of the natural abundance of the isotope, 0.76/0.24) can also be expected. This becomes important when interpreting mass spectra, where observing one peak and a co-eluting peak with mass 1.9970 amu greater and intensity of approximately 1/3 the larger peak may suggest a chlorinated compound is present. Similar principles apply for other isotopes, which can also be used for molecular fingerprinting and provide some information to the true elemental composition, but for brevity, other isotopic fingerprints are not discussed here. Figure 4-4 shows the expected mass spectrum for chlorinated

pyrrole, incorporating other possible substitutions of N, C, and H isotopes. Again, modern HRMS instrument software incorporates these molecular fingerprinting techniques.

Thus, for high-accuracy instruments (HRMS instruments), measurement of mass can be used to find the elemental composition of a molecule, and from that a structure can be proposed. This informed guess is then typically confirmed using high-purity analytical standards based on chromatographic retention time and isotopic fingerprinting. The following sections describe three types of instruments (time-of-flight, Fourier-transform ion cyclotron resonance mass spectrometry, and Orbitrap) that can take measurements of mass accurately enough to perform calculations similar to Eq 2.

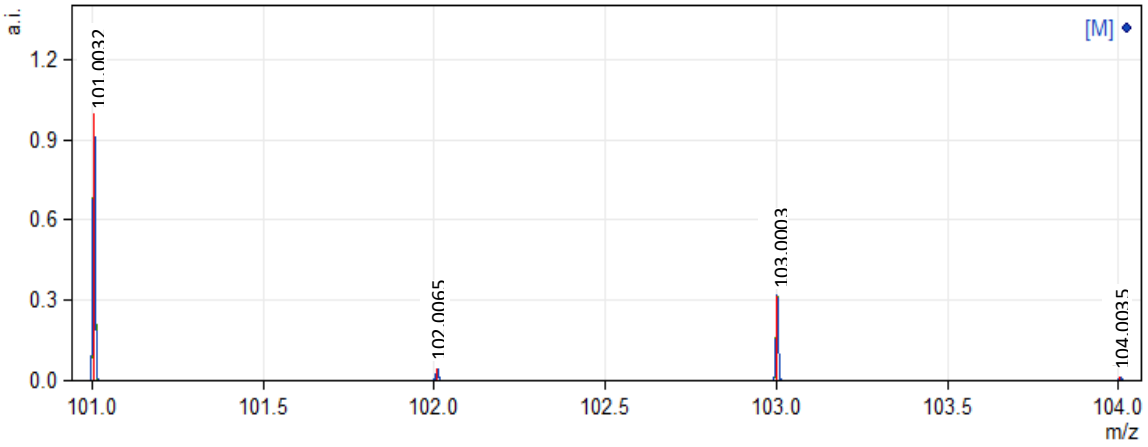

Figure 4-4 Expected mass spectra of C4H4NCl.The first peak, 101.0032 amu, contains the highest abundance isotopes of C, H, N, and Cl. The peak at 103.0003 amu represents the same compound, but with the less abundant $_{37}$Cl isotope. Other peaks represent combinations of various lower natural abundance isotopic combinations of $_{13}$C, $_{2}$H, $_{15}$N. a.i. = arbitrary units, m/z = mass to charge ratio. Figure generated with nMass v5.5.0 (Strohalm et al. 2010).

Time-of-Flight

Time-of-flight (TOF) instruments are similar to their quadrupole counterparts in that they operate under high vacuum to remove interfering molecules and that an indiscriminate electrical signal is produced by any ion that impacts the detector. The source, or the part of the instrument that turns molecules into ions, is also similar, as is the chromatograph, either liquid or gas. Different, however, is that while quadrupole instruments function on the principle of using electromagnetic fields to remove ions that are of no interest, TOF instruments send all ions to the detector. Ions are pushed up a flight tube by an intermittent electromagnetic pulse (on, off, on, off) at a rate of thousands of times per second. Ions enter the vacuum space above the "pusher," and upon activation of the pusher (i.e., generation of an electrical field), are repelled up the flight tube. Larger (heavier, or greater mass) ions travel more slowly and thus impact the detector later than lighter ions. TOF instruments measure the time from pusher activation to ion impact extremely accurately, and then translate, through a calibrant of known mass, flight duration into mass.

Because multiple ions of varying mass are pushed up the flight tube, multiple impacts are recorded with various flight durations, which are then translated into mass. In other words, no ions are intentionally filtered out, and the mass spectra of all ions entering the mass spectrometer are captured with high sensitivity. This comes with the additional benefit that flight duration is simple to measure very accurately, and thus measurement of mass is very accurate (good approximation of the fourth decimal place for compounds in the 50–1,000 amu range). A diagram of a TOF mass spectrometer flight tube is shown in Figure 4-5.

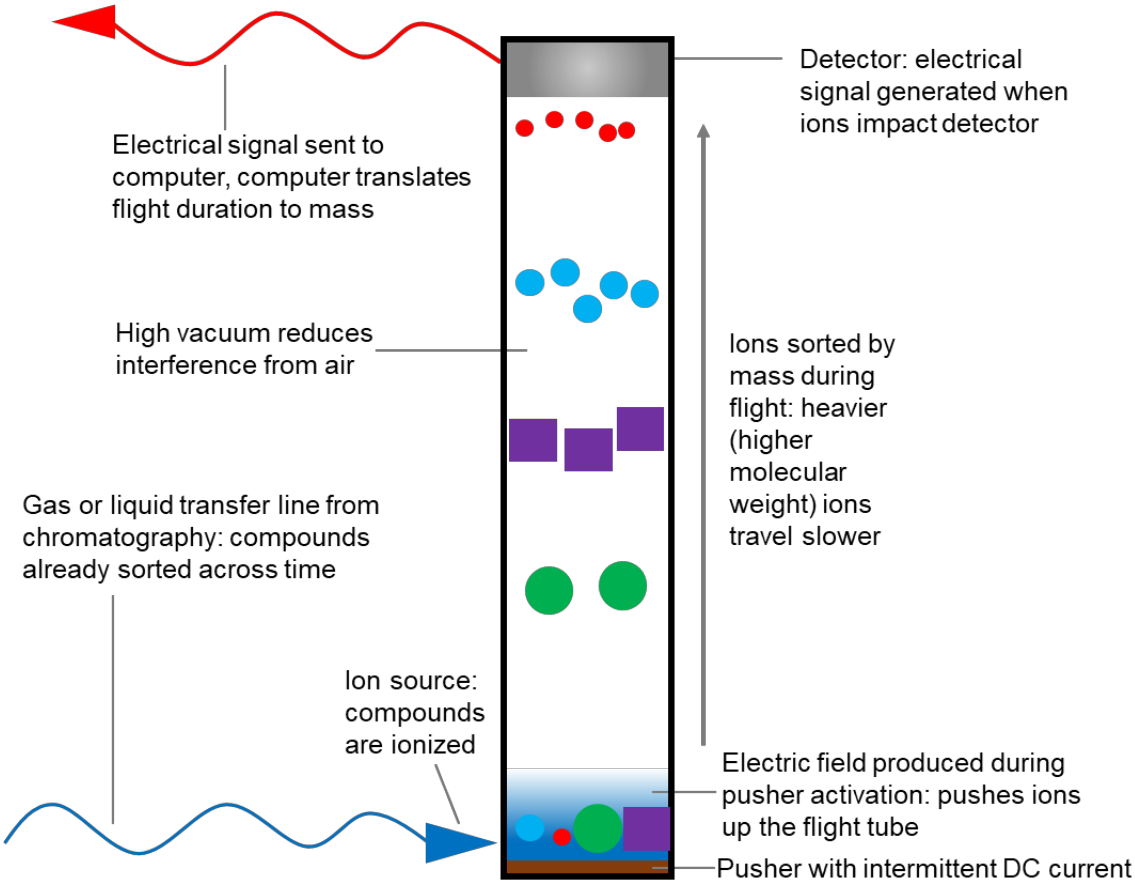

Figure 4-5 Diagram of TOF flight tube. Most instruments contain an ion reflector at the top of the tube and move the detector to the bottom of the tube, which causes the ions to fly in a parabolic arc similar to a pop fly in baseball and effectively doubles the flight tube length and flight duration, further separating ions by mass and increasing mass accuracy.

In very simple samples with few molecular solutes present, it may be possible to completely skip chromatography and directly inject the sample into the TOF mass spectrometer. All ions are detected and so all compounds are likely to be shown in the mass spectrum, given that they ionize well (i.e., if Waldo tells us his weight accurately enough, there's no need to have anyone run the race, we can simply make everyone stand on very accurate scales). Of course, if the sample contains two compounds with

the same elemental composition (e.g., pyrrole and allyl cyanide are both C_4H_5N), this method isn't appropriate and requires other fingerprinting techniques or chromatography to deconvolute the separate molecules.

With the accurate masses of many compounds, structures may be proposed and again confirmed using analytical standards. Some TOF instruments also incorporate a quadrupole in front of the flight tube to intentionally fragment an unidentified compound, and the fragments can be used to confirm the structure of the proposed compound or verified against an external analytical standard.

TOF instruments are popular because they are relatively inexpensive compared to other high-resolution instruments; a LC/qTOF mass spectrometer that can identify environmental unknowns generally costs around $350,000. However, there are limitations; for example, if we want to know how much of a specific molecule is present but are not interested in other dissolved compounds, TOF instruments are less sensitive for targeted quantification than quadrupole instruments because the intermittent electromagnetic pusher field results in some ions being lost during the flight of other ions. Also, like many mass spectrometers, TOF instruments are quite large and cumbersome, with flight tubes extending approximately 1 m above the instrument itself. This requires adequate bench space and ceiling clearance, in addition to gas requirements and vacuum pump exhaust.

Fourier Transform Ion Cyclotron Resonance Mass Spectrometry

Another limitation of TOF-based mass spectrometry for identification of unknowns is that mass resolutions are typically on the order of 25,000–50,000, which may not be high enough to unambiguously assign a molecular formula to a peak (particularly for higher-mass compounds) or to resolve two very closely spaced peaks.

For instance, two peaks at *m*/*z* of 1,000.01 and 1,000.02 would require mass resolution of 100,000 to discern the two. After initial rapid gains in mass resolution by TOF instrument technology (e.g., extending TOF path length by adding reflectors to the top of the flight tube to increase effective length), improvements to mass resolution have been incremental.

To dramatically increase mass resolution, an entirely different approach is used for mass separation: ions are electromagnetically trapped in a circular chamber under a high magnetic field (typically >5 tesla) in an instrument called a Fourier-transform ion cyclotron resonance (FT-ICR) mass spectrometer. In this situation, ions orbit in an electromagnetic field at a frequency proportional to the field strength and inversely proportional to their mass (Eq 3).

$$f = (qB)/(2\pi m) \qquad (3)$$

where *q* is the charge of the ion (typically 1 elementary charge = 1.6×10^{-19} C), *B* is the magnetic field strength in tesla (*T* = *kg*/C × s), and *m* is the ion mass (kg).

The movement of the orbiting ion produces a small electromagnetic field, which is measured at a location in the orbit such that each pass of the ion is detected as oscillating electrical current. This oscillating electrical signal is then mathematically transformed via a Fourier transform into a series of peaks corresponding to different orbital frequencies, which each corresponds to a unique mass. Calibration with mass standards allows an assignment of the mass corresponding to each orbital frequency (Figure 4-6).

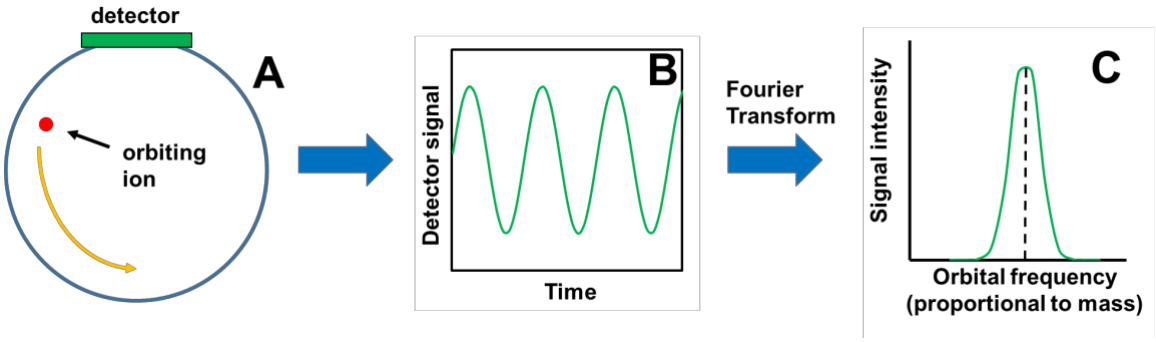

Figure 4-6 (A) Schematic of an ion orbiting in an FT-ICR instrument, (B) Output signal from FT-ICR instrument, (C) Fourier transformed output signal with peak corresponding to a unique mass.

Because the frequency of ion orbit can be measured very accurately, FT-ICR instruments can achieve extremely high mass resolution (>1,000,000 or the fifth and even approximations of the sixth decimal place in compounds with mass between 50 and 1,000 amu), allowing unambiguous determinations of atomic composition for each peak and avoiding peak overlap issues common with TOF-based instruments. However, unlike TOF instruments, FT-ICR instruments are prohibitively expensive to own and operate for single investigator labs or even most universities, so they're typically housed at national laboratories or specialized research institutes (e.g., the National High Magnetic Field Laboratory in Tallahassee, Fla.).

Orbitrap

As a compromise between the accessibility of TOF instruments and the mass resolution of FT-ICR instruments, Orbitrap instruments have recently become popular. Orbitrap instruments are miniaturized FT-ICR mass spectrometers that fit on a benchtop and can be obtained for between $500,000 and $1,000,000, opening up accessibility for academic departments or even certain individual investigators. The first Orbitrap

instrument, the LTQ Orbitrap, was introduced by Thermo Scientific in 2005, and successive models have refined the technology. Typical commercial Orbitraps can achieve mass resolutions of 240,000 (approximately the fifth decimal place for environmental applications), which is usually high enough to resolve all mass peaks for small molecules, and usually feature a quadrupole in front of the Orbitrap detector to allow intentional fragmentation.

However, there are tradeoffs for high mass resolution, and the Orbitrap has not completely dominated the high-resolution mass spectrometer market. Most obviously, because Thermo Scientific holds the exclusive patent on parts of the Orbitrap technology, the prices remain significantly higher than for TOF instruments, which are produced by several vendors. Technologically, the Orbitrap is not without disadvantages either. The highest mass resolutions are only achievable with relatively long scan times, extending the run time per sample, so Orbitraps are typically operated at lower than maximum resolution (e.g., 70,000—only slightly better than a typical TOF instrument) to increase throughput. Resolution may then be adjusted in a second injection of the sample if peaks overlapped in the first trial. Additionally, all ion trap instruments can suffer from the space charge effect, in which the trap becomes too full and the ions begin to repel one another (as a result of having the same polarity charge), resulting in reduced mass accuracy. For these reasons, TOF instruments remain popular despite their lower resolution.

Hopefully by now, the notion of television sci-fi chemical analysis has met reality, and Waldo is seeking treatment for his bicycle accident. Though this article is simply an introduction for people interested in learning more about how mass spectrometry works, it should help individuals working in the water industry understand the complexity involved in chemical analysis and what is involved to determine a low concentration

pollutant's presence and structure in a water sample. It should help water professionals understand what's going on "under the hood" in their own analytical instruments, allowing them to better problem solve instrumentation issues and the full capabilities of the tools in their labs. Finally, understanding these analytical techniques should help water professionals better evaluate the work of others and think more critically about water research.

Chapter 5 Summation of Disinfection By-Product CHO Cell Relative Toxicity Indices: Sampling Bias, Uncertainty, and a Path Forward

Relevance to Thesis

This following publication critically examines a popular method of DBP analysis, summation of predicted geno- and cytotoxicity, which fits my Thesis Objective 3: criticism of a common data interpretation method. The objective of this manuscript was to bring attention to an analytical method that has been frequently used in the industry. Many publications used predicted toxicities to describe and compare water samples across different treatments. We show through manipulating published datasets that this method biases results and caution water professionals to use this tool carefully. My contributions to the manuscript include leading the manuscript as first author, conducting the research and analyzing the data, producing Figures 5-1 to 5-4, all SI figures and tables (found in Appendix C), and drafting of the manuscript with help from coauthors. The section on Statistical Methods in Summed Calculations was primarily written by Dr. Kyle Thompson. A citation to the publication is included below, and the manuscript follows. (McKenna et al. 2020b)

Citation:

McKenna, E., Thompson, K.A., Taylor-Edmonds, L., McCurry, D.L., and Hanigan, D. 2020b. Summation of disinfection by-product CHO cell relative toxicity indices: sampling bias, uncertainty, and a path forward. Environmental Science: Processes and Impacts 22, 708-718.

Abstract

The cyto- and genotoxic potencies of disinfection by-products (DBPs) have been evaluated in published literature by measuring the response of exposed Chinese hamster ovary cells. In recent publications, DBP concentrations divided by their individual toxicity indices are summed to predict the relative toxicity of a water sample. We hypothesized that the omission or inclusion of certain DBPs over others is equivalent to statistical sampling bias and may result in biased conclusions. To test this hypothesis, we removed or added actual or simulated DBP measurements to that of published studies which evaluated granular activated carbon as a treatment to reduce the relative toxicity of the effluent. In several examples, it was possible to overturn the conclusions (i.e., activated carbon is detrimental or beneficial in reducing toxicity) by preferentially including specific DBPs. In one example, removing measured haloacetaldehydes caused the predicted cytotoxicity of a treated sample to decrease by up to 47%, reversing the initial conclusion that activated carbon increased the toxicity of the water. We also discuss measurements of statistical error, which are rarely included in publications related to predicted toxicity, but strongly influence the outcomes. Finally, we discuss future research needs in the light of these and other concerns.

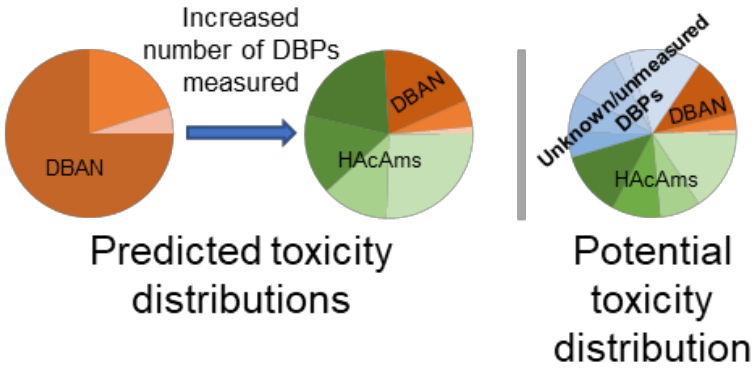

Introduction

Disinfection by-products (DBPs) form from reactions of inorganic or organic matter with disinfectants during water treatment. The most abundant species by molar mass in drinking water are trihalomethanes (THMs) and haloacetic acids (HAAs), which are currently regulated by the United States Environmental Protection Agency (EPA) (USEPA 2006). THMs and HAAs are formed to a greater extent by free chlorine than chloramines (Norman et al. 1980). Therefore, many treatment plants have switched from free chlorine to chloramination to reduce the formation of THMs and HAAs (Li 2011, Seidel et al. 2005). While lower concentrations of the regulated THMs and HAAs form during chloramination than chlorination, certain other DBPs form to a greater extent (Guay et al. 2005, Norman et al. 1980). Therefore, there are tradeoffs in DBP formation from use of different disinfectants and researchers have focused recent efforts on determining which DBPs are the most important to mitigate formation of to limit the risk to human health (Li and Mitch 2018, Stalter et al. 2016).

Some DBPs elicit cyto- and genotoxic responses and the "potency" (i.e., the LC_{50}, or concentration required to achieve an effect in 50% of the cells) of roughly 100 individual DBPs has been assessed by multiple *in vitro* and *in vivo* assays (Hanigan et al. 2017, Laingam et al. 2012, Lan et al. 2018, Li et al. 2015, Pals et al. 2017, Parvez et al. 2017, Plewa et al. 2002, Plewa et al. 2017, Wagner and Plewa 2017). The most comprehensive data set uses Chinese hamster ovary (CHO) cells and the published potencies serve as a unique and valuable dataset for comparing the potency of DBPs and of classes of DBPs (Wagner and Plewa 2017). The published potencies have also been used to calculate "predicted toxicity" (i.e., the measured concentration of an individual DBP is divided by the published potency to calculate the relative toxicological contribution of each DBP, which are then summed). Predicted toxicity is part of an ever-

evolving approach to understanding the human health impact of DBPs and has been used in studies to evaluate treatment process efficacy (Chuang et al. 2019b). This approach is particularly attractive for labs without biological assay capabilities.

It was recently postulated that granular activated carbon (GAC) treatment may increase the toxicity of disinfected water, despite an overall removal of organic matter, based on the observation that GAC does not remove bromide, which may result in higher concentrations of brominated DBPs (Krasner et al. 2016b). Brominated DBPs are generally more potent than their chlorinated analogues based on results from the CHO comet assay (Richardson et al. 2007). As hypothesized, in rapid small-scale column tests, predicted toxicity increased due to an increase in brominated DBP formation, in particular, dibromoacetonitrile (DBAN). However, genotoxicity was also directly assayed with the SOS Chromotest and unlike predicted toxicity, the measured genotoxicity was consistently reduced with GAC treatment and tracked well with removal of bulk organic carbon. Of the 30 DBPs measured prior to and following GAC treatment, dibromoacetonitrile (DBAN) accounted for ~53% of the predicted toxicity and it was suggested that further GAC studies focus on HANs, particularly brominated HANs. The conclusion that HANs are the drivers of risk for disinfected water samples has only emerged in the past few years, but has been pervasive among predicted toxicity publications (Chuang and Mitch 2017, Chuang et al. 2019b, Furst et al. 2019, Krasner et al. 2016b, Kristiana et al. 2017, Le Roux et al. 2017, Li et al. 2019, Liu et al. 2018, Liu et al. 2017, Stanford et al. 2019b, Vatankhah et al. 2019, Wagner and Plewa 2017, Zeng et al. 2016, Zhang et al. 2017).

Previously published studies focusing on predicted toxicity typically measured 30 to 40 DBPs, but a more recent study measured 70 (Cuthbertson et al. 2019, Stanford et al. 2019b). The team found that the overall mass of 70 DBPs decreased across GAC,

but the number of brominated DBPs, including DBAN, increased. Because brominated DBPs are generally more potent than chlorinated DBPs as measured by the comet assay (Richardson et al. 2007), it was expected that the predicted toxicity would also increase, following other published studies, despite the overall reduced mass concentration of DBPs. Instead, the investigators found that the predicted toxicity decreased. The authors did not definitively reconcile the opposing conclusions of this research and other published literature, but we attribute the discrepancy to differences in number and speciation of measured DBPs.

Both the published literature and the more recent research discussed above conclude that DBAN precursors are poorly removed by GAC, thus DBAN contributed similar amounts of predicted toxicity before and after GAC (Chuang et al. 2019b, Krasner et al. 2016b, Kristiana et al. 2017, Stanford et al. 2019b). However, by measuring a greater number of DBPs compared with prior studies and including precursors that are well removed by GAC, specifically dibromoacetamide and bromochloroacetamide, the more recent study effectively diluted the weight of DBAN in the predicted toxicity calculation. This highlights how published literature may have unintentionally biased the toxicity calculations by including a comparatively potent DBP that preferentially forms in conditions that GAC selects for, while neglecting to measure DBPs that are effectively mitigated by GAC. Although inclusion of other DBPs reduced this bias, it is possible that other toxic DBPs which were not measured or remain unidentified could have altered the conclusion. Thus, we find the competing conclusions in the literature to be an excellent example of how predicted toxicity can be difficult to interpret.

We and others have suggested that the overall variability in conclusions across studies and assays is caused by the inherent uncertainty associated with this method of

risk attribution. First, DBPs that are not measured or have not yet been discovered or assayed for toxicity might substantially contribute to the predicted toxicity, even at low concentrations, given that DBPs have toxic potencies that span greater than six orders of magnitude (i.e., sampling error or sampling bias) (Wagner and Plewa 2017). Second, a typical suite of DBPs measured in advanced analytical publications (~30-70 DBPs) are representative of only about 30% of the overall DBPs as measured by adsorbable organic halides (AOX) (Li and Mitch 2018, Richardson and Postigo 2012), which still does not account for DBPs that do not contain halogen atoms. Finally, published potencies are derived from individual DBP exposures, which ignore agonistic or antagonistic effects of mixtures (Peng et al. 2019). Although these limitations are well known among experts in the field and discussed conceptually throughout perspective and review publications (Li and Mitch 2018, Plewa et al. 2017), they are infrequently discussed in publications in which predicted toxicity is applied, potentially because they are only reviewed broadly, and there is no published demonstration of their potential impacts.

Although the impact of agonistic and antagonistic effects may be extremely important, for brevity, we limited the objective of this manuscript to demonstrating the impact of the number of DBPs measured and the statistical uncertainty on the reported toxicity. First, we removed groups of DBPs from published datasets to determine if the conclusions regarding the efficacy of GAC changed dependent on the number of DBPs measured. The removal of groups of DBPs was not focused on a specific subset of DBPs; we evaluated the theoretical removal of all groups of DBPs individually. Next, we aggregated published haloacetamide (HAcAm) data and inserted the aggregates into datasets from publications that assessed GAC treatment but did not measure HAcAms (i.e., we simulated the measurement of additional DBPs) and compared the conclusions

from the publications to hypothetical datasets. We chose to supplement the datasets with HAcAms because they are relatively potent, measured frequently enough for there to be data available, and because HAcAms can be formed by hydrolysis of HANs (Yu and Reckhow 2015). Finally, we discuss measurements of summative error, which are absent in many publications, and comment on the potential impacts of discounting rigorous statistical analysis. Because many DBPs are not genotoxic, published predicted toxicity literature tends to focus on predicted cytotoxicity rather than genotoxicity. We also focus on cytotoxicity because of the greater dataset available but discuss genotoxicity where possible.

Methods

CHO cell DBP potencies were obtained from two publications (Plewa et al. 2002, Wagner and Plewa 2017) and a personal correspondence (Plewa 2019). The predicted toxicity was calculated by dividing measured concentrations of DBPs by their respective geno- or cytotoxic potency (LC_{50} [cytotoxicity], or 50% tail DNA or midpoint of DNA tail moment [genotoxicity]), resulting in a unitless toxicity (See Table C-1 for toxic potencies). DBP concentrations from pre- and post-GAC treatment were from multiple publications (See Table C-2 for background on treatments) (Krasner et al. 2016b, McKie et al. 2015, Stanford et al. 2019b). HAcAm concentrations were derived from two publications that measured HAcAms before and after GAC treatment at a total of 18 drinking water treatment plants (Table C-1, pre-GAC concentrations in Table C-3) (Kosaka et al. 2016a, Stanford et al. 2019b). The GAC influent water samples were either not oxidized, or pre-oxidized with varying oxidation techniques (chlorine, chloramine, ozone, $NaMnO_4$, $KMnO_4$, see Table C-2), representing a broad array of pre-oxidation conditions. HAcAms measured in the GAC effluent samples in both the data

that was aggregated from and supplemented to were primarily chlorinated, except two samples, which were chloraminated (WTP D and WTP E in Fig. 5-1 and 5-2) (Stanford et al. 2019a).

Table 5-1 Post-GAC HAcAm concentrations derived from two publications. Data from Kosaka *et al*. (2016a) is the average from 6 treatment plants and Stanford *et al*. (2019b) from 12 treatment plants.

	Mean concentration from Kosaka *et al.* (2016a) (nM)	Mean from Stanford *et al.* (2019b) (nM)	Mean of both datasets (nM)
DCAM	1.69 ± 0.54	22.47 ± 30	12.08 ± 10.3
DBAM	2.61 ± 1.7	7.84 ± 3.3	5.23 ± 2.6
BCAM	2.13 ± 0.55	8.34 ± 5.2	5.23 ± 3.1
TCAM	0.62	3.08 ± 0.9	1.85 ± 1.2
CAM	1.43 ± 0.50	Not Measured	1.43 ± 0.50
BAM	1.57 ± 1.06	Not Measured	1.57 ± 1.06

In cases where a HAcAm was not detected, a concentration equal to half the provided MDL was assumed. DCAM, DBAM, BCAM, and TCAM were measured post-GAC by Stanford *et al.* (2019b), and therefore the toxic potencies provided here are averages of the initial data set combined with that from Kosaka *et al.* (2016a). In the study by McKie *et al*.(2015) DBAN was not measured, thus, in addition to supplementing the HAcAm data from Kosaka *et al*. (2016a), the average of sixteen samples after GAC treatment from Krasner *et al*. (2016b) and Stanford *et al.* (2019b) were included (5.12 ± 3.39 nM DBAN, Table C-4). DCAM is not genotoxic and thus was not included in genotoxicity. We are unaware of additional sources of HAcAm occurrence data in drinking water facilities with GAC treatment.

Results and Discussion

Simulating the Omission of Specific DBP Subsets in Published Data

We removed groups of DBPs from published data sets to demonstrate that omission of specific analytes can alter the conclusion of the analysis. We discuss in detail only one example here, but additional data aggregated from publications are provided in the SI, and similar conclusions follow (Figure C-1: Panels 2 and 4, and Figure C-2: Panels 1 and 2.3). In Figure 5-1, we show the contribution of individual DBPs to predicted toxicity from the initial data set. In Panel 4, we show that predicted cytotoxicity decreased 20% across GAC (22,000 bed volumes [BV]) when HAcAms were included in the initial measurements. However, removal of HAcAms (pink compounds) from the data (i.e., simulating measurement of fewer compounds) results instead in a 6% increase in predicted cytotoxicity after GAC treatment. Similarly, in Panel 3, GAC treatment reduced the predicted cytotoxicity by 13% to 4%. However, had HALs (purple compounds) been omitted from the analysis, the initial untreated sample would have been predicted to be 5% to 14% more cytotoxic than the GAC treated samples, at the two BV sampled (shown with HALs as the top bars in Figure C-3A for clarity). Finally, in Panel 6, GAC treatment increased the predicted cytotoxicity by 15% to 19%, mostly due to increased formation of chloroacetaldehyde. Omission of HALs, including chloroacetaldehyde, caused the predicted toxicity to decrease across GAC by 47% to 28% (also shown in Figure C-3B with CAL as the top stacked back for clarity).

Removal of other DBPs in these three panels or in Panels 1, 2, 5, and 7 resulted in changes to the magnitude of the predicted toxicity change, but generally no change to the initial conclusion, that GAC reduced the toxicity profile of the samples. Thus, omission of specific classes of DBPs does not always change the interpretation of the data and the magnitude of the changes presented here are a relatively small percent

contribution to the toxicity profile of the samples. Given that observed reductions or increases in predicted toxicity across the GAC are relatively small in most cases, we caution that without rigorous statistical analysis, conclusions as to the benefit or cost of a treatment process are not appropriate. Additionally, in some cases, the conclusion that a technology results in better or worse water quality is dependent on which DPBs were measured, which is troublesome considering the investment required to implement such technology in water treatment systems.

The contribution from THMs' predicted toxicity are relatively small compared to those of other DBPs. Total THMs contributed 0.2% to 2.4% of predicted cytotoxicity to each water sample without the addition of our simulated HAcAms (Figure 5-1). THMs do not elicit a genotoxic response, and therefore did not impact predicted genotoxicity. HAAs contributed 0.2% to 23% of predicted cytotoxicity, which was generally less than other classes of measured DBPs. HAAs dominated genotoxicity in some samples, but not in others (Figure C-4). The US EPA currently regulates THMs and HAAs, but these species did not contribute appreciably to predicted toxicity in the cases here or in other publications (Chuang and Mitch 2017, Chuang et al. 2019a). We believe this is an especially useful application of predicted toxicity; to compare the relative importance of individual compounds or classes of DBPs in a single sample, but not between samples or treatment groups. Finally, to interpret such data as an indication that a certain class of DBPs should be subject to regulation instead of or in addition to THMs and HAAs is likely an overextension of the data (i.e., THMs are probably not important in the given data, but it is not known whether DBAN is important, only that it is more important than THMs, [see *Importance of DBAN*]).

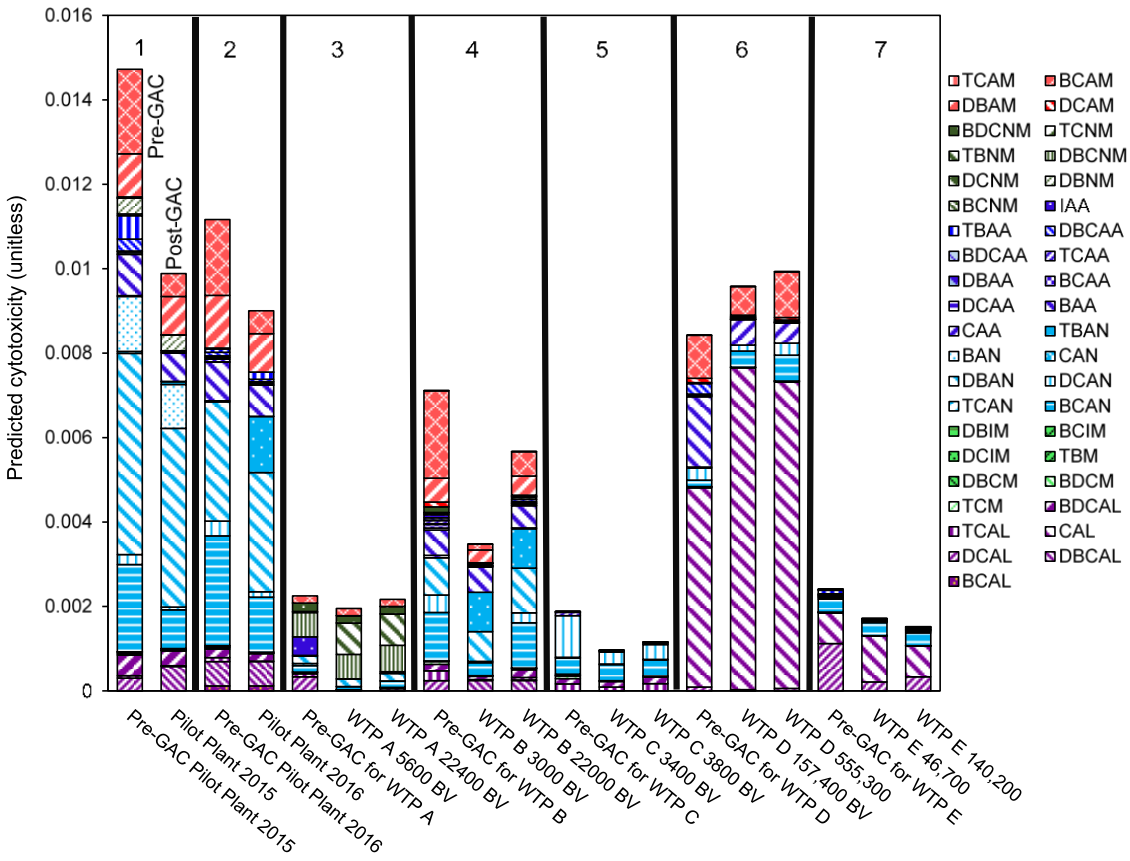

Figure 5-1 Components of predicted cytotoxicity for data from Stanford et al. (2019b) and Cuthbertson et al. (2019) Pink colored compounds are HAcAms. Left-most bar in each panel is pre-GAC predicted cytotoxicity, other bars are GAC effluent samples. Only 41 DBPs are shown, rather than the 70 that were measured, because 29 DBPs were not detected. Compound abbreviations are provided in Table C-1 and raw data provided in Table C-5. Panels 3, 4, and 6 are instances where omission or inclusion of specific DBPs or groups of DBPs may cause an inversion of the conclusion that GAC treatment was beneficial or detrimental.

Incorporation of Unmeasured DBPs

We initially supplemented aggregated HAcAm data from 18 WTPs (Table 5-1) into the same pre- and post-GAC example dataset because the number of DBPs measured is relatively comprehensive. HAcAms were measured in some of the treatment plants and we supplemented the data for other plants or added specific HAcAm compounds to those that did not measure all six HAcAms. The supplemented HAcAm data contributed an average of 51% ± 31% of the predicted toxicity for pre-GAC data and an average of 38% ± 23% for post-GAC data (Figure 5-2). Predicted cytotoxicity decreased across GAC for five of the seven cases, and the addition of HAcAm data (red bars) did not change this conclusion. However, in Panel 4, the initial dataset without HAcAms indicates that the predicted toxicity of the GAC effluent initially decreased across GAC (3,000 BV), but then increased to greater than the pre-GAC sample (22,000 BV), suggesting that GAC caused the total predicted toxicity of the treated sample to be greater than the untreated sample. Much of this can be attributed to the increase in tribromoacetonitrile (TBAN) formation. However, with the simulated measurement of HAcAms (i.e., addition of aggregated data), the predicted toxicity of the GAC treated samples tends to increase with increasing GAC use, but does not exceed the predicted toxicity of the pre-GAC sample, suggesting that GAC decreased the predicted toxicity of the water relative to the untreated sample. This is attributable to a decreased weighting of TBAN due to a greater number of compounds measured.

In Panel 2, predicted toxicity decreased relative to the untreated sample despite a large increase in TBAN and independent of the addition of HAcAms. However, had an additional sample been taken at a later point in time, predicted toxicity may have increased because of the large increase in TBAN across GAC and decreasing DBP precursor removal across GAC over time. Amending aggregated HAcAm data would

reduce the impact of TBAN and potentially result in decreased predicted toxicity. In Panel 6, predicted cytotoxicity increased independent of the inclusion of HAcAms, but does so to a lesser extent when HAcAms are amended. Again, the relative changes observed here are small and only in select instances, but the impacts on decision making are substantial if the results are assumed to be statistically significant.

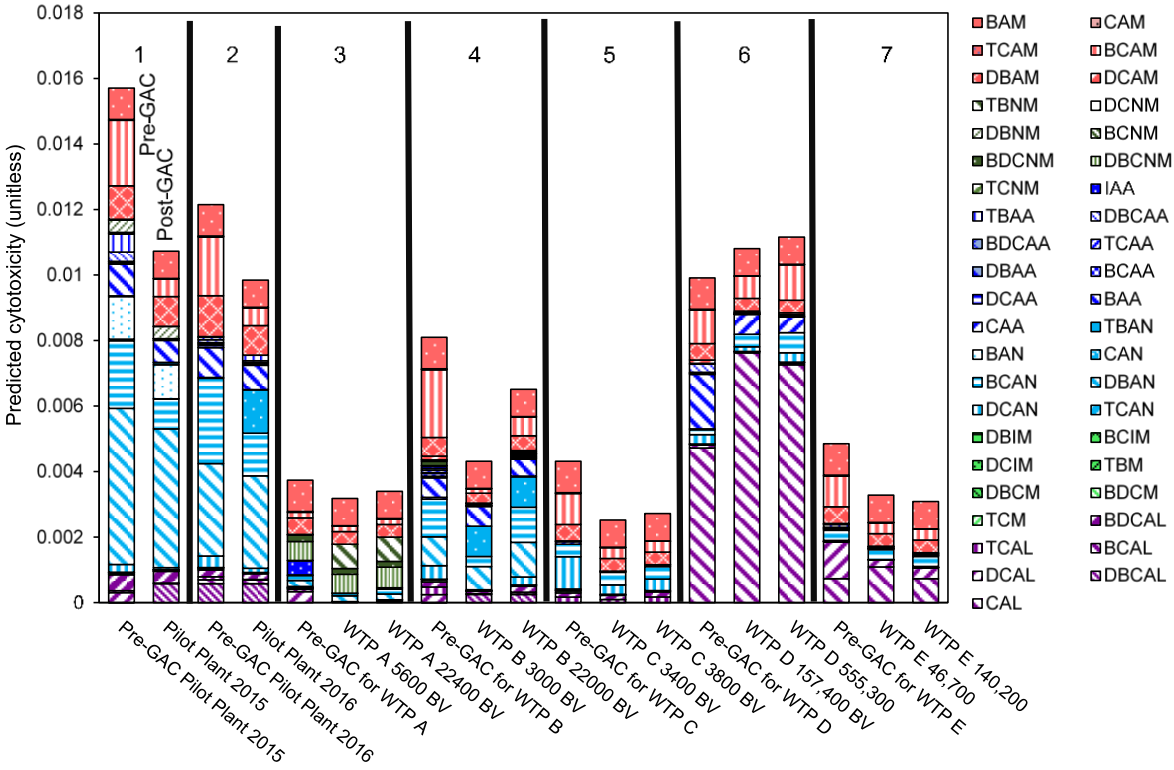

Figure 5-2 Components of predicted cytotoxicity for data from Stanford et al. (2019b) and Cuthbertson et al. (2019) Pink colored compounds are either measured HAcAms from the study or supplemented HAcAms derived from the mean concentrations at 18 WTPs (Table 5-1) (2016a, 2019b). Left-most bar in each panel is pre-GAC predicted cytotoxicity, other bars are GAC effluent samples. Only 41 DBPs are shown, rather than the 70 that were measured, because 29 DBPs were not detected. Compound abbreviations are provided in Table C-1 and raw data provided in Table C-5. All panels are

supplemented with CAM and BAM data from Table 5-1. Additionally, panels 1 and 2 are supplemented with TCAM data, panel 3 is supplemented with DBAM and TCAM data, panel 5 is supplemented with DBAM and BCAM data, panel 6 is supplemented with DBAM data, and panel 7 is supplemented with DBAM, BCAM, and TCAM data. Panels 2 and 4 are instances where inclusion of supplemented HAcAms may have significantly impacted conclusions. Conclusions from other panels are impacted to a lesser extent.

In another published dataset in which a relatively small number of DBPs was measured (N=15), predicted genotoxicity increased slightly across biologically active GAC (e.g., biofiltration) partially due to increased CAA formation (Figure 5-3 Panels 4 through 8). However, including simulated HAcAm data caused predicted toxicity to decrease by 52% to 75% across the biofilters. The publication also measured absorbable organic halogens (AOX) and SOS genotoxicity via the SOS Chromotest and found strong correlations between SOS genotoxic response and AOX, THMs, and HAAs, and particularly strong correlation between THMs and SOS genotoxic response after biofiltration (R_2 = 0.97). It is well recognized that THMs and HAAs are not likely to be the primary toxicological drivers based on their potency and occurrence (see *Simulating the Omission of Specific DBP Subsets in Published Data*) but they may be well correlated for specific assays. One additional published data set is provided in Appendix C and simulated addition of HAcAms follows the conclusions here but is not discussed in depth for brevity (Figure C-5: Panels 1 and 2.3).

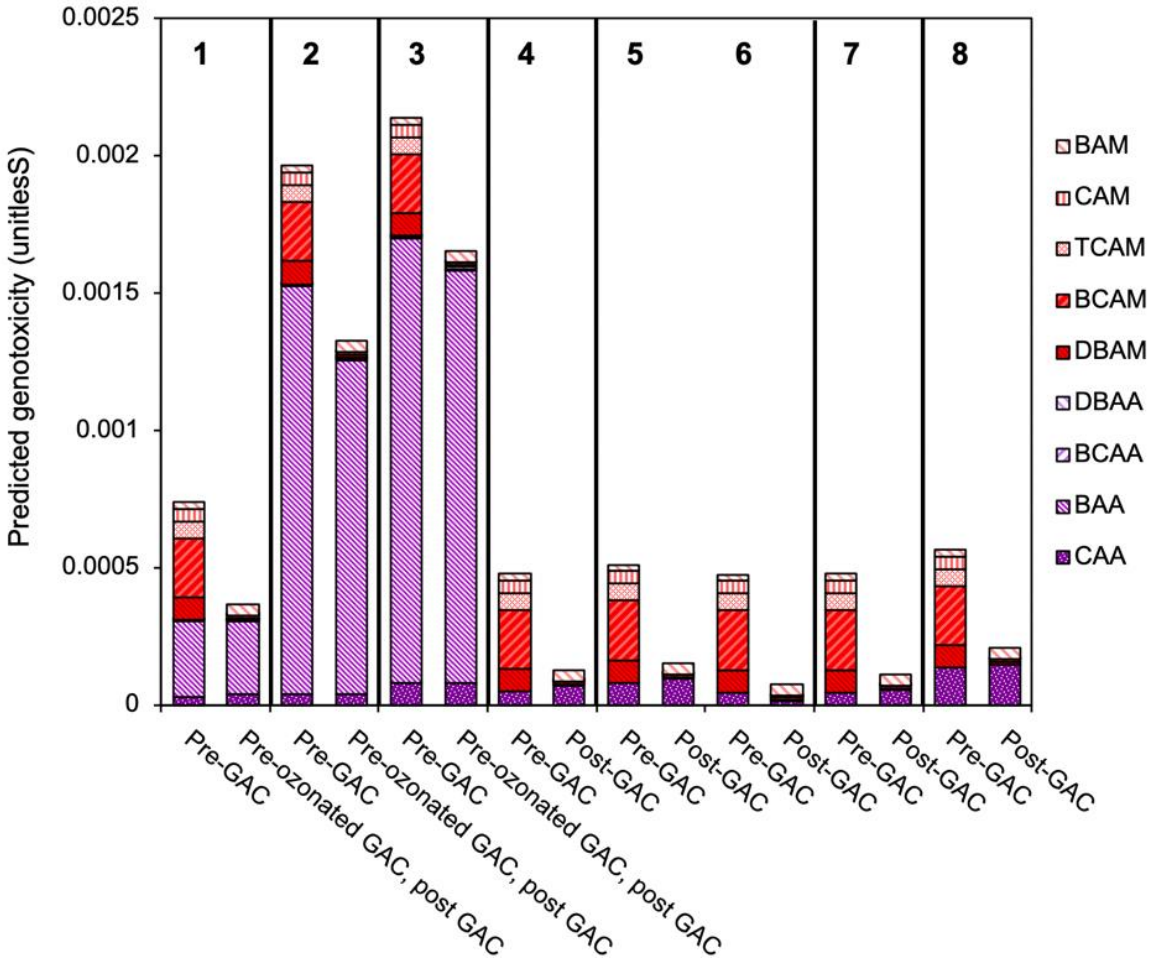

Figure 5-3 DBP components of predicted genotoxicity from McKie et al. (2015) Red colored compounds are supplemented HAcAms (see Table C-3). Left-most bar in each panel is pre-GAC, other bars are post-GAC. Panels 1-3 represent samples from Lake Ontario taken in three different months. Panels 4-8 are samples from the Otonabee River taken from five separate sampling events. Only 9 DBPs are shown, rather than the 15 that were measured, because 6 DBPs were not detected or do not have published genotoxic indices. Compound abbreviations are provided in Table C-1 and raw data provided in Table C-6. Panels 4 through 8 are strongly influenced by the inclusion of haloacetamides while panels 1 through 3 are driven by BAA.

Importance of DBAN

Because of its extraordinarily high toxicity index, detecting DBAN with a detection limit between 0.2 µg/L (Liu et al. 2018) and 1 µg/L (Krasner et al. 2016b) results in a contribution of 3.5×10^{-4} to 1.8×10^{-3} to predicted cytotoxicity, the same order of magnitude as the total predicted toxicity for most drinking water samples. Because of this, a large number of publications have implicated DBAN as the primary driver of toxicity, (Chuang and Mitch 2017, Chuang et al. 2019b, Krasner et al. 2016b, Kristiana et al. 2017, Le Roux et al. 2017, Li et al. 2019, Liu et al. 2018, Liu et al. 2017, Stanford et al. 2019b, Vatankhah et al. 2019, Zeng et al. 2016, Zhang et al. 2017) and therefore we also examined the importance of DBAN before and after the addition of aggregated HAcAm data, which also have relatively high toxicity indices, but are not always measured alongside HANs. In Figure 5-4, we show the contribution of DBAN to the overall predicted cytotoxicity in sampling events from three publications with varying treatment processes and source waters. The addition of HAcAms to the post-GAC samples caused a 10% to 63% percent decrease in the contribution of DBAN to predicted cytotoxicity for two studies (Krasner et al. 2016b, McKie et al. 2015). DBAN associated toxicity in the third study decreased to a lesser extent because four of the six HAcAms were measured in the initial study, which diluted the effect of adding additional HAcAms. However, inclusion of two additional HAcAms (i.e., CAM and BAM) reduced the percent contribution of DBAN to predicted cytotoxicity by an additional 2% to 4%. In Figure C-6, we show the percent contribution from DBAN to predicted genotoxicity, which generally agrees with the conclusions presented for cytotoxicity. Although this exercise might seem intuitive, we note here that increasing the number of total compounds measured will diminish the relative contribution of DBAN to predicted

toxicity. Therefore, the conclusion that DBAN drives overall toxicity may be an artifact of 1) the number of DBPs measured, and 2) the relative toxic potency of DBAN.

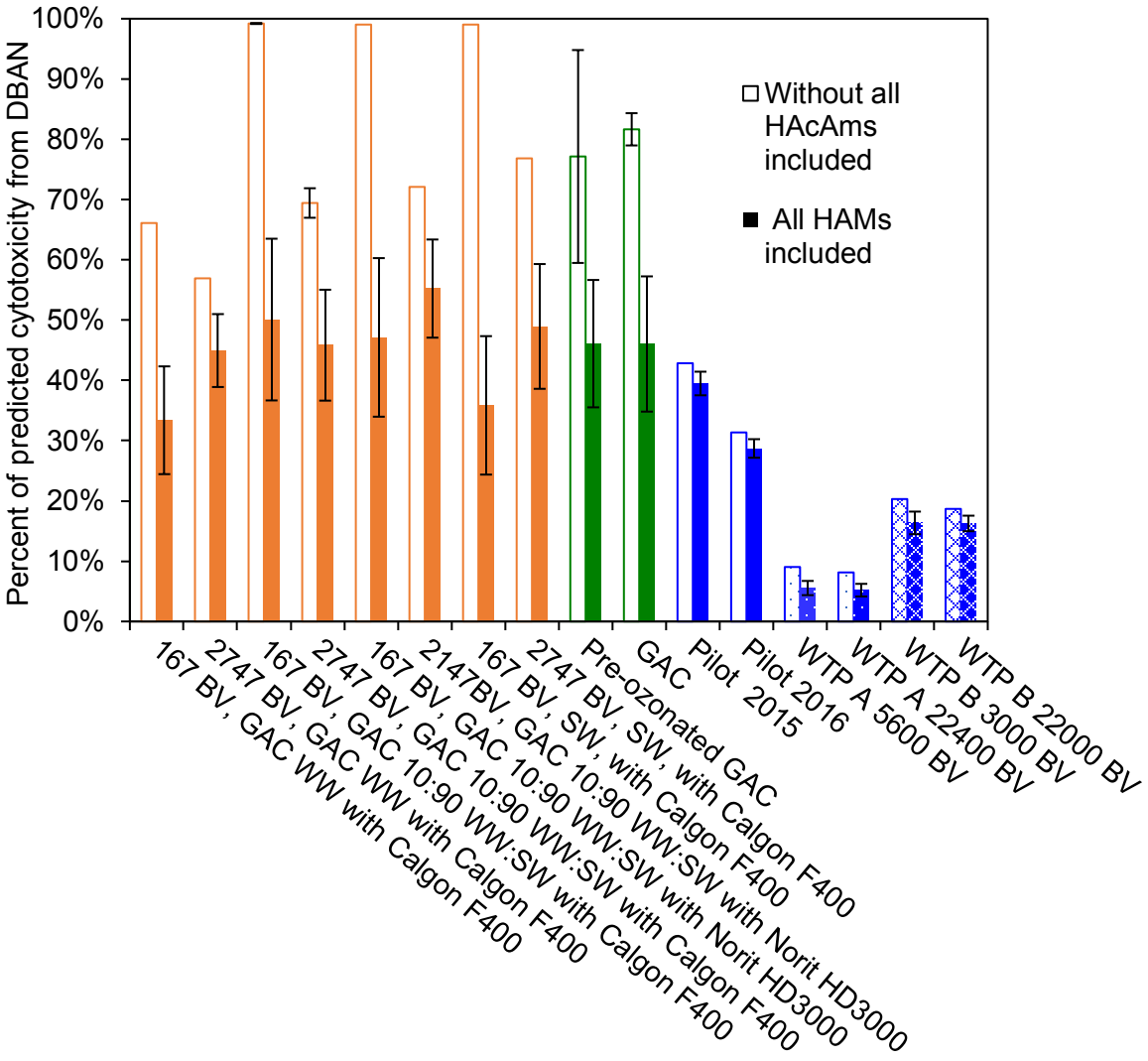

Figure 5-4 Contribution of DBAN to predicted cytotoxicity of GAC treated samples in which HAcAms were not measured (published data) or with addition of aggregated HAcAm data. Orange data is from Krasner et al. (2016b) (Table C-6), green data is from McKie et al. (2015) (Table C-6), and blue data is from Stanford et al. (2019b) (Table C-5). Stanford et al. (2019b) measured several HAcAms, others were supplemented. The

pilot plants included DCAM, DBAM, and BCAM, WTP A included DCAM and BCAM, and WTP B included DCAM, DBAM, BCAM, and TCAM. McKie et al. (2015) did not measure DBAN; the mean GAC effluent DBAN concentrations from Krasner et al. (2016b) and Stanford et al. (2019b) are presented. Error bars for data including HAcAms (filled bars) are derived from the standard deviation of HAcAm data from Kosaka et al. (2016a) and the HAcAms measured in Stanford et al. (2019b) (DCAM, DBAM, BCAM, TCAM). Error bars for data without HAcAms (open bars) are derived from the publications. Raw data provided in Table C-7.

Statistical Methods in Summed Calculations

Like any measurement, predicted toxicity has some statistical uncertainty. There is uncertainty in both the measurement of a DBP's concentration, and the measurement of its toxic potency. However, the standard deviation of the predicted toxicity is not reported, or is in some cases reported incorrectly, potentially leading to a misunderstanding of the measurement's precision.

Regarding the DBP concentration, during quantification of compounds at low µg/L or low ng/L, relative standard deviation (i.e., standard deviation divided by the mean) of 20% is generally considered acceptable, and some highly genotoxic to CHO cell DBPs regularly occur at or near their limit of quantification (e.g., DBAN). One way to reduce the measurement error is through replicate measurement. However, replicate measurement only accounts for measurement error. If the goal is to compare water treatment processes, it is necessary to measure replicate samples from the experiment to account for both experimental and measurement error. This becomes cost prohibitive, and many data are reported with only measurement replication, rather than experimental.

Regarding measurement of toxic potency, CHO cytotoxicity and genotoxicity assays are considered relatively precise among *in vitro* bioanalytical assays. For example, Wagner and Plewa (2017) used a bootstrap method to estimate a relative standard error of 12% for the cytotoxic potency of chloroacetamide. While it is possible to estimate the standard error of the toxic potency of a DBP using the raw data and a bootstrap method, this descriptive statistic has not been published for the majority of DBPs tested with the CHO comet assays. Nevertheless, the toxic potencies measured by these assays also have some uncertainty which should be considered when using them to compare DBPs or water samples.

Multiplying two uncertain values increases the overall standard error. Treating the DBP concentration and its geno- or cytotoxic potency as independent random variables, the standard error of their product is:

$$s_{A\times B} = \sqrt{\left(s_A{}^2 + \bar{x}_A{}^2\right)\left(s_B{}^2 + \bar{x}_B{}^2\right) - \bar{x}_A{}^2\bar{x}_B{}^2} \qquad (1)$$

Where *A* is the DBP molar concentration, *B* is the toxic potency (1/LC_{50} or 1/50% DNA tail moment), *s* is standard error, and $\bar{x}$ is mean DBP concentration or mean bootstrap output. For example, for a DBP with concentration measurement relative standard error of 20% and with geno- or cytotoxic potency relative standard error of 12%, the toxicity-weighted concentration standard error is 23.4%. The assumption of independence is valid in this case because there is no relationship between the result of a toxicity assay on a DBP and that DBP's concentration in a sample collected years and miles apart.

When adding random variables, the relative standard error decreases, but to an extent that depends on how much one variable dominates the equation. The standard error for the sum of independent random variables is:

$$s_{(Z_1+Z_2+\cdots Z_n)} = (\sum_{i=1}^{i=n} {s_{Z_i}}^2)^{\frac{1}{2}} \quad (2)$$

Where *n* is the number of variables summed and Z_1, Z_2, etc. are the variables summed. Consider a hypothetical scenario in which a water sample has 30 detected DBPs, each of which has a relative standard error of 20% for the product of DBP concentration and toxic potency. If each DBP contributes to the predicted toxicity equally, the overall relative standard error is just 3.7%. This low relative standard error is because it is unlikely that all 30 DBPs would have been low estimates in a single sample (assuming independence), and any one extreme value by a single DBP represents a low percentage of the total predicted toxicity. However, if a single DBP contributes 50% of the index (e.g., DBAN) and the other 29 detected DBPs contribute equally to the other 50%, the overall relative standard error is 10.2%. Additionally, the concentration of multiple DBPs measured in a sample may not be completely independent, since the same factors that might dilute, concentrate, or contaminate the measurement of one DBP could also affect the others. Considering covariance, Eqn 2 becomes:

$$s_{(Z_1+Z_2+\ldots+Z_n)} = \sqrt{\sum_{i=1}^{i=n} {s_{Z_i}}^2 + \frac{2\sum_{i,j:i<j} \operatorname{cov}\left(Z_i, Z_j\right)}{N}} \quad (3)$$

As an example of how rigorous analysis of error may alter interpretation, we examine one study in which it was observed that pre-chlorination of surface water before GAC resulted in a lower predicted cyto- and genotoxicity than GAC alone.(Stanford et al. 2019b) The predicted cyto- and genotoxicity were reduced 17% and 16%, respectively, if pre-chlorination was applied before the GAC. In Figure 5-5 we show the predicted cyto- and genotoxicities with error bars assuming a relative standard error of 12% for all DBP

toxic potencies and 15% for all DBP concentrations. Based on these assumptions and Eqns. 1 and 2, the relative standard errors of the predicted cyto- and genotoxicities are 10.3% and 10.6%, respectively, before treatment with GAC. After GAC treatment, the relative standard errors of the predicted cyto- and geno-toxicities are 9.3% and 9.9%, respectively. Although in this case a change across GAC is statistically significant, the predicted toxicities with and without pre-chlorination are within 2 standard errors of each other, and thus not statistically significant (p-value > 0.05). Large experimental replication would have been required to reduce the standard error and verify a change in predicted toxicities of this magnitude. Given that descriptive statistical measures of variance are not generally available and that there is complex interplay between standard errors, small changes in predicted toxicities should be interpreted with caution.

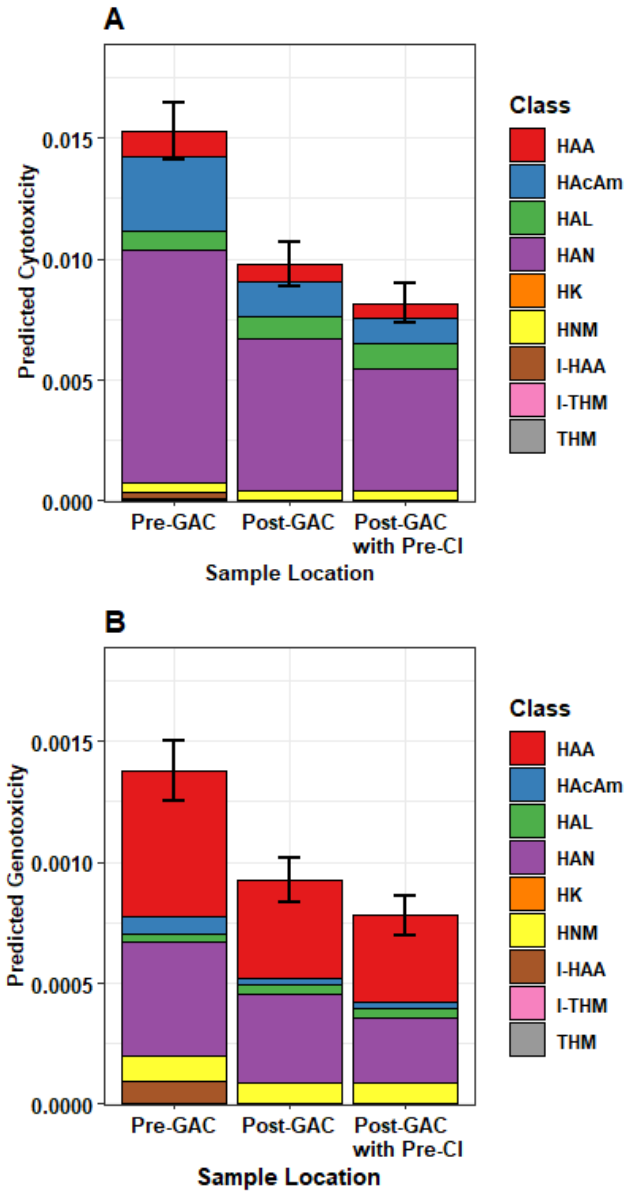

Figure 5-5 Predicted toxicities of a pilot plant treating surface water with GAC with and without chlorination before GAC, including measurements of error, which are not frequently presented. (A) Cytotoxicity and (B) Genotoxicity. Water quality and treatment details are in Stanford et al.(2019b). HAA = haloacetic acids (non-iodinated), HAcAm = haloacetamides, HAL = haloacetaldehydes, HAN = haloacetonitriles, HK = haloketones, HNM = halonitromethanes, I-HAA = iodinated haloacetic acids, I-THM = iodinated trihalomethanes. THM = trihalomethanes (non-iodinated).

Conclusions and Future Research Needs

Predicted toxicity has been used previously to show that regulated DBPs (THMs and HAAs) contribute much less to the overall toxicological profile of a treated water sample than other DBPs that are present at significantly lower concentrations (i.e., DBAN tends to contribute more to toxicity than THMs and therefore is likely to be more important). This is a function of individual DBPs toxicity index and their concentration. Predicted toxicity is a valuable tool for determining primary contributors to DBPs among the DBPs measured and is one of many approaches for determining the potential public health effects of DBPs. But we show here that the uncertainties inherent to the method render it challenging and requiring careful interpretation for comparing treatment processes (i.e., GAC treated water is more or less toxic than untreated water). Comparisons between treated and untreated samples using predicted toxicity may be biased towards measured DBP species that have both high toxicity indices in CHO cell assays and precursors that are unaffected by the treatment being studied. Other methods exist to compare toxicity between samples, such as bioassays, but they also have limitations. Primarily that they require extraction of the DBPs to produce a sample that is concentrated enough to produce a response, and the extraction step causes the loss of most volatile DBPs, and likely some unknown DBPs. Further, there are many bioassays that measure various endpoints and it is not yet known which is the most relevant in capturing human health impacts of DBPs.

In the short term, further research is needed to viably advance predicted toxicity and other toxicity measurements to determine the benefits of a treatment technology. Additional research to determine how well predicted toxicity and CHO cell toxicity are correlated with other whole mixture bioassays (e.g., SOS Chromotest) would be valuable and would determine if cost effective and quick assays are representative of overall

toxicity. Continuation of the discovery of DBPs and their respective toxic potency will continue to improve our understanding of the importance of specific DBPs. If it were possible to measure all DBPs and their toxicity indices, predictive toxicity would no longer be subject to sampling bias, but this is not possible in the short term, and likely will not be in the long term either, and therefore we must accept that certainty may not be within our grasp. However, better availability and use of metrics of statistical certainty and uncertainty would help to definitively determine if technologies are effective in reducing overall toxicity.

Another short-term goal for DBP researchers should be to assess the role of agonism or antagonism in DBP mixtures, which may be achieved by comparing the predicted toxicity of a clean mixture to that of its actual toxicity to CHO cells (Chuang et al. 2019c). Predicted toxicity assumes that the toxicity of each DBP is additive and ignores the possibility of agonistic or antagonistic effects. Toxicity is generally additive if each compound is toxic through a different mechanism. However, prevailing evidence suggests that DBPs are genotoxic though indirect DNA damage and products of oxidative stress (i.e., similar mechanisms) (Lan et al. 2018, Pals et al. 2013, Pals et al. 2011).

Toxicity threshold values should also be incorporated into predicted toxicity, because some DBPs could be below a threshold concentration at which they would pose no cytotoxic risk. DBPs that are directly genotoxic by chemically reacting with DNA theoretically have no toxicity threshold (Hrudey 2009). However, DBPs that are indirectly carcinogenic through cytotoxicity or oxidative stress are expected to have toxicity thresholds below which they pose zero risk (Hrudey 2009). Ideally, a DBP that is detectable but below this threshold should be excluded from any metric of total DBP risk. Lowest observed effect levels have been published for the CHO genotoxicity and

cytotoxicity assays on DBPs (Wagner and Plewa 2017), and could be used to exclude DBPs below these concentrations.

A long-term goal may be to assess the differences in toxic response between hamster ovary cells or other bioassays and target human organs. For example, some DBPs are only toxic after hepatic metabolism and liver S9 activation has been developed to act as a surrogate (George et al. 2001, Peto et al. 1991, Wagner et al. 2014). We must accept that both the long- and short-term goals presented here are significant challenges, and that obtaining perfection may not be attainable in the near future. However, we believe that overcoming the challenges presented will help to guide and understand the implications of future regulatory action.

Chapter 6 Synthesis

Each chapter in this thesis concentrated on an aspect of trace organic compounds in the context of potable water reuse research: experimentation (Chapters 2 & 3), instrumentation (Chapter 4), and data interpretation (Chapter 5). As I gained more laboratory experience, I better understood the data and methods used in Chapter 5's paper and obtained the technical GC-MS experience to contribute to Chapter 4's paper explaining mass spectrometry. The relationships between these components are best demonstrated in Figure 6-1.

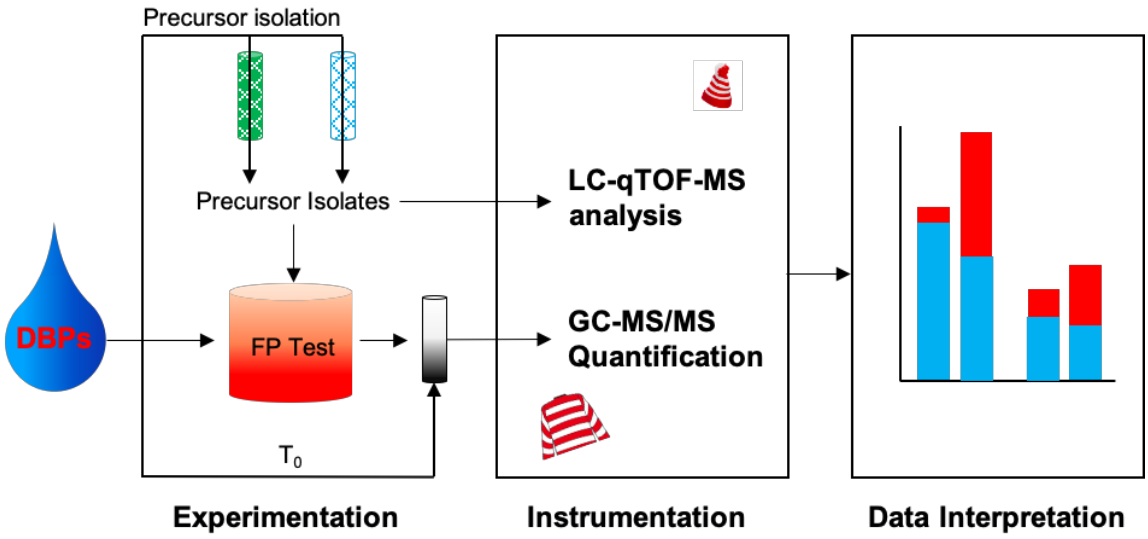

Figure 6-1 The sections of this thesis as they relate to each other.

The experimental data I produced in the laboratory either used samples from OCWD's AWPF or simulated conditions at this facility. Some experiments were guided by unanswered questions from previous AWPF experiments. For example, benzotriazole was previously detected in the RO permeate, but was removed by UV/AOP. So, I tested whether benzotriazole's UV/AOP products could form reactive nitrosamine precursors,

while using enough benzotriazole to theoretically yield enough nitrosamines to be detected on the GC-MS.

Developing a paper to help water professionals use their own instruments helped me troubleshoot instrument problems, interpret the data (i.e. What counts as a peak? What does this peak shape indicate?) and determine experimental parameters (i.e. target yield 10x above the LOQ). Due to instrument malfunction, many samples had to be put on hold for months before analysis could be completed, showing how important instrumentation is to the research process. Learning to maintain a ~15-year-old GC-MS prepared me for adjusting to a new instrument. Additionally, understanding instrumentation provided more context for how the DBP data was quantified in the published papers used for Chapter 5's toxicity publication.

Finally, interpreting the data is important to figure out what story the data tells. In the case of chemical additions in Chapter 2, data was interpreted with a conservative dilution factor, which required an understanding of the experimental methods and reuse facility operations. However, knowing the data was so diluted resulted in the conclusion that negligible nitrosamine precursors were contributed by the chemical additions. Data must be interpreted carefully to avoid bias in the results, as shown with the manuscript in Chapter 5. Because the experimentation and instrumentation methods required to measure all DBPs would be impossible, using toxicities of selected compounds to compare water treatments results in biased conclusions.

Chapter 7 Conclusions and Recommendations for Future Work

In Chapter 2, I found that the AWPF's chemical additions contributed few nitrosamine precursors. After FP tests and an incorporated 10,000x dilution factor, the most NDMA formed was about 1.2 ng/L due to the AWPF's stock H_2O_2, while other nitrosamine formation was not detected. Due to the conservative dilution factor and the expected NDMA rebound of 0.7 ng/L·h, I concluded that the chemical additions were an unlikely source of NDMA precursors.

The second half of Chapter 2 found that there was little difference in nitrosamine precursor removal depending on the type of oxidant used (HOCl or H_2O_2) prior to UV/AOP. NDMA precursors extracted using MCX cartridges had recoveries of 69% to 113%, but these cartridges were ineffective for other nitrosamines. HLB cartridges did not recover nitrosamine precursors with the exception of NDBA, which had recoveries of 65% to >100%. Further research is needed to test NDBA (and other nitrosamines with high alkyl composition) at higher concentrations of known precursors to verify these results.

In the next experimental section, Chapter 3, I found that the simulated AWPF UV/AOP experiments did not produce reactive precursors from five of the six compounds I tested. The exception was diphenhydramine, which formed 268 ng/L of NDMA, resulting in a 1% NDMA yield from precursors. Future experiments should explore diphenhydramine NDMA precursor yields at UV doses between 0 and 1000 mJ/cm_3, as well as include NOM in the UV reactor to simulate wastewater conditions. Compounds similar to diphenhydramine, such as those containing secondary or tertiary

amines unbounded by a ring, should be tested for reactive nitrosamine precursor generation in UV/AOP processes.

High-resolution mass spectrometry likely requires a mass spectrometer expert to operate instruments. However, an understanding of the mechanics behind water quality analysis techniques helps practitioners to understand results and limitations of published research. My expectation was that the breakdown of a few instruments in Chapter 4 would help future graduate students and other researchers better understand the instruments they work with frequently. Further explanation of mass spectrometry that would be useful to beginners could delve into different types of ionization, interpreting results, common problems encountered and how to solve them, and maintenance.

Measurements from such instrumentation provide a broad view of water quality and some of the measured compounds have known toxicological indices. I showed in Chapter 5 that summing toxicity indices from multiple compounds results in a biased understanding of the samples' overall toxicity when compared to other samples. In one example, I found that removing haloacetaldehydes (the equivalent of not measuring this group of DBPs), caused the predicted cytotoxicity of a GAC treated sample to decrease by about 47% - reversing the initial conclusion that GAC increased the water toxicity. I recommend that future work should carefully interpret relative toxicity data and that it is better used for understanding what should or should not be better regulated. Ideally, a method for determining the toxicity of a water sample will be developed rather than determining toxicity piecemeal based on measurements of individual compounds. Table 7-1 summarizes the conclusions drawn from the work done in each chapter of this thesis.

Table 7-1 Summary of the conclusions and future work for each thesis chapter.

Chapter	Conclusions	Future Work
Contributions of Treatment Facility Chemical Additions and Cleaning Agents as Precursors to NDMA Formation	• Cleaning agents and chemical additions produced negligible NDMA precursors that could not be attributed to the formation of NDMA later in the distribution system. • NDMA precursors decreased throughout the facility for both oxidant treatment trains. • MCX cartridges had the highest precursor recoveries for NDMA. HLB cartridges recovered NDBA precursors the best.	• HLB extraction experiments require higher, known concentrations of NDBA precursors to verify the recoveries found in this chapter. • Nitrosamines with more lipophilic properties (i.e. NDPA) should also be tested for HLB precursor recovery.
Potential Transformation of Nitrogenous Organic Matter During UV/AOP into Reactive NDMA Precursors	• NDMA yields were highest for diphenhydramine (~1%). • The other five compounds tested returned low yields similar to those of the MQ blanks.	• Determine whether diphenhydramine produces precursors at UV doses between 0 and 1000 mL/cm$_3$. • Determine yields for similar compounds (contain a tertiary amine unbounded by a ring). • Add NOM to the UV/AOP experiments to simulate wastewater conditions.
Summation of Disinfection By-Product CHO Cell Relative Toxicity Indices: Sampling Bias, Uncertainty, and a Path Forward	• Using predicted toxicity to compare water treatments can bias conclusions because it is impossible to measure every DBP that contributes to toxicity. • When used carefully, this method can show what class of compounds dominate a water sample's toxicity profile and help determine which DBPs are most important for regulation.	• Assess the role of agonism or antagonism in DBP mixtures. • Determine how CHO cells differ from human cells in toxic responses. • Determine toxicity thresholds for DBPs.

References

Abdessemed, A.P., Appel; Klaliny Amer, E.L.; (2015) Combined Chlorine Degradationcombin, LAP Lambert Academic Publishing.

Bellar, T.A., Lichtenberg, J.J. and Kroner, R.C. (1974) Occurrence of Organohalides in Chlorinated Drinking Waters. Journal American Water Works Association 66(12), 703-706.

Boyd, J.M., Hrudey, S.E., Richardson, S.D. and Li, X.F. (2011) Solid-phase extraction and high-performance liquid chromatography mass spectrometry analysis of nitrosamines in treated drinking water and wastewater. Trac-Trends in Analytical Chemistry 30(9), 1410-1421.

Buerge, I.J., Poiger, T., Muller, M.D. and Buser, H.R. (2003) Caffeine, an anthropogenic marker for wastewater contamination of surface waters. ENVIRONMENTAL SCIENCE & TECHNOLOGY 37(4), 691-700.

CDPH (2009) NDMA and Other Nitrosamines – Drinking Water Issues. http://www.cdph.ca.gov/certlic/drinkingwater/Pages/NDMA.aspx.

Chen, W.H. and Young, T.M. (2008) NDMA formation during chlorination and chloramination of aqueous diuron solutions. ENVIRONMENTAL SCIENCE & TECHNOLOGY 42(4), 1072-1077.

Chen, Y., Hu, C., Hu, X.X. and Qu, J.H. (2009) Indirect Photodegradation of Amine Drugs in Aqueous Solution under Simulated Sunlight. ENVIRONMENTAL SCIENCE & TECHNOLOGY 43(8), 2760-2765.

Chen, Y., Ye, J.S., Li, C.S., Zhou, P.L., Liu, J. and Ou, H.S. (2018) Degradation of 1H-benzotriazole by UV/H2O2 and UV/TiO2: kinetics, mechanisms, products and toxicology. Environmental Science-Water Research & Technology 4(9), 1282-1294.

Chuang, Y.-H. and Mitch, W.A. (2017) Effect of Ozonation and Biological Activated Carbon Treatment of Wastewater Effluents on Formation of N-nitrosamines and Halogenated Disinfection Byproducts. ENVIRONMENTAL SCIENCE & TECHNOLOGY 51(4), 2329-2338.

Chuang, Y.-H., Szczuka, A., Shabani, F., Munoz, J., Aflaki, R., Hammond, S.D. and Mitch, W.A. (2019a) Pilot-scale comparison of microfiltration/reverse osmosis and ozone/biological activated carbon with UV/hydrogen peroxide or UV/free chlorine AOP treatment for controlling disinfection byproducts during wastewater reuse. Water Research 152, 215-225.

Chuang, Y.H., Parker, K.M. and Mitch, W.A. (2016) Development of Predictive Models for the Degradation of Halogenated Disinfection Byproducts during the UV/H2O2

Advanced Oxidation Process. ENVIRONMENTAL SCIENCE & TECHNOLOGY 50(20), 11209-11217.

Chuang, Y.H., Szczuka, A. and Mitch, W.A. (2019b) Comparison of Toxicity-Weighted Disinfection Byproduct Concentrations in Potable Reuse Waters and Conventional Drinking Waters as a New Approach to Assessing the Quality of Advanced Treatment Train Waters. ENVIRONMENTAL SCIENCE & TECHNOLOGY 53(7), 3729-3738.

Chuang, Y.H., Szczuka, A., Shabani, F., Munoz, J., Aflaki, R., Hammond, S.D. and Mitch, W.A. (2019c) Pilot-scale comparison of microfiltration/reverse osmosis and ozone/biological activated carbon with UV/hydrogen peroxide or UV/free chlorine AOP treatment for controlling disinfection byproducts during wastewater reuse. Water Research 152, 215-225.

Cornell, J.S., Pillard, D.A. and Hernandez, M.T. (2000) Comparative measures of the toxicity of component chemicals in aircraft deicing fluid. Environmental Toxicology and Chemistry 19(6), 1465-1472.

Cuthbertson, A.A., Kimura, S.Y., Liberatore, H.K., Summers, R.S., Knappe, D.R.U., Stanford, B.D., Maness, J.C., Mulhern, R.E., Selbes, M. and Richardson, S.D. (2019) Does Granular Activated Carbon with Chlorination Produce Safer Drinking Water? From Disinfection Byproducts and Total Organic Halogen to Calculated Toxicity. ENVIRONMENTAL SCIENCE & TECHNOLOGY 53(10), 5987-5999.

EPA, U. (1979) National interim primary drinking water regulations: control of trihalomethanes in drinking water: final rules. Fed. Reg. 44.

Eschenbrenner, A.B. (1945) Induction of Hepatomas in Mice by Repeated Oral Administration of Chloroform, with Observations of Sex Differences. Journal of the National Cancer Institute, 251-255.

Fenn, J.B., Mann, M., Meng, C.K., Wong, S.F. and Whitehouse, C.M. (1989) Electrospray ionization for mass spectrometry of large biomolecules. Science 246(4926), 64-71.

Fiddler, W.P., J.W.; Doerr, R.C.; Wasserman, A.E.; (1972) Formation of N-nitrosodimethylamine from naturally occurring quaternary ammonium compounds and tertiary amines. Nature 236.

Furst, K.E., Coyte, R.M., Wood, M., Vengosh, A. and Mitch, W.A. (2019) Disinfection Byproducts in Rajasthan, India: Are Trihalomethanes a Sufficient Indicator of Disinfection Byproduct Exposure in Low-Income Countries? Environmental Science & Technology 53(20), 12007-12017.

George, J., Rao, K.R., Stern, R. and Chandrakasan, G. (2001) Dimethylnitrosamine-induced liver injury in rats: the early deposition of collagen. Toxicology 156, 129-138.

Giger, W., Schaffner, C. and Kohler, H.P.E. (2006) Benzotriazole and tolyltriazole as aquatic contaminants. 1. Input and occurrence in rivers and lakes. ENVIRONMENTAL SCIENCE & TECHNOLOGY 40(23), 7186-7192.

Guay, C., Rodriguez, M. and Serodes, J. (2005) Using ozonation and chloramination to reduce the formation of trihalomethanes and haloacetic acids in drinking water. Desalination 176(1-3), 229-240.

Gumbrecht, J.H.a.J. (2019) FDA finds low levels of cancer-linked impurity in common heartburn drugs, CNN.

Hanigan, D., Liao, X.B., Zhang, J.W., Herckes, P. and Westerhoff, P. (2016) Sorption and desorption of organic matter on solid-phase extraction media to isolate and identify N-nitrosodimethylamine precursors. Journal of Separation Science 39(14), 2796-2805.

Hanigan, D., Thurman, E.M., Ferrer, I., Zhao, Y., Andrews, S., Zhang, J.W., Herckes, P. and Westerhoff, P. (2015) Methadone Contributes to N-Nitrosodimethylamine Formation in Surface Waters and Wastewaters during Chloramination. Environmental Science & Technology Letters 2(6), 151-157.

Hanigan, D., Truong, L., Simonich, M., Tanguay, R. and Westerhoff, P. (2017) Zebrafish embryo toxicity of 15 chlorinated, brominated, and iodinated disinfection by-products. Journal of Environmental Sciences 58, 302-310.

Hrudey, S.E. (2009) Chlorination disinfection by-products, public health risk tradeoffs and me. Water Res 43(8), 2057-2092.

James, A.T. and Martin, A.J. (1952) Gas-liquid partition chromatography; the separation and micro-estimation of volatile fatty acids from formic acid to dodecanoic acid. Biochemical Journal 50(5), 679-690.

Karthikeyan, K.G. and Meyer, M.T. (2006) Occurrence of antibiotics in wastewater treatment facilities in Wisconsin, USA. Science of the Total Environment 361(1-3), 196-207.

Kemper, J.M., Westerhoff, P., Dotson, A. and Mitch, W.A. (2009) Nitrosamine, dimethylnitramine, and chloropicrin formation during strong base anion-exchange treatment. Environ Sci Technol 43(2), 466-472.

Kinney, C.A., Furlong, E.T., Werner, S.L. and Cahill, J.D. (2006) Presence and distribution of wastewater-derived pharmaceuticals in soil irrigated with reclaimed water. Environmental Toxicology and Chemistry 25(2), 317-326.

Kosaka, K., Ohkubo, K. and Akiba, M. (2016a) Occurrence and formation of haloacetamides from chlorination at water purification plants across Japan. Water Research 106, 470-476.

Kosaka, K., Ohkubo, K. and Akiba, M. (2016b) Occurrence and formation of haloacetamides from chlorination at water purification plants across Japan. Water Res 106, 470-476.

Krasner, S.W. (2009) The formation and control of emerging disinfection by-products of health concern. Philosophical Transactions of the Royal Society a-Mathematical Physical and Engineering Sciences 367(1904), 4077-4095.

Krasner, S.W., Lee, T.C., Westerhoff, P., Fischer, N., Hanigan, D., Karanfil, T., Beita-Sandí, W., Taylor-Edmonds, L. and Andrews, R.C. (2016a) Granular Activated Carbon Treatment May Result in Higher Predicted Genotoxicity in the Presence of Bromide. Environ Sci Technol 50(17), 9583-9591.

Krasner, S.W., Lee, T.C.F., Westerhoff, P., Fischer, N., Hanigan, D., Karanfil, T., Beita-Sandí, W., Taylor-Edmonds, L. and Andrews, R.C. (2016b) Granular Activated Carbon Treatment May Result in Higher Predicted Genotoxicity in the Presence of Bromide. ENVIRONMENTAL SCIENCE & TECHNOLOGY 50(17), 9583-9591.

Krasner, S.W., Mitch, W.A., McCurry, D.L., Hanigan, D. and Westerhoff, P. (2013) Formation, precursors, control, and occurrence of nitrosamines in drinking water: a review. Water Res 47(13), 4433-4450.

Krasner, S.W., Westerhoff, P., Mitch, W.A., Hanigan, D., McCurry, D.L. and von Gunten, U. (2018) Behavior of NDMA precursors at 21 full-scale water treatment facilities. Environmental Science-Water Research & Technology 4(12), 1966-1978.

Kristiana, I., Liew, D., Henderson, R.K., Joll, C.A. and Linge, K.L. (2017) Formation and control of nitrogenous DBPs from Western Australian source waters: Investigating the impacts of high nitrogen and bromide concentrations. Journal of Environmental Sciences 58, 102-115.

Laingam, S., Froscio, S.M., Bull, R.J. and Humpage, A.R. (2012) In vitro toxicity and genotoxicity assessment of disinfection by-products, organic N-chloramines. Environmental & Molecular Mutagenesis 53(2), 83-93.

Lan, J., Rahman, S.M., Gou, N., Jiang, T., Plewa, M.J., Alshawabkeh, A. and Gu, A.Z. (2018) Genotoxicity Assessment of Drinking Water Disinfection Byproducts by DNA Damage and Repair Pathway Profiling Analysis. Environmental Science & Technology 52(11), 6565-6575.

Lau, S.S., Wei, X., Bokenkamp, K., Wagner, E.D., Plewa, M.J. and Mitch, W.A. (2020) Assessing Additivity of Cytotoxicity Associated with Disinfection Byproducts in Potable Reuse and Conventional Drinking Waters. ENVIRONMENTAL SCIENCE & TECHNOLOGY 54(9), 5729-5736.

Le Roux, J., Plewa, M.J., Wagner, E.D., Nihemaiti, M., Dad, A. and Croué, J.-P. (2017) Chloramination of wastewater effluent: Toxicity and formation of disinfection byproducts. Journal of Environmental Sciences 58, 135-145.

Leavey-Roback, S.L., Sugar, C.A., Krasner, S.W. and Suffet, I.H. (2016) NDMA formation during drinking water treatment: A multivariate analysis of factors influencing formation. Water Research 95, 300-309.

Li, C. (2011) Trends and Effects of Chloramine in Drinking Water. Water Conditioning & Purification 53(10), 52-56.

Li, J., Wang, W., Moe, B., Wang, H. and Li, X.-F. (2015) Chemical and Toxicological Characterization of Halobenzoquinones, an Emerging Class of Disinfection Byproducts. Chemical Research in Toxicology 28(3), 306-318.

Li, X.-F. and Mitch, W.A. (2018) Drinking Water Disinfection Byproducts (DBPs) and Human Health Effects: Multidisciplinary Challenges and Opportunities. ENVIRONMENTAL SCIENCE & TECHNOLOGY 52(4), 1681-1689.

Li, Z., Liu, X., Huang, Z., Hu, S., Wang, J., Qian, Z., Feng, J., Xian, Q. and Gong, T. (2019) Occurrence and ecological risk assessment of disinfection byproducts from chlorination of wastewater effluents in East China. Water Research 157, 247-257.

Liu, C., Ersan, M.S., Plewa, M.J., Amy, G. and Karanfil, T. (2018) Formation of regulated and unregulated disinfection byproducts during chlorination of algal organic matter extracted from freshwater and marine algae. Water Research 142, 313-324.

Liu, C., Olivares, C.I., Pinto, A.J., Lauderdale, C.V., Brown, J., Selbes, M. and Karanfil, T. (2017) The control of disinfection byproducts and their precursors in biologically active filtration processes. Water Research 124, 630-653.

Lopez, N., Plaza, S., Afkhami, A., Marco, P., Gimenez, J. and Esplugas, S. (2017) Treatment of Diphenhydramine with different AOPs including photo-Fenton at circumneutral pH. Chemical Engineering Journal 318, 112-120.

Massachusetts Department of Environmental Protection (2004) Massachusetts Department of Environmental Protection.

McKenna, E., Sharma, P., McCurry, D.L. and Hanigan, D. (2020a) A Layman's Guide to High-Resolution Mass Spectrometry. Journal American Water Works Association 112(4), 40-49.

McKenna, E., Thompson, K.A., Taylor-Edmonds, L., McCurry, D.L. and Hanigan, D. (2020b) Summation of disinfection by-product CHO cell relative toxicity indices: sampling bias, uncertainty, and a path forward. Environ Sci Process Impacts.

McKie, M.J., Taylor-Edmonds, L., Andrews, S.A. and Andrews, R.C. (2015) Engineered biofiltration for the removal of disinfection by-product precursors and genotoxicity. Water Research 81, 196-207.

Mitch, W.A., Gerecke, A.C. and Sedlak, D.L. (2003) A N-Nitrosodimethylamine (NDMA) precursor analysis for chlorination of water and wastewater. Water Res 37(15), 3733-3741.

Mitch, W.A. and Sedlak, D.L. (2002) Formation of N-nitrosodimethylamine (NDMA) from dimethylamine during chlorination. ENVIRONMENTAL SCIENCE & TECHNOLOGY 36(4), 588-595.

Mitch, W.A. and Sedlak, D.L. (2004) Characterization and fate of N-nitrosodimethylamine precursors in municipal wastewater treatment plants. ENVIRONMENTAL SCIENCE & TECHNOLOGY 38(5), 1445-1454.

Mitch, W.A.S., D.L.; (2002) Factors controlling nitrosamine formation during wastewater chlorination. Water Science and Technology 2(3), 191-198.

Munch, J.W. and Basset, M.V. (2005) Method 521 Determination of Nitrosamines in Drinking Water by Solid Phase Extraction and Capillary Column Gas Chromatography with Large Volume Injection and Chemical Ionization Tandem Mass Spectrometry (MS/MS), U.S. EPA, Washington, DC.

National Cancer Institute (1976) Report on the Carcinogenesis Bioassay of Chloroform. NTIS Report No PB264018.

Nier, K.A., Yergey, A.L. and Gale, P.J. (2015) The Encyclopedia of Mass Spectrometry : Historical Perspective, Elsevier Science & Technology.

Norman, T.S., Harms, L.L. and Looyenga, R.W. (1980) The use of chloramines to prevent trihalomethane formation. Journal American Water Works Association 72(3), 176-180.

OEHHA (2006) Public Health Goal for Chemicals in Drinking Water: N-Nitrosodimethylamine. http://www.oehha.ca.gov/water/phg/pdf/122206NDMAphg.pdf.

Pals, J., Attene-Ramos, M.S., Xia, M., Wagner, E.D. and Plewa, M.J. (2013) Human Cell Toxicogenomic Analysis Linking Reactive Oxygen Species to the Toxicity of Monohaloacetic Acid Drinking Water Disinfection Byproducts. Environmental Science & Technology 47(21), 12514-12523.

Pals, J.A., Ang, J.K., Wagner, E.D. and Plewa, M.J. (2011) Biological Mechanism for the Toxicity of Haloacetic Acid Drinking Water Disinfection Byproducts. Environmental Science & Technology 45(13), 5791-5797.

Pals, J.A., Wagner, E.D., Plewa, M.J., Xia, M. and Attene-Ramos, M.S. (2017) Monohalogenated acetamide-induced cellular stress and genotoxicity are related to electrophilic softness and thiol/thiolate reactivity. Journal of Environmental Sciences 58, 224-230.

Park, S.H., Piyachaturawat, P., Taylor, A.E. and Huang, C.H. (2009a) Potential N-nitrosodimethylamine (NDMA) formation from amine-based water treatment polymers in the reactions with chlorine-based oxidants and nitrosifying agents. Water Supply 9(3), 279-288.

Park, S.H., Wei, S., Mizaikoff, B., Taylor, A.E., Favero, C. and Huang, C.H. (2009b) Degradation of Amine-Based Water Treatment Polymers during Chloramination as N-Nitrosodimethylamine (NDMA) Precursors. ENVIRONMENTAL SCIENCE & TECHNOLOGY 43(5), 1360-1366.

Parvez, S., Rice, G.E., Teuschler, L.K., Simmons, J.E., Speth, T.F., Richardson, S.D., Miltner, R.J., Hunter, E.S., Pressman, J.G., Strader, L.F., Klinefelter, G.R., Goldman, J.M. and Narotsky, M.G. (2017) Method to assess component contribution to toxicity of complex mixtures: Assessment of puberty acquisition in rats exposed to disinfection byproducts. Journal of Environmental Sciences 58, 311-321.

Peng, B., Liu, M., Han, Y., Wanjaya, E.R. and Fang, M. (2019) Competitive Biotransformation Among Phenolic Xenobiotic Mixtures: Underestimated Risks for Toxicity Assessment. Environmental Science & Technology 53(20), 12081-12090.

Peter, K.T., Tian, Z., Wu, C., Lin, P., White, S., Du, B., McIntyre, J.K., Scholz, N.L. and Kolodziej, E.P. (2018) Using High-Resolution Mass Spectrometry to Identify Organic Contaminants Linked to Urban Stormwater Mortality Syndrome in Coho Salmon. Environ Sci Technol 52(18), 10317-10327.

Peto, R., Gray, R., Brantom, P. and Grasso, P. (1991) Dose and time relationships for tumor induction in the liver and esophagus of 4080 inbred rats by chronic ingestion of N-nitrosodiethylamine or N-nitrosodimethylamine. Cancer Research 51, 6452-6469.

Pitt, J.J. (2009) Principles and applications of liquid chromatography-mass spectrometry in clinical biochemistry. Clin Biochem Rev 30(1), 19-34.

Plewa, M.J. (2019) Comparative quantitative toxicology of the haloacetonitriles: forcing agents of water disinfection by-product toxicity, Personal Communication.

Plewa, M.J., Kargalioglu, Y., Vankerk, D., Minear, R.A. and Wagner, E.D. (2002) Mammalian cell cytotoxicity and genotoxicity analysis of drinking water disinfection by products. Environmental and molecular mutagenesis 40(2), 134-142.

Plewa, M.J., Wagner, E.D., Muellner, M.G., Hsu, K.M. and Richardson, S.D. (2008) Comparative Mammalian Cell Toxicity of N-DBPs and C-DBPs. Disinfection by-Products in Drinking Water: Occurrence, Formation, Health Effects, and Control 995, 36-50.

Plewa, M.J., Wagner, E.D. and Richardson, S.D. (2017) TIC-Tox: A preliminary discussion on identifying the forcing agents of DBP-mediated toxicity of disinfected water. Journal of Environmental Sciences 58, 208-216.

Plumlee, M.H., Ishida, K. (2020) IAP Memo. Personal Communication.

Prakash, B., Lipps, W., Wang, D., Chopra, S., Lock, N. and Chambers, L. (2016) Determination of N-Nitrosamines by USEPA Method 521 using Triple Quadrupole Gas Chromatography Mass Spectrometry. Shimadzu Corporation (Application Note).

Richardson, S. and Postigo, C. (2012) Emerging Organic Contaminants and Human Health. Barceló, D. (ed), pp. 93-137, Springer Berlin Heidelberg.

Richardson, S.D., Plewa, M.J., Wagner, E.D., Schoeny, R. and DeMarini, D.M. (2007) Occurrence, genotoxicity, and carcinogenicity of regulated and emerging disinfection by-products in drinking water: A review and roadmap for research. Mutation Research/Reviews in Mutation Research 636(1–3), 178-242.

Ries, J. (2020) FDA Orders Zantac Taken Off Store Shelves Due to Cancer-Causing Chemical, Healthline.

Roback, S.L., Ferrer, I., Thurman, E.M., Ishida, K.P., Plumlee, M.H., Poustie, A., Westerhoff, P. and Hanigan, D. (2018) Non-target mass spectrometry analysis of NDMA precursors in advanced treatment for potable reuse. Environmental Science-Water Research & Technology 4(12), 1944-1955.

Roback, S.L.I., K.P.; Plumlee, M.H. (2017) Post-treatment challenges at advanced potable reuse plants: corrosion, metals mobilization and the reappearance of disinfection byproducts. 253rd National Meeting of the American Chemical Society A.C. Society.

Rook, J.J. (1974) FORMATION OF HALOFORMS DURING CHLORINATION OF NATURAL WATERS. Water Treatment Examination 23, 234-243.

Russell, C.G., Blute, N.K., Via, S., Wu, X.Y. and Chowdhury, Z. (2012) Nationwide assessment of nitrosamine occurrence and trends. Journal American Water Works Association 104(3), 57-58.

Schmidt, C.K. and Brauch, H.J. (2008) N,N-dimethosulfamide as precursor for N-nitrosodimethylamine (NDMA) formation upon ozonation and its fate during drinking water treatment. ENVIRONMENTAL SCIENCE & TECHNOLOGY 42(17), 6340-6346.

Schreiber, I.M. and Mitch, W.A. (2006) Nitrosamine formation pathway revisited: the importance of chloramine speciation and dissolved oxygen. Environ Sci Technol 40(19), 6007-6014.

Seidel, C.J., McGuire, M.J., Summers, R.S. and Via, S. (2005) Have utilities switched to chloramines? Journal (American Water Works Association) 97(10), 87-97.

Selbes, M., Kim, D., Ates, N. and Karanfil, T. (2013) The roles of tertiary amine structure, background organic matter and chloramine species on NDMA formation. Water Research 47(2), 945-953.

Sgroi, M., Roccaro, P., Oelker, G. and Snyder, S.A. (2016) N-nitrosodimethylamine (NDMA) formation during ozonation of wastewater and water treatment polymers. Chemosphere 144, 1618-1623.

Sgroi, M., Roccaro, P., Oelker, G.L. and Snyder, S.A. (2015) N-nitrosodimethylamine (NDMA) formation at an indirect potable reuse facility. Water Res 70, 174-183.

Sgroi, M., Vagliasindi, F.G.A., Snyder, S.A. and Roccaro, P. (2018) N-Nitrosodimethylamine (NDMA) and its precursors in water and wastewater: A review on formation and removal. Chemosphere 191, 685-703.

Shen, R. and Andrews, S.A. (2011) Demonstration of 20 pharmaceuticals and personal care products (PPCPs) as nitrosamine precursors during chloramine disinfection. Water Research 45(2), 944-952.

Soltermann, F., Lee, M., Canonica, S. and von Gunten, U. (2013) Enhanced N-nitrosamine formation in pool water by UV irradiation of chlorinated secondary amines in the presence of monochloramine. Water Res 47(1), 79-90.

Stalter, D., O'Malley, E., von Gunten, U. and Escher, B.I. (2016) Fingerprinting the reactive toxicity pathways of 50 drinking water disinfection by-products. Water Research 91, 19-30.

Stalter, D., O'Malley, E., Von Gunten, U. and Escher, B.I. (2020) Mixture effects of drinking water disinfection by-products: implications for risk assessment. Environmental Science: Water Resources Technology.

Stanford, B.D., Knappe, D.R.U., Maness, C., Zhang, C., Summers, R.S., Mulhern, R.E., Richardson, S.D., Cuthbertson, A., Kimura, S.Y., Liberatore, H., Dickenson, E.R.V., Verdugo, E., Glover, C., Ghosh, A., Seidel, C.J., Selbes, M., Reinert, A., Pierce, M. and Rosenfeldt, E. (2019a) GAC Control of Regulated and Emerging DBPs of Health Concern. Water Research Foundation Final Report (final Draft provided by authors on 6/20/18) Water Research Foundation: Denver, CO.

Stanford, B.D., Selbes, M., Reinert, A., Pierce, M., Rosenfeldt, E., Knappe, D.R.U., Maness, C., Zhang, C., Summers, R.S., Mulhern, R.E., Richardson, S.D., Cuthbertson, A., Kimura, S.Y., Liberatore, H., Dickenson, E.R.V., Verdugo, E., Glover, C., Ghosh, A. and Seidel, C.J. (2019b) GAC Control of Regulated and Emerging DBPs of Health Concern. Water Research foundation Final Report Water Research Foundation: Denver, CO.

Strohalm, M., Kavan, D., Novak, P., Volny, M. and Havlicek, V. (2010) mMass 3: a cross-platform software environment for precise analysis of mass spectrometric data. Anal Chem 82(11), 4648-4651.

Swain, D.L. (2015) A tale of two California droughts: Lessons amidst record warmth and dryness in a region of complex physical and human geography. Geophysical Research Letters 42(22), 9999-10003.

U.S. EPA (1993) Integrated Risk Information System N-nitrosodimethlyamine; CASRN 62-75-9.

USEPA (2006) 40 CFR Parts 9, 141, and 142. National primary drinking water regulations: stage 2 disinfectants and disinfection byproducts rule; final rule. Federal Register (Part II) 71(2), 388.

USEPA (2016) Contaminant Candidate List 4-CCL4.

Vatankhah, H., Szczuka, A., Mitch, W.A., Almaraz, N., Brannum, J. and Bellona, C. (2019) Evaluation of Enhanced Ozone-Biologically Active Filtration Treatment for the Removal of 1,4-Dioxane and Disinfection Byproduct Precursors from Wastewater Effluent. ENVIRONMENTAL SCIENCE & TECHNOLOGY 53(5), 2720-2730.

Voutsa, D., Hartmann, P., Schaffner, C. and Giger, W. (2006) Benzotriazoles, alkylphenols and bisphenol a in municipal wastewaters and in the Glatt River, Switzerland. Environmental Science and Pollution Research 13(5), 333-341.

Wagner, E.D., Osiol, J., Mitch, W.A. and Plewa, M.J. (2014) Comparative in vitro toxicity of nitrosamines and nitramines associated with amine-based carbon capture and storage. Environ Sci Technol 48(14), 8203-8211.

Wagner, E.D. and Plewa, M.J. (2017) CHO cell cytotoxicity and genotoxicity analyses of disinfection by-products: An updated review. Journal of Environmental Sciences 58, 64-76.

Yu, Y. and Reckhow, D.A. (2015) Kinetic Analysis of Haloacetonitrile Stability in Drinking Waters. Environ Sci Technol 49(18), 11028-11036.

Zeisel, S.H., Dacosta, K.A. and Fox, J.G. (1985) Endogenous Formation of Dimethylamine. Biochemical Journal 232(2), 403-408.

Zeng, T. and Mitch, W.A. (2015) Contribution of N-Nitrosamines and Their Precursors to Domestic Sewage by Greywaters and Blackwaters. ENVIRONMENTAL SCIENCE & TECHNOLOGY 49(22), 13158-13167.

Zeng, T. and Mitch, W.A. (2016) Impact of Nitrification on the Formation of N-Nitrosamines and Halogenated Disinfection Byproducts within Distribution System Storage Facilities. Environ Sci Technol 50(6), 2964-2973.

Zeng, T., Plewa, M.J. and Mitch, W.A. (2016) N-Nitrosamines and halogenated disinfection byproducts in U.S. Full Advanced Treatment trains for potable reuse. Water Research 101, 176-186.

Zhang, J.W., Hanigan, D., Westerhoff, P. and Herckes, P. (2016) N-Nitrosamine formation kinetics in wastewater effluents and surface waters. Environmental Science-Water Research & Technology 2(2), 312-319.

Zhang, Y., Chu, W., Yao, D. and Yin, D. (2017) Control of aliphatic halogenated DBP precursors with multiple drinking water treatment processes: Formation potential and integrated toxicity. Journal of Environmental Sciences 58, 322-330.

Appendix A UV/AOP Simulation SOP

1. Make a 0.1 M stock phosphate buffer by combining monobasic sodium phosphate and dibasic sodium phosphate in a volumetric flask. For a phosphate buffer recipe to help you determine how much of each compound to add depending on your desired volume, use this phosphate buffer calculator. Add some MQ water to dissolve the solids, then slowly add dilute NaOH until you reach a pH of 7.2. Add MQ water to the volumetric flask marking and mix well.
2. Calculate the amount of target compound required to reach a concentration of 18.5 µM in the UV reactor.
3. Make chloramines following the procedure detailed in **NDMA Formation Potential, NDMA t_0, and Extraction & Concentration**
4. Turn on UV lamp 20 minutes prior to sample exposure to warm up the light. Make sure lamp is set to 254 nm.
5. Into a volumetric flask, add the following:
    a. Stock phosphate buffer for a final concentration of 0.02 M
    b. The calculated amount of the target compound
    c. H_2O_2 for a final concentration 3 mg/L (note- try to add this as late as possible to minimize reactions or photodegradation).
    d. MQ water to the desired volume
6. Stir until lamp is ready for samples.
7. For the 0-min sample, add 2mL of the volumetric flask's contents to a 500 mL MQ water sample. Add chloramines and borate buffer, then store for 72 hours in the dark.

8. Pipette the contents of the volumetric flask into a quartz cuvette (15.7 cm_3 to 37.7 cm_3). Make sure there are no air bubbles. Cap the cuvette tightly with Teflon caps. Wipe cuvette with KimWipe to remove any fingerprints or dust.
9. For set up, cuvette must be as close to the lamp as possible. In Figure A-1, the cuvette sits on a pipette box inside of a bin so that the lamp may be placed as closely as possible to the cuvette.
10. Cuvette should be placed on top of a sheet of aluminum foil (Figure A-1)
11. Place the lamp over the cuvette (Figure A-2) and wrap foil around the lamp (Figure A-3) to encase both lamp and sample together.
12. At the desired time, remove lamp from sample. Pipette 2 mL of the sample into 500 mL MQ water. Add chloramines and borate buffer as per the NDMA Formation Potential procedure (Chapter 2), then store for 72 hours in the dark.
13. Wipe cuvette with KimWipe and place sample back on top of the aluminum foil and under the lamp. Repeat steps 11-13 until experiment is finished.

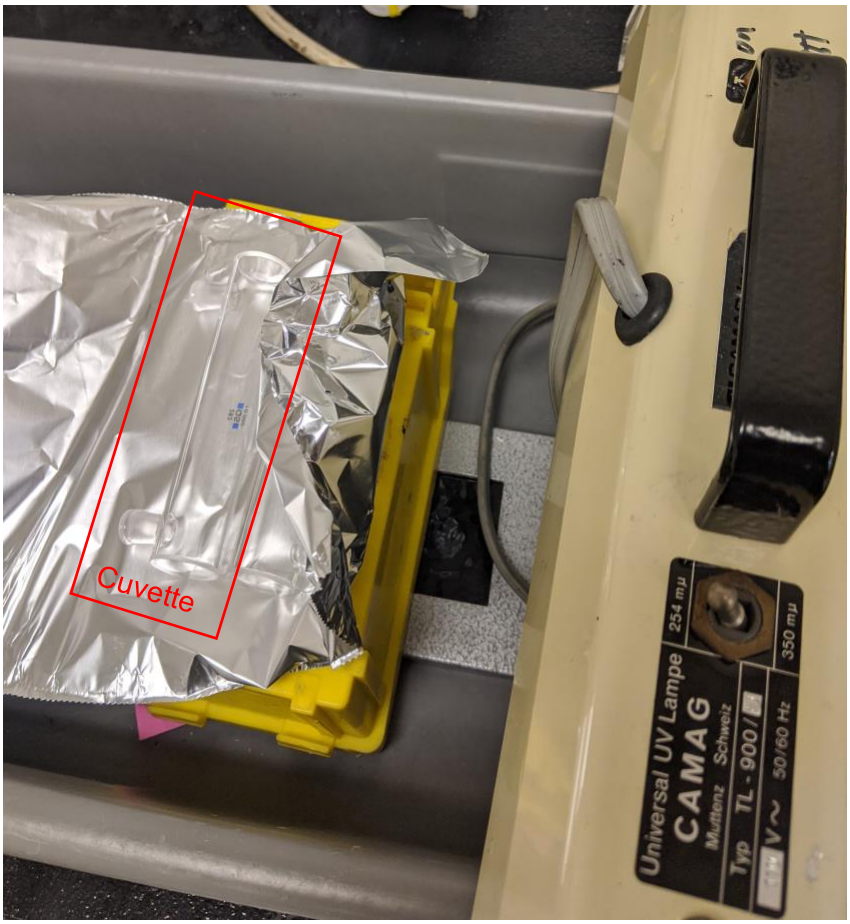

Figure-A-1 Cuvette (37.7 cm_3) placed on top of aluminum foil and a pipette box to keep sample close to lamp.

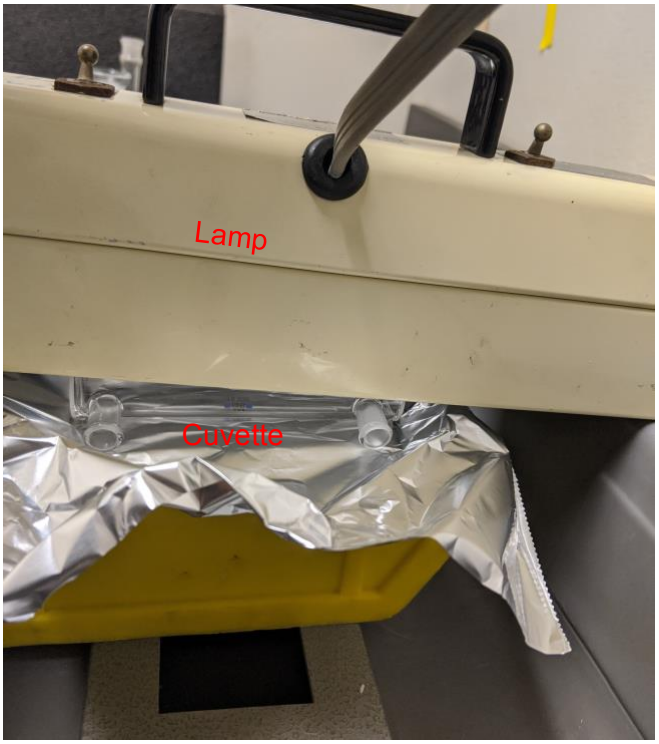

Figure-A-2 Lamp placed directly on top of sample.

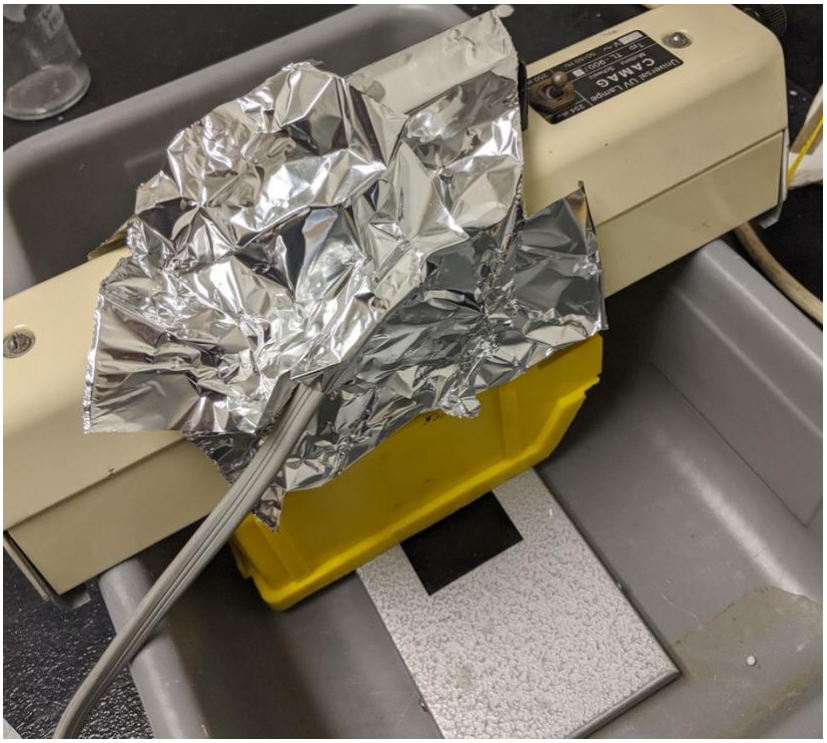

Figure-A-3 Aluminum foil wrapped around sample and lamp.

Appendix B GC-MS/MS SOP

1. Check gas levels of helium and argon tanks. Around 500 psi, keep a close eye on the tanks and order a backup tank. There are currently two oxygen traps and one scrubber in series between the helium and the GC. While oxygen is well removed, it is important to check these occasionally to see if they have expired.
2. Check pump oil levels and color. If oil level is low, add oil. If it looks brown or yellow, change the pump oil. Make sure you turn off the vacuum pump using the software BEFORE servicing the pump: Click the “Vacuum Control” button in the left purple column. Then click “Auto Shutdown” in the pop-up window. This will take at least 20 minutes to properly shut down the pump. This function also reduces source and inlet heat, so it is a good opportunity to clean the source, change the inlet liner, change the septa, and change the column if necessary.

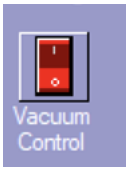

3. Ensure solvents are filled in the AutoSampler and that correct solvents are in the correct location vial. Vials A, B, and C correspond to methanol, methanol, and DCM (this is also labeled in tape on top of the GC). Manually push the “reset” button on the AutoSampler.
4. Open “GCMS Real Time Analysis” Program. It will ask for a password with the “admin” user, but none is set. Click “OK.”
5. If you get the error 1317, “The hardware configuration for this method…” just click “OK.” This usually means the column was changed and does not match the selected method.

a. When the program opens, check to see that the column installed matches the one set in the program. Click “System Configuration” in the left-hand panel. If you do not see this, click the blue arrow “Top” in the left-hand panel.

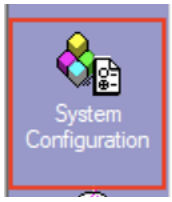

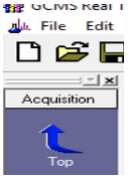

b. After clicking “System Configuration,” double click “Column” on the right. Click the column in use and click “Select” then “OK.” If you have a new column, click “Add” and input the column’s parameters.

6. Next is Tuning. Click the Tuning button in the left-hand panel. Make sure that the most recent method is set to MRM if you plan on running samples in MRM mode. This ensures that the instrument will be tuned with collision gas. To see what method is loaded, select the “Method” tab at the bottom of the screen (1).

   a. If the selected method is not MRM, press the blue arrow “Top,” then click “Data Acquisition,” then go to File > Open Method File… and select your method file.

After verifying a method, “New” blank page icon in the top left corner (2). In the pop-up box, select “High Sensitivity.” Finally, click “Start Auto Tuning” button (3).

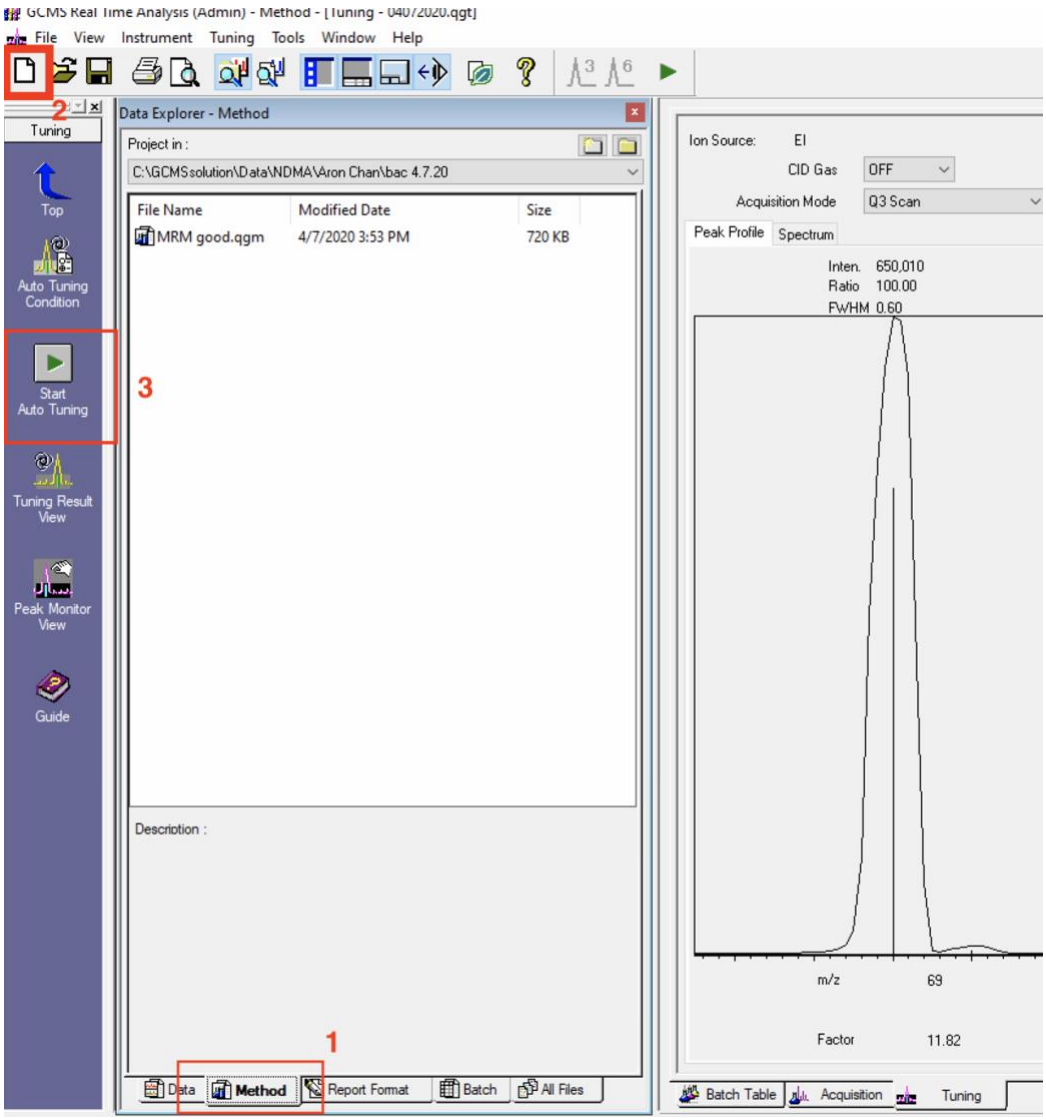

7. After auto tuning (about 30 minutes), you will be prompted to save THREE times: 1) first pdf page of the tuning report, 2) second page of tuning report with collision gas on, and 3) the tuning file itself (.qgt) to be used during acquisition. The tuning reports are saved to the desktop in the folder, “TUNING FILES.” The tuning files are saved in the folder (C:) > GCMS Solution > System > Tune 1.

8. Log some tuning data to quickly determine if the source needs to be cleaned. On the desktop, open the Excel file, “TUNE DATA.” Open the two pdf tuning files you just saved. In the Excel file, enter the following data from your pdf files: Tuning date, Lens 1-4, CC Lens 1-4, Detector, Low Vacuum, High Vacuum. Source generally needs to be cleaned when you notice an increase in detector voltage. After cleaning the source, indicate this in the logbook as done previously.
9. Create a folder that will house all your data files, standards, method file, and batch file. Most folders are stored here: (C:) > GCMSolution > Data
10. Return to the GCMS program. Click the blue arrow “Top” then click “Data Acquisition.” Load your method or create a new one from the “File” button. The best NDMA method file is located in (C:) > GCMSolution > Data > NDMA, “ORIGINAL MRM for NDMA...qgm.” Do not edit this original NDMA MRM method. If you use this file, COPY it, and paste it into the folder you created in Step 9. Change the name to avoid confusion. You should now be able to see this file in the GCMS program. If you cannot see it, click the “Select Project” folder icon to navigate to the correct folder:

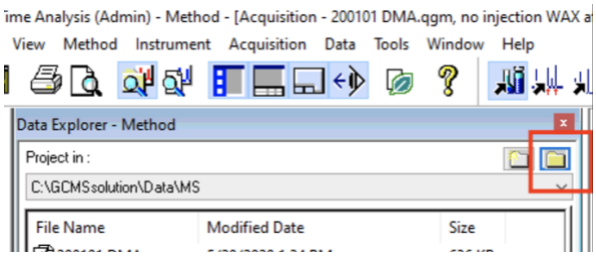

Double click on the displayed method file to open it. Your method parameters can be viewed and edited in the “Acquisition” tab on the BOTTOM right half of the screen. You can then toggle between the Sampler, GC, and MS settings.

11. Next select the “Batch **Table**” tab, adjacent to the “Acquisition” tab (bottom RIGHT tabs). Go to File > New Batch File. Then, Click File > Save As… to save your file (.qgb) in the Step 9 folder.
12. The following columns are shown in your new batch table, but only the **BOLDED** ones will be discussed here: **Vial #, Sample name,** Sample ID, **Sample Type, Analysis type, Method File, Data File, Level #, Inj. Volume,** ISTD Amount, Report Output, Report File, **Tuning File**, Data description.
    a. Vial # - Make sure the vial # entered matches with the sample’s location on the autosampler tray.
    b. Sample Name – Enter sample’s unique description or name.
    c. Sample Type – Click inside the box, then click the small arrow that appears on the right side. If the sample is a calibration standard, select “Standard.” If it is your first standard, click “Initialize Calibration Curve.” The rest of your standards should automatically have “Add Calibration Level” selected. If you are entering an unknown (i.e. a sample), select “Unknown” in the left panel.
    d. Analysis Type – Should always be IT QT
    e. Method File – Click in the box, then click the small arrow to open up a file viewer. Load your method file (.qgm).
    f. Data File – It is easiest to auto generate names for this column. To do so, Right Click and select “Settings” from the menu. Click the “Data File Name” tab. Check the box “Create filenames automatically.” Choose what parameters you want in the datafile name. I have found it is best to just use “Sample Name” to avoid long file names, as well as auto-increment set to “1, 2, …” Your data file’s output will be Sample Name_1.qgd. After

adjusting these settings, the column will turn yellow and will auto-populate AFTER analysis.

g. Level # - To be used with standards only. This indicates what point in the calibration curve each standard corresponds to. For example, 0.5 ppb = Level 1, 1 ppb = Level 2, etc.

h. Inj. Volume – For NDMA, set the injection volume to 2 µL. The automatic setting is 1 µL, so up to you if you choose to change it.

i. Tuning File – As created in Step 7, you will now load your tuning file. Click the cell, then click the small arrow to select the correct .qgt file.

13. Highlight all samples, then click the green triangle to start your batch of samples. MAKE SURE all rows you want processed are listed in “Selected Rows.” Then click “Start.”

14. To view your processed samples, go back to your computer’s desktop and open “GCMS Postrun Analysis.” Go to File > Open Data File and select a data file from your Step 9 folder. When you select one data file, you will be able to see all files in the Step 9 folder in the data explorer. If you do not see a list of files, click the “Toggle Data Explorer” button:

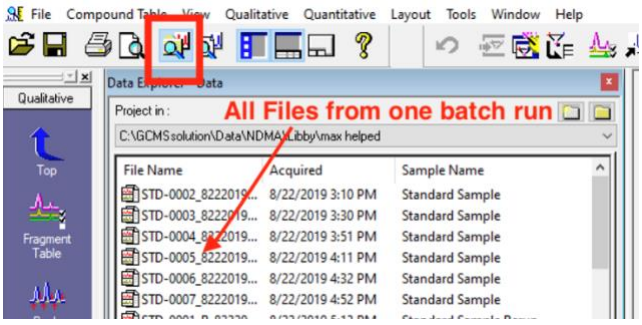

15. Go to File > Load Method to open the method file you just used (make sure this is the method in your Step 9 folder – not the original one).

16. If a “Select Method Parameters” box pops up, select all the check boxes.

17. Select all data files. Then (in the same row as your “File” button), click Quantitative > Peak Integrate for All IDs.
18. Click the “Calibration Curve” button in the left purple panel. If you do not see this, click the blue arrow “top.”
19. Drag the data files for each standard from the data explorer to the corresponding level in the Calibration Curve box.

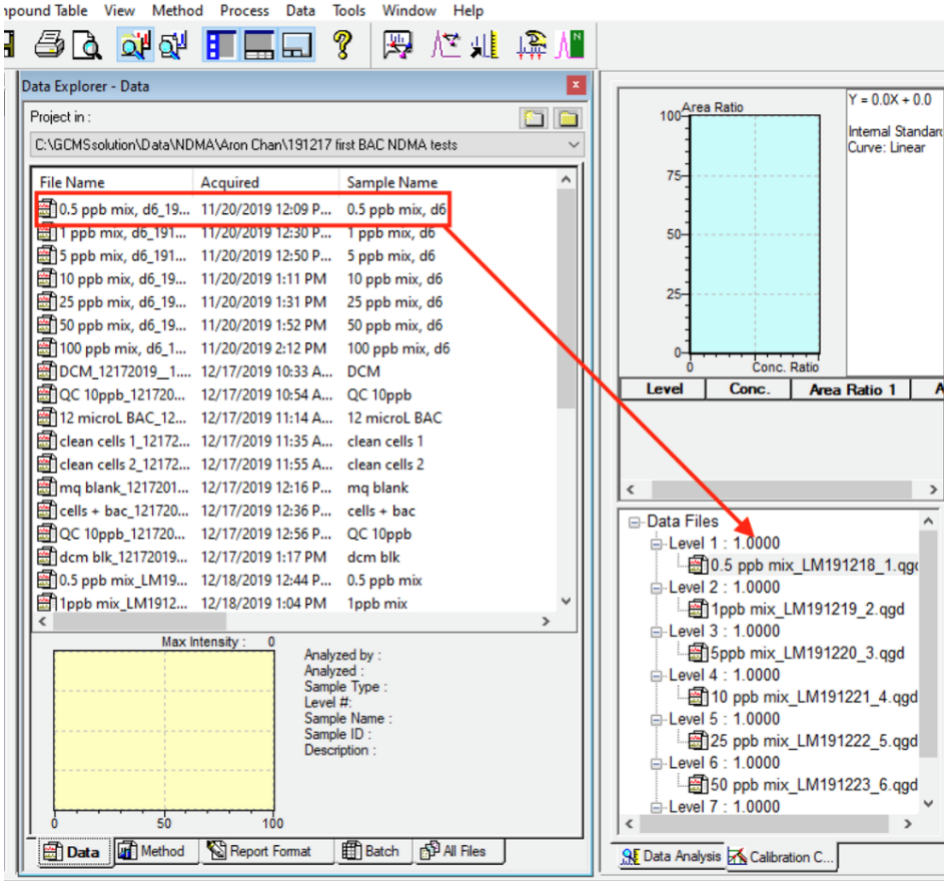

20. If you want to change the concentration of the calibration curve (1), go to the right most window click the “Param’s” tab. Click “Edit” (2) and then change the concention value. Finally click “View” (2) to save it. Remember, the concentration

of internal standard (ISTD) should always be 1 (3).

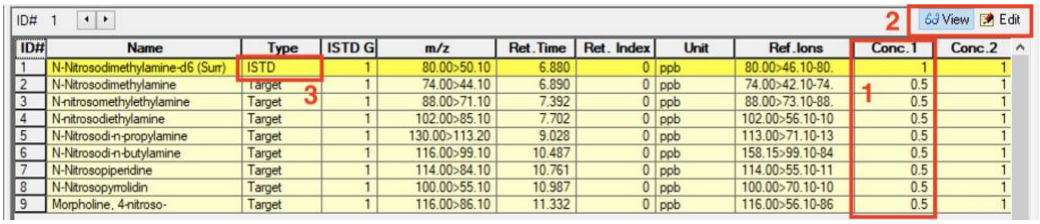

ID#	Name	Type	ISTD G	m/z	Ret.Time	Ret. Index	Unit	Ref.Ions	Conc.1	Conc.2
1	N-Nitrosodimethylamine-d6 (Surr)	ISTD	1	80.00>50.10	6.880	0	ppb	80.00>46.10-80.	1	1
2	N-Nitrosodimethylamine	Target	1	74.00>44.10	6.890	0	ppb	74.00>42.10-74.	0.5	1
3	N-nitrosomethylethylamine	Target	1	88.00>71.10	7.392	0	ppb	88.00>73.10-88.	0.5	1
4	N-nitrosodiethylamine	Target	1	102.00>85.10	7.702	0	ppb	102.00>56.10-10	0.5	1
5	N-Nitrosodi-n-propylamine	Target	1	130.00>113.20	9.028	0	ppb	113.00>71.10-13	0.5	1
6	N-Nitrosodi-n-butylamine	Target	1	116.00>99.10	10.487	0	ppb	158.15>99.10-84	0.5	1
7	N-Nitrosopiperidine	Target	1	114.00>84.10	10.761	0	ppb	114.00>55.10-11	0.5	1
8	N-Nitrosopyrrolidin	Target	1	100.00>55.10	10.987	0	ppb	100.00>70.10-10	0.5	1
9	Morpholine, 4-nitroso-	Target	1	116.00>86.10	11.332	0	ppb	116.00>56.10-86	0.5	1

21. In the right-most window click the “Results” tab (1). Click on ID numbers to see calibration curves for each compound (2). Use the horizontal scroll bar (3) to see other parameters, such as S:N ratio. Click the check boxes (4) to remove any standards that might not fit with your calibration curve. This is helpful to remove lower concentration samples and set a detection limit. In this example, the 3rd standard, 5 ppb, is not on the calibration curve. If the wrong peak has been integrated, move the small blue triangle (5) (triangle is difficult to see in this picture, but it is at the top of the peak) to the correct peak. If this is not possible, right-click to either manually integrate or manually select peak.

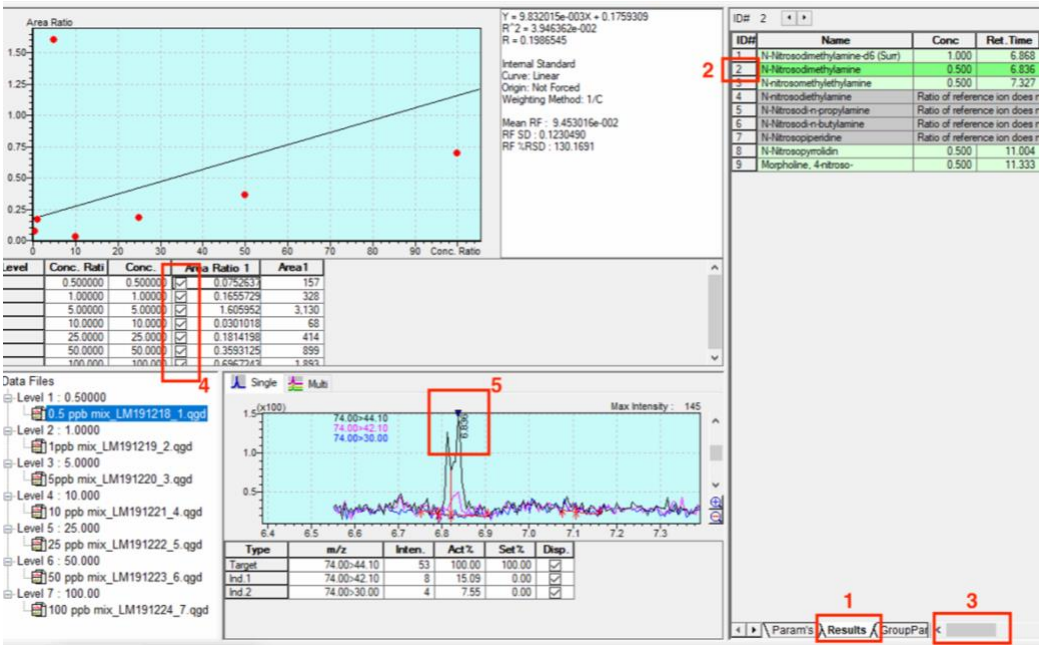

22. When you are satisfied with your calibration curve, save it directly with  or Click File > Save Method File. Next, click the “Data Analysis” tab (next to “Calibration Curve” tab).
23. Double click on a data file from the file explorer. Similar to Step 21, click the Results tab, then click any of the ID# rows to see peaks for each compound. The concentration for each compound is displayed in the second column. Check that the software correctly identified peaks. The retention time is extremely important. A compound may have a peak in the same range as the target compound’s retention time but may be off by 0.1 seconds. Check your standards’ retention times against the peak in question.

Appendix C Supplementary Information for Summation of Disinfection By-product CHO Cell Relative Toxicity Indices: Sampling Bias, Uncertainty, and a Path Forward

6 Figures

7 Tables

18 Pages

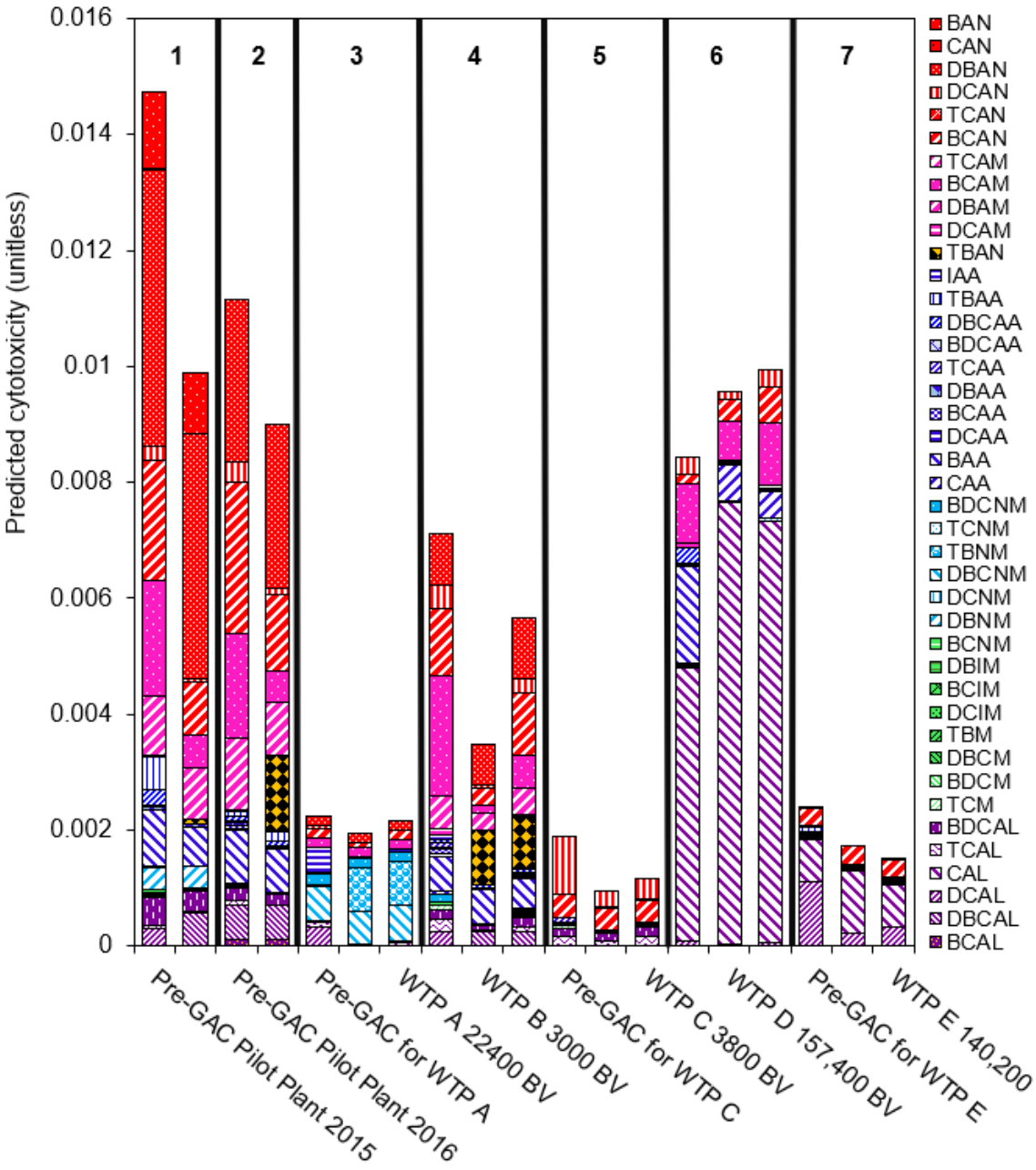

Figure-C-1 Components of predicted cytotoxicity for data from Stanford *et al*. (2019a) and Cuthbertson *et al*. (2019). Red/pink compounds are HANs and HAcAms. Left-most bar in each panel is pre-GAC predicted cytotoxicity, other bars are GAC effluent samples. Only 41 DBPs are shown, rather than the 70 that were measured, because 29 DBPs were not detected.

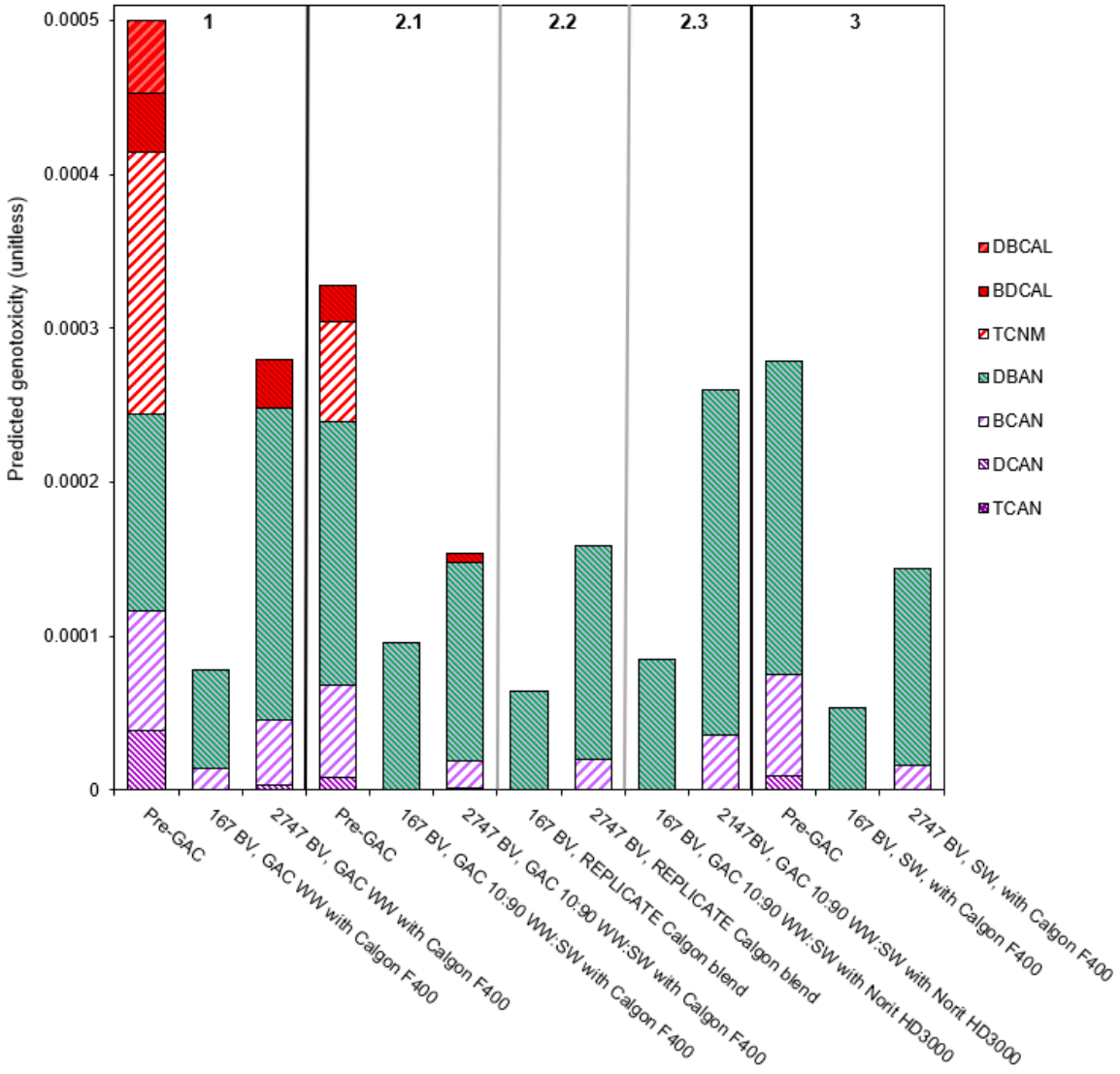

Figure-C-2 DBP components of predicted genotoxicity for Krasner *et al.* (2016b) data. Red compounds are measured HALs and TCNM. Left-most bar in each panel is pre-GAC genotoxicity, other bars are post-GAC.

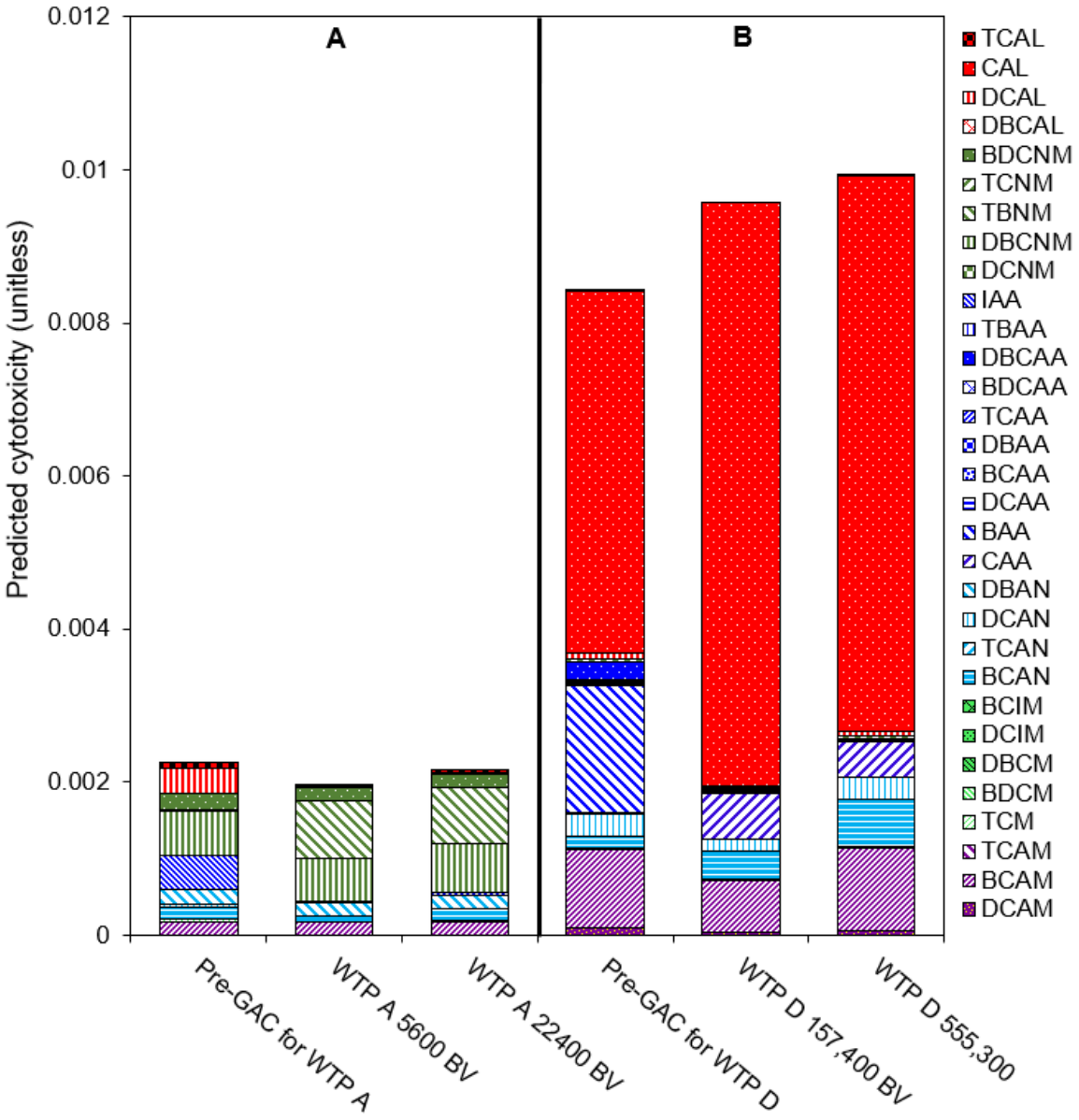

Figure-C-3 DBP components of predicted cytotoxicity for data from Stanford *et al*. (2019a) and Cuthbertson *et al.* (2019). Red compounds are measured HALs.1,4 Left-most bar in each panel is pre-GAC predicted cytotoxicity, other bars are GAC effluent samples. Only 41 DBP's are listed (rather than 70 as previously mentioned) because DBPs not detected in a sample are not included.

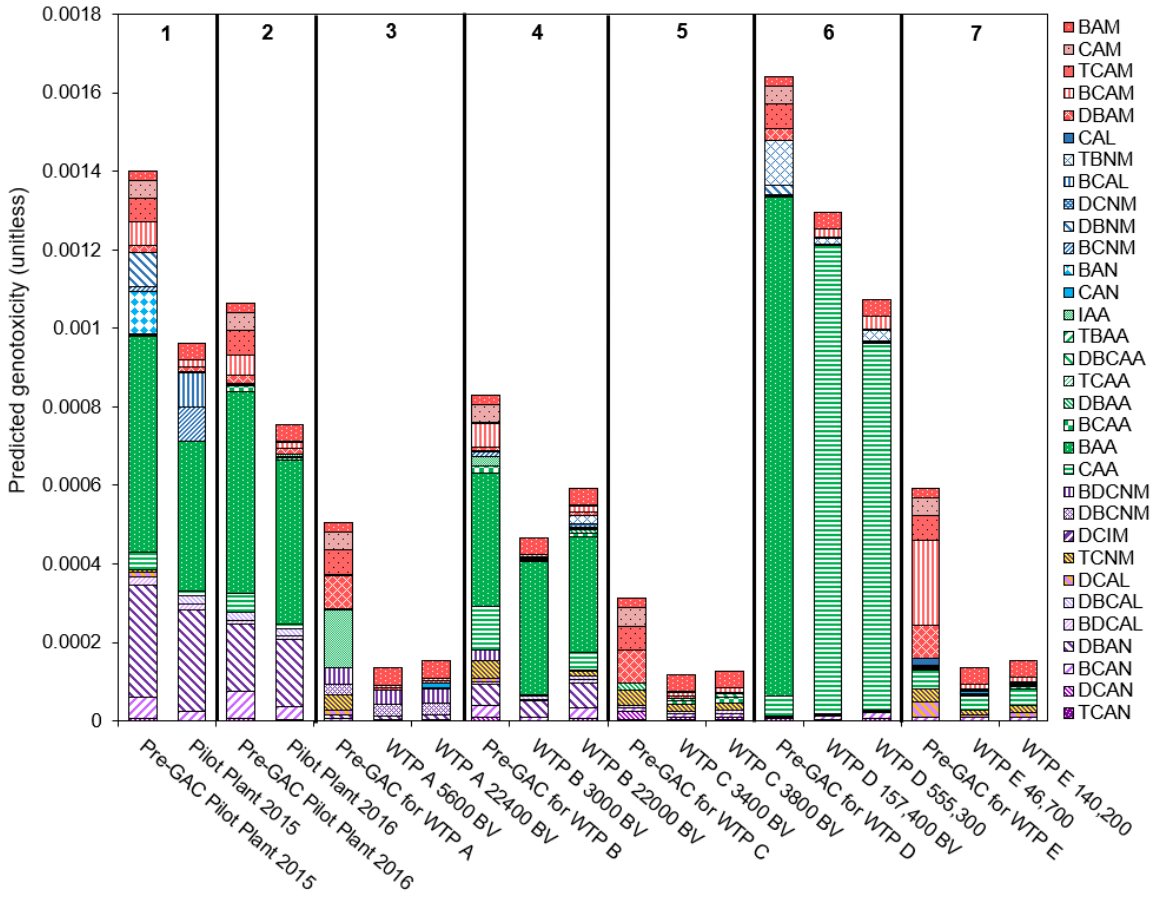

Figure-C-4 DBP components of predicted cytotoxicity for data from Stanford *et al*. (2019a) and Cuthbertson *et al.* (2019). Red colored compounds are either measured HAcAms from the study or supplemented HAcAms derived from the mean concentrations at 18 WTPs (Table 5-1).1,4 Left-most bar in each panel is pre-GAC predicted genotoxicity, other bars are GAC effluent samples. Only 41 DBPs are shown, rather than the 70 that were measured, because 29 DBPs were not detected.

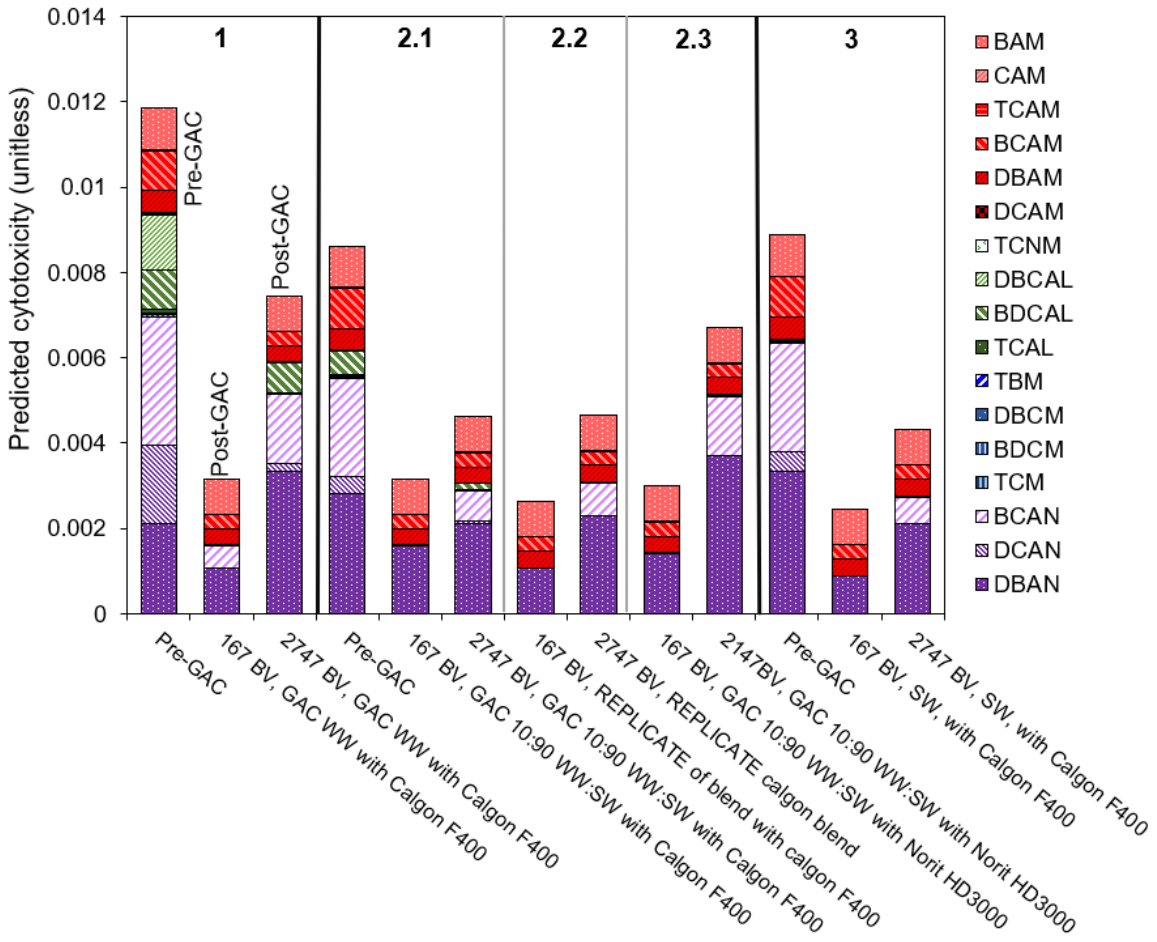

Figure-C-5 DBP components of predicted cytotoxicity for Krasner *et al*. (2016b) data. Red compounds are either measured HAcAms from the study or assumed HAcAms (see Table 5-1). Left-most bar in each panel is pre-GAC cytotoxicity, other bars are post-GAC.

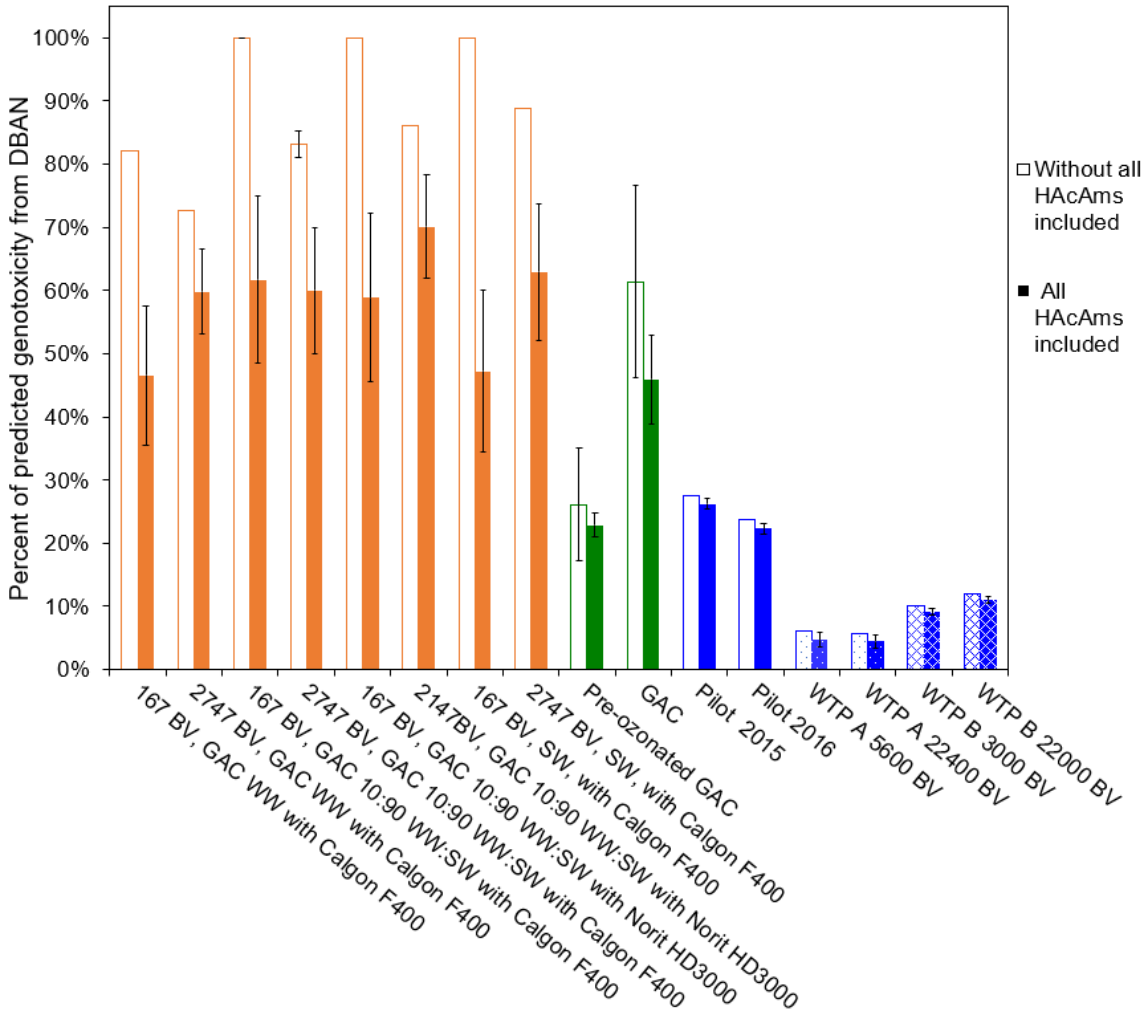

Figure-C-6 Percent of post-GAC predicted genotoxicity from DBAN without HAcAms (original data) or with addition of assumed HAcAms (data averaged from Kosaka *et al.* (2016b)) as well as DCAM, DBAM, BCAM, and TCAM data from Stanford *et al*. (2019a)) Orange data is from Krasner *et al.* (2016), green data is from McKie *et al*. (2015) and blue data is Stanford *et al*. (2019). Data from Stanford *et al.* (2019) initially included some HAcAms and therefore the filled bars only include assumed concentrations for the additional HAcAms. Stanford *et al.* (2019) (blue bars) have different pattern fills because each data set included different HAcAms – The pilots included DCAM, DBAM, and BCAM, WTP A included DCAM and BCAM, and WTP B included DCAM, DBAM, BCAM,

and TCAM. McKie *et al.* (2015) did not measure DBAN and thus the average, post-GAC DBAN concentrations from Krasner *et al.* (2016) and Stanford *et al.* (2019) were included. Error bars for data including HAcAms (filled bars) are derived from the standard deviation of HAcAm data from Kosaka *et al.* (2016a) and the HAcAms that Stanford *et al.* (2019) measured (DCAM, DBAM, BCAM, TCAM). Error bars for data without HAcAms (open bars) are derived from data included in the original publications.

Table C-1 Toxic potencies derived from Wagner and Plewa (2017). TBAN cytotoxicity from a personal correspondence with Plewa (2019).

Abbreviation	Compound's full name	Genotoxic potency (unitless)	Cytotoxic potency (unitless)
TCM	Trichloromethane	Not genotoxic	9.62E-03
BDCM	Bromodichloromethane	Not genotoxic	1.15E-02
DBCM	Dibromochloromethane	Not genotoxic	5.36E-03
TBM	Tribromomethane	Not genotoxic	3.96E-03
TCAN	Trichloroacetonitrile	1.01E-03	1.60E-04
DCAN	Dichloroacetonitrile	2.75E-03	5.73E-05
BCAN	Bromochloroacetonitrile	3.24E-04	8.46E-06
DBAN	Dibromoacetonitrile	4.71E-05	2.85E-06
CAN	Chloroacetonitrile	6.01E-04	6.83E-05
BAN	Bromoacetonitrile	3.85E-05	3.21E-06
TBAN	Tribromoacetonitrile	Not genotoxic	2.71E-06
CAL	Chloroacetaldehyde	1.43E-04	3.51E-06
TCAL	Trichloroacetaldehyde	Not genotoxic	1.16E-03
BCAL	Bromochloroacetaldehyde	6.21E-04	5.34E-06
BDCAL	Bromodichloroacetaldehyde	4.70E-04	2.04E-05
DBCAL	Dibromochloroacetaldehyde	1.44E-04	5.15E-06
DCAL	Dichloroacetaldehyde	7.95E-04	2.92E-05
DCIM	Dichloroiodomethane	Not genotoxic	4.13E-03
BCIM	Bromochloroiodomethane	Not genotoxic	2.42E-03
DBIM	Dibromoiodomethane	Not genotoxic	1.91E-03
CAA	Chloroacetic acid	4.11E-04	8.10E-04
BAA	Bromoacetic acid	1.70E-05	9.60E-06
IAA	Iodoacetic acid	8.70E-06	2.95E-06
DCAA	Dichloroacetic acid	Not genotoxic	7.30E-03
BCAA	Bromochloroacetic acid	3.64E-03	7.78E-04
DBAA	Dibromoacetic acid	1.80E-03	5.90E-04
TCAA	Trichloroacetic acid	Not genotoxic	2.40E-03
DBCAA	Dibromochloroacetic acid	1.40E-02	2.02E-04
BDCAA	Bromodichloroacetic acid	Not genotoxic	6.85E-04
TBAA	Tribromoacetic acid	2.50E-03	8.50E-05
DCAM	Dichloroacetamide	Not genotoxic	1.92E-03
DBAM	Dibromoacetamide	7.44E-04	1.22E-05
BCAM	Bromochloroacetamide	5.83E-04	1.71E-05
TCAM	Trichloroacetamide	6.54E-03	2.50E-03
CAM	Chloroacetamide	1.38E-03	1.48E-04

BAM	Bromoacetamide	3.68E-05	1.89E-06
TCNM	Trichloronitromethane	9.34E-05	5.36E-04
DBCNM	Dibromochloronitromethane	1.43E-04	6.88E-06
BDCNM	Bromodichloronitromethane	6.32E-05	1.32E-05
BCNM	Bromochloronitromethane	1.65E-04	4.05E-05
DBNM	Dibromonitromethane	2.62E-05	6.09E-06
DCNM	Dichloronitromethane	4.21E-04	3.73E-04
TBNM	Tribromonitromethane	6.99E-05	8.57E-06

Table C-2 GAC and oxidation treatment characteristics.

	Corresponding Figure	Influent water	Pre-GAC oxidant	Post-GAC oxidant
Data from McKie *et al.* and Krasner *et al.* (HAcAms supplemented to)				
Pre-ozonated GAC	Figure 5-3, Panels 1-3	Lake	Ozone	Chlorine
GAC	Figure 5-3, Panels 4-8	River	None	Chlorine
167 BV with Calgon F400	Figure 5-4	Wastewater	None	Chlorine
2747 BV with Calgon F400	Figure 5-4	Wastewater	None	Chlorine
167 BV with Calgon F400	Figure 5-4	10:90 WW:SW	None	Chlorine
2747 BV with Calgon F400	Figure 5-4	10:90 WW:SW	None	Chlorine
167 BV with Norit HD3000	Figure 5-4	10:90 WW:SW	None	Chlorine
2147 BV with Norit HD3000	Figure 5-4	10:90 WW:SW	None	Chlorine
167 BV with Calgon F400	Figure 5-4	Surface water	None	Chlorine
2747 BV with Calgon F400	Figure 5-4	Surface water	None	Chlorine
Stanford *et al.* and Cuthbertson *et al.* (DCAM, DBAM, BCAM, TCAM aggregated from. CAM and BAM supplemented to)				
Pilot scale plant 1	Figures 5-1 & 5-2, Panel 1	Tertiary filtered ww	Chlorine	Chloramine and chlorine
Pilot scale plant 2	Figures 5-1 & 3-2, Panel 2	UF membrane permeate from surface water treatment plant	Chlorine	Chlorine
WTP A	Figures 5-1 & 3-2, Panel 3	Lake	Chlorine	Chlorine
WTP B	Figures 5-1 & 5-2, Panel 4	River	KMnO4	Chlorine
WTP C	Figures 5-1 & 5-2, Panel 5	Reservoir	NaMnO4	Chlorine
WTP D	Figures 5-1 & 5-2, Panel 6	River	KMnO4, chloramine	Chloramine
WTP E	Figures 5-1 & 5-2, Panel 7	River	Chloramine	Chloramine
HAcAm data from Kosaka *et al.* (HAcAms aggregated from)				

Event 1, WTP 5	Figures 5-2, 5-3, 5-4	Surface water	None	Chlorine
Event 2, WTP 5	Figures 5-2, 5-3, 5-4	Surface water	None	Chlorine
Event 1, WTP 10	Figures 5-2, 5-3, 5-4	Surface water	Ozone	Chlorine
Event 2, WTP 10	Figures 5-2, 5-3, 5-4	Surface water	Ozone	Chlorine
Event 1, WTP 12	Figures 5-2, 5-3, 5-4	Surface water	Ozone	Chlorine
Event 2, WTP 12	Figures 5-2, 5-3, 5-4	Surface water	Ozone	Chlorine

Table C-3 Aggregated HAcAm data from Kosaka et al. (2016).

Pre-GAC HAcAm concentrations (M)							
		[DCAM]	**[DBAM]**	**[BCAM]**	**[TCAM]**	**[CAM]**	**[BAM]**
Event 1	WPP 5	2.58E-08	7.84E-09	2.26E-08	6.16E-09	7.49E-09	4.35E-09
Event 2	WPP 5	1.80E-08	5.99E-09	1.57E-08	4.93E-09	5.35E-09	2.90E-09
Event 2	WPP10	1.09E-08	4.61E-10	4.06E-09	2.46E-09	2.14E-09	7.25E-10
Event 2	WPP10	9.38E-09	9.22E-10	4.06E-09	2.46E-09	2.14E-09	7.25E-10
Event 1	WPP12	4.69E-09	2.31E-09	4.64E-09	6.16E-10	1.07E-09	7.25E-10
Event 2	WPP12	4.69E-09	3.23E-09	5.80E-09	1.23E-09	2.14E-09	1.45E-09
Column Avg:		1.22E-08	3.46E-09	9.47E-09	2.98E-09	3.39E-09	1.81E-09
Post-GAC HAcAm concentrations (M)							
		[DCAM]	**[DBAM]**	**[BCAM]**	**[TCAM]**	**[CAM]**	**[BAM]**
Event 1	WPP 5	2.34E-09	2.77E-09	2.90E-09	6.16E-10	2.14E-09	2.17E-09
Event 2	WPP 5	2.34E-09	1.38E-09	1.74E-09	6.16E-10	1.07E-09	7.25E-10
Event 2	WPP10	1.56E-09	1.38E-09	2.32E-09	6.16E-10	2.14E-09	7.25E-10
Event 2	WPP10	1.56E-09	4.61E-10	1.16E-09	6.16E-10	1.07E-09	7.25E-10
Event 1	WPP12	1.56E-09	4.61E-09	2.32E-09	6.16E-10	1.07E-09	3.62E-09
Event 2	WPP12	7.82E-10	5.07E-09	2.32E-09	6.16E-10	1.07E-09	1.45E-09
Column Avg:		1.69E-09	2.61E-09	2.13E-09	6.16E-10	1.43E-09	1.57E-09

Table C-4 DBAN concentrations from Krasner et al. (2016b) and Stanford et al. (2019b) The average was used for McKie et al. (2015).

Source	Water Source	DBAN (nM)
Stanford *et al.*(2019b)	WW	12.07
	UF Permeate	8.05
	Lake	0.50
	Lake	0.50
	River	2.01
	River	3.02
Krasner *et al.*(2016a)	100% WW	3.02
	100% WW	9.56
	10:90 WW:SW	4.53
	10:90 WW:SW	6.03
	10:90 WW:SW	3.02
	10:90 WW:SW	6.54
	10:90 WW:SW	4.02
	10:90 WW:SW	10.56
	100% SW	2.51
	100% SW	6.03
Average DBAN (nM)		5.12
Standard deviation		3.39

Table C-5 Raw data from Stanford et al. measuring post-GAC concentrations of DBPs. Dashes indicate non-detect.

DBP (ug/L)	Stanford *et al.* (2019a)											
	Pilot 2015	Pilot 2016	WTP A 5,600 BV	WTP A 22,400 BV	WTP B 3,000 BV	WTP B 22,000 BV	WTP C 3,400 BV	WTP C 3,800 BV	WTP D 157,400 BV	WTP D 555,300 BV	WTP E 46,700 BV	WTP E 140,200 BV
TCM	2.2	3.59	6.1	22.5	10.2	30.2	21.9	29.5	16.3	15.5	8.5	8.5
BDCM	12.3	12.55	4.9	9.5	5.9	16.7	1.7	1.8	2.4	2.5	1.3	1.3
DBCM	24.5	25.93	--	--	4	7.3	--	--	0.3	0.4	0.3	0.4
TBM	17.1	--	--	--	0.5	0.4	--	--	--	--	0.5	0.5
TCAN	--	--	--	--	--	--	0.3	0.3	--	--	--	--
DCAN	0.4	0.8	0.0025	0.0025	0.2	1.5	1.8	2.2	0.9	1.8		0.2
BCAN	1.2	1.7	0.1	0.2	0.4	1.4	0.5	0.5	0.5	0.8	0.4	0.4
DBAN	2.4	1.6	0.1	0.1	0.4	0.6	--	--	--	--	--	--
TCAL	0.8	1.9	0.9	7.5	1.1	9.9	16	29.4	--	1.2	0.2	0.3
BDCAL	1.4	0.7	--	--	0.3	0.7	0.5	0.6	--	--	--	--
DBCAL	0.7	0.7	--	--	0.3	0.3	--	--	--	--	--	--
DCAL	0.05	--	0.05	0.05	0.05	0.05	--	--	0.1	0.2	0.7	1.1
TCNM	0.003	--	0.003	0.003	0.003	0.2	0.3	0.3	--	--	0.2	0.3
DCIM	0.4	--	0.006	0.006	0.006	0.006	--	--	--	--	--	--
BCIM	0.5	0.5	0.0195	0.0195	0.0195	0.0195	--	--	--	--	--	--
DBIM	0.6	0.7	--	--	--	--	--	--	--	--	--	--
DBCNM	--	--	1.2	1.3	--	--	--	--	--	--	--	--
BDCNM	--	--	0.8	0.8	0.05	0.05	--	--	--	--	--	--
DCAM	0.8	0.7	0.1	0.2	0.8	4.1	0.3	0.7	7.4	14.3	2.4	2.7
DBAM	2.4	2.4			0.8	1.2	--	--	0.6	0.5	--	--
BCAM	1.6	1.6	0.5	0.5	0.4	1.7	--	--	2	3.2	--	--
TCAM	--	--	--	--	0.4	0.8	0.4	0.5	0.4	0.5	--	--
CAA	0.5	0.423	--	--		1.7	--	--	46.3	36.3	1.3	1.6
BAA	0.9	0.986	--	--	0.8	0.7	--	--	--	--	--	--
DCAA	1.6	1.63	--	4	2.4	12	11.3	18.8	1.6	3.3	6.5	8.2
BCAA	0	3.99	--	--	2.1	4.7	--	--	0.2	--	1.4	1.6
DBAA	5.8	5.18	--	--	1.3	1.4	--	--	0.2	--	--	--
TCAA	0.6	--	--	--	1	7.3	8.6	12.9	3.9	4.3	0.8	2.7
BDCAA	--	1.11	--	--	1.6	3.3	--	--	1.5	1.3	1.2	1.3
DBCAA	--	2.92	--	--	2	2.6	--	--	0.9	0.9	0.8	0.9
TBAA	--	4.28	--	--	--	--	--	--	0.3	--	0.4	0.6
IAA	--	--	0.0025	0.02	0.0025	0.0025	--	--	--	--	0.007	--
CAN	0.004	--	--	--	--	--	--	--	--	--	--	--
BAN	0.4	--	--	--	--	--	--	--	--	--	--	--

TBAN	0.05	1	--	--	0.7	0.7	--	--	--	--	--	--
BCNM	0.012	--	--	--	0.012	0.3	--	--	--	--	--	--
DBNM	0.5	--	--	--			--	--	--	--	--	--
DCNM	0.014	--	--	--	0.014	1.1	--	--	0.8	1.5	0.1	0.1
BCAL	--	.1	--	--	--	--	--	--	--	--	--	--
TBNM	--	--	1.9	1.9	--	--	--	--	--	--	--	--
CAL	--	--	--	--	--	--	--	--	2.1	2	0.3	0.2

Table C-6 Raw data from Krasner *et al.* and McKie *et al.* measuring post-GAC concentrations of DBPs. Dashes indicate non-detect.

DBP (ug/L)	Krasner *et al.*[1]									McKie *et al.*[4]					
	167 BV, GAC WW with Calgon F400	2747 BV, GAC WW with Calgon F400	167 BV, GAC 10:90 WW:SW with Calgon F400	167 BV, GAC REPLICATE of blend with Calgon F400	2747 BV, REPLICATE of 10:90 Calgon	167 BV, GAC 10:90 WW:SW with Norit HD3000	2147BV, GAC 10:90 WW:SW with Norit HD3000	2747 BV, GAC 10:90 WW:SW with Calgon F400	167 BV, SW, with Calgon F400	2747 BV, SW, with Calgon F400	Pre-ozonated GAC			GAC		
TCM	1.8	5.9	1.7	1.4	3.9	1.7	8.6	3.4	0	3.4	13.12	13.3	10.8	164	158.2	63.4	96.4	73.4
BDCM	2.8	9.2	2.8	2.4	7.2	4	17.8	7	2.1	6.8	11.7	13.3	11.8	25.1	3.73	17.8	19.9	19.8
DBCM	4.3	10.8	6.3	4.9	11.4	7.4	21	11.5	4.6	11.3	4.53	6.3	5.09	--	--	--	--	--
TBM	2.7	3.8	4.1	3.4	5.3	3.6	6	4.9	3.4	5.8	--	--	--	--	--	--	--	--
DCAN	--	1.1	--	--	--	--	--	0.4	--	--	--	--	--	--	--	--	--	--
BCAN	0.7	2.1	--	--	1	--	1.8	0.9	--	0.8	--	--	--	--	--	--	--	--
DBAN	0.6	1.9	0.9	0.6	1.3	0.8	2.1	1.2	0.5	1.2	--	--	--	--	--	--	--	--
TCAL	--	2.6	--	--	0.7	--	2.4	0.8	--	0.6	--	--	--	--	--	--	--	--
BDCAL	--	2.8	--	--	--	--	--	0.6	--	--	--	--	--	--	--	--	--	--
CAA	--	--	--	--	--	--	--	--	--	--	1.47	1.55	3.12	2.66	3.67	0.59	2.05	5.78
BAA	--	--	--	--	--	--	--	--	--	--	0.63	2.87	3.55	--	--	--	--	--
DCAA	--	--	--	--	--	--	--	--	--	--	2.34	5.47	6.08	36.8	36	23.1	29.8	48.6
BCAA	--	--	--	--	--	--	--	--	--	--	0.9	2.14	2.06	--	--	--	--	--
DBAA	--	--	--	--	--	--	--	--	--	--	0.79	3.25	2.81	--	--	--	--	--
TCAA	--	--	--	--	--	--	--	--	--	--	1.61	0.74	2.03	55.8	33.9	40.4	33.1	42

Table C-7 Raw data for Figure 5-4, cytotoxicity.

	Percent of total cytotoxicity from DBAN without HAcAms included	Percent of total cytotoxicity from DBAN including HAcAms	Error for Data with HAcAms included	Error for data with replicated sampling events
167 BV, GAC WW with Calgon F400	66.11%	33.4%	8.94%	
2747 BV, GAC WW with Calgon F400	56.93%	44.9%	6.05%	
167 BV, GAC 10:90 WW:SW with Calgon F400	99.21%	50.1%	13.42%	0.08%
Krasner et al. 167 BV, GAC REPLICATE of blend with calgon F400	99.04%	40.1%	12.25%	
2747 BV, GAC 10:90 WW:SW with Calgon F400	69.43%	45.8%	9.20%	2.45%
Krasner et al. 2747 BV, DUP 10:90 calgon	74.32%	49.3%	9.83%	
167 BV, GAC 10:90 WW:SW with Norit HD3000	99.03%	47.1%	13.16%	
2147BV, GAC 10:90 WW:SW with Norit HD3000	72.10%	55.2%	8.14%	
167 BV, SW, with Calgon F400	99.03%	35.9%	11.49%	
2747 BV, SW, with Calgon F400	76.83%	48.9%	10.35%	
Pre-ozonated GAC	77.14%	46.1%	10.57%	17.6%
Pre-ozonated GAC	42.46%	30.3%	5.30%	
Pre-ozonated GAC	37.42%	27.6%	4.48%	
GAC	81.65%	46.0%	11.22%	2.6%
GAC	84.14%	46.8%	11.56%	
GAC	89.23%	48.3%	12.23%	

GAC	87.47%	47.8%	12.00%	
GAC	84.29%	46.9%	11.58%	
Pilot 2015	42.84%	39.5%	1.96%	
Pilot 2016	31.36%	28.7%	1.54%	
WTP A 5600 BV	9.04%	5.5%	1.18%	
WTP A 22400 BV	8.13%	5.2%	1.05%	
WTP B 3000 BV	20.31%	16.4%	1.88%	
WTP B 22000 BV	18.67%	16.3%	1.29%	